^{182}W and ^{187}Os Constraints on the Origin of Siderophile Isotopic Heterogeneity in the Mantle

Richard J. Walker[a], Andrea Mundl-Petermeier[a,b], Igor S. Puchtel[a], Robert W. Nicklas[c], Jan L. Hellmann[a], Lina M. Echeverría [d], Kyle D. Ludwig[a], Katherine R. Bermingham[e], Esteban Gazel[f], Charlotte L. Devitre[f], Matthew G. Jackson[g], Catherine Chauvel[h]

a - Department of Geology, University of Maryland, College Park, MD, USA
b - University of Vienna, Department of Lithospheric Research, 1090 Vienna, Austria
c - Department of Earth and Environmental Sciences, Boston College, Chestnut Hill, MA, USA
d - Corning Inc. retired.
e - Department of Earth and Planetary Science, Rutgers University, Piscataway, NJ, USA
f - Department of Earth and Atmospheric Sciences, Cornell University, Ithaca, NY, USA
g - Department of Earth Science, University of California Santa Barbara, Santa Barbara, CA, USA
h - Université Paris Cité, Institut de Physique du Globe de Paris, CNRS, F-75005 Paris, France

email addresses for authors:
Richard Walker: rjwalker@umd.edu
Andrea Mundl-Petermeier: andrea.mundl@univie.ac.at
Igor Puchtel: puchtel@umd.edu
Robert Nicklas: nicklasr@bc.edu
Jan Hellmann: hellmann@umd.edu
Lina Echeverría: lina.echeverria2@gmail.com
Kyle Ludwig: kyle.ludwig.kl@gmail.com
Katherine Bermingham: kb1012@eps.rutgers.edu
Esteban Gazel: egazel@cornell.edu
Charlotte L. Devitre: cld243@cornell.edu
Matthew G. Jackson: jackson@geol.ucsb.edu
Catherine Chauvel: chauvel@ipgp.fr

Corresponding Author: Richard J. Walker: rjwalker@umd.edu

Submitted to *Geochimica et Cosmochimica Acta* June 28, 2023

October 20, 2023 Revision

Abstract

Major and trace element abundances, including highly siderophile elements, and ^{187}Os and ^{182}W isotopic compositions were determined for *ca*. 89 Ma mafic and ultramafic rocks from the islands of Gorgona (Colombia) and Curaçao (Dutch Caribbean). The volcanic systems of both islands were likely associated with a mantle plume that generated the Caribbean Large Igneous Province. The major and lithophile trace element characteristics of the rocks examined are consistent with the results of prior studies, and indicate derivation from both a chemically highly-depleted mantle component, and an enriched, or less highly-depleted mantle component. Highly siderophile element abundances for these rocks are generally similar to rocks with comparable MgO globally, indicating that the major source components were not substantially enriched or depleted in these elements. Rhenium-Os isotopic systematics of most rocks of both islands indicate derivation from a mantle source with an initial $^{187}Os/^{188}Os$ ratio between that of the contemporaneous average depleted mid-ocean ridge mantle and bulk silicate Earth. The composition may reflect either an average lower mantle signature, or global-scale Os isotopic heterogeneity in the upper mantle. Some of the basalts, as well as two of the komatiites, are characterized by calculated initial $^{187}Os/^{188}Os$ ratios 10-15% higher than the chondritic reference. These more radiogenic Os isotopic compositions do not correlate with major or trace element systematics, and indicate a mantle source component that was most likely produced by either sulfide metasomatism or ancient Re/Os fractionation. Tungsten-182 isotopic compositions measured for rocks from both islands are characterized by variable $\mu^{182}W$ values ranging from modern bulk silicate Earth-like to strongly negative values. The $\mu^{182}W$ values do not correlate with major/trace element abundances or initial $^{187}Os/^{188}Os$ compositions. As with some modern ocean island basalt systems, however, the lowest $\mu^{182}W$ value (-53) measured, for a Gorgona olivine

gabbro, corresponds with the highest $^{3}He/^{4}He$ previously measured from the suite (15.8 R/R_A). Given the lack of correlation with other chemical/isotopic compositions, the mantle component characterized by negative $\mu^{182}W$ and possibly high $^{3}He/^{4}He$ is most parsimoniously explained to have formed as a result of isotopic equilibration between the mantle and core at the core-mantle boundary.

Keywords: Tungsten-182, Osmium-187, highly siderophile elements, Gorgona Island, Curaçao

1. Introduction

The Caribbean Large Igneous Province (CLIP), also referred to as the Cretaceous Caribbean Plateau and the Caribbean–Colombian Oceanic Plateau, is characterized by the spatial association of various Cretaceous mafic-ultramafic rocks, including those present in Colombia, Ecuador, Costa Rica, Panama, and several Caribbean islands. It has been suggested that the Galápagos hotspot represents the current manifestation of the mantle plume that generated the CLIP (e.g., Sen et al., 1988; Sinton et al., 1998; Hauff et al., 2000; Madrigal et al., 2016; Gazel et al., 2018; Dürkefälden et al., 2019a). The processes leading to the chemical and isotopic heterogeneities observed in rocks of the CLIP have been vigorously debated (e.g., Sinton et al., 1998; Révillon et al., 1999, 2000, 2002; Kerr et al., 2002), and are further examined here.

Mafic-ultramafic rocks present on the islands of Gorgona (Colombia) and Curaçao (Dutch Caribbean) include komatiites, peridotites, picrites, gabbros and basalts (**Fig. 1**). These rocks have been interpreted by some studies to be early-stage products of the putative mantle plume that generated the CLIP (e.g., Duncan and Hargraves, 1984; Kerr et al., 1996a-b), although arguments for the generation of the Gorgona rocks from a different plume have also been advanced (e.g., Thompson et al., 2003; Hoernle et al., 2004; Kerr, 2005). Based on broadly similar chemical and isotopic compositions and ages, it is assumed here that the igneous rocks of Gorgona and Curaçao tapped the same or closely spatially associated mantle sources. The diversity of rock types, including komatiites on Gorgona, make these two islands particularly valuable for teaming lithophile and siderophile geochemical tracers for constraining the large-scale processes involved in generating the CLIP.

For the present study, rocks from Gorgona and Curaçao were examined for chemical and isotopic compositions with a focus on siderophile element concentrations and isotopic

compositions (^{182}W and ^{187}Os). The ^{182}Hf→^{182}W short-lived isotope system ($t_{½}$ of ^{182}Hf = 8.9 Myr; Vockenhuber et al., 2004) was live during only the first ~ 60 Myr of Solar System history. It is of particular interest here because heterogeneities in ^{182}W/^{184}W ratios observed in modern plume-derived systems have been variably attributed to large-scale global processes, including early-Earth silicate fractionation and core-mantle interactions (Mundl et al., 2017; Rizo et al., 2019; Mundl-Petermeier et al., 2020; Tusch et al., 2022; Archer et al., 2023). Such processes would likely have led to collateral effects with respect to absolute and relative abundances of some trace elements, especially the highly siderophile elements (HSE: including Os, Ir, Ru, Pt, Pd, Re), and consequently ^{187}Os, the decay product of ^{187}Re ($t_{½}$ = 42 Ga).

The relative youth of the Cretaceous Gorgona and Curaçao rocks, and the probable genetic overlap between certain mafic and ultramafic rocks on the two islands, provide a rare opportunity to link lithophile and siderophile elemental/isotopic tracers in order to discriminate among the possible processes associated with the CLIP plume. High MgO rocks such as komatiites, peridotites and picrites are superior for constraining the HSE abundances and ^{187}Os characteristics of their mantle sources. Such rocks are normally produced by higher degrees of partial melting of mantle lithologies than mafic rocks, which leads to the removal of most host phases of HSE (e.g., sulfides, alloys) from the mantle residue into the melt. This means that the abundances of certain HSE present in the crystallization products of high MgO melts may be broadly similar to their abundances in their mantle source (e.g., Puchtel et al., 2009). Further, characteristically low Re/Os ratios in such rocks mean that age corrections used to calculate initial ^{187}Os/^{188}Os ratios are typically minor. By contrast, mafic rocks such as basalts, are more advantageous for characterizing the ^{182}W and lithophile element characteristics of their mantle sources. This is because their typically considerably higher concentrations of incompatible trace elements, including W, make

them less likely to be strongly modified by lithospheric contamination. Such rocks, however, tend to have lower, more highly fractionated abundances of HSE, which makes them problematic for precisely constraining HSE abundances in their mantle sources. In addition, except for relatively young rocks, the typically high Re/Os ratios of mafic rocks require significant age corrections, leading to larger uncertainties in calculated initial $^{187}Os/^{188}Os$ ratios.

No prior studies have examined ^{182}W in rocks from the CLIP, although Mundl-Petermeier et al. (2020) reported anomalous $\mu^{182}W$ values for some Galápagos lavas as low as -22 (where $\mu^{182}W$ refers to the parts per million deviation in $^{182}W/^{184}W$ ratio relative to laboratory standards believed to reflect the isotopic composition of the Bulk Silicate Earth; BSE). Consequently, a major objective of this study is to compare ^{182}W isotopic data with HSE concentration and ^{187}Os isotopic data, as well as with lithophile trace element data and published data for a long-lived radiogenic isotopic system comprised of lithophile elements ($^{147}Sm \rightarrow ^{143}Nd$). In addition, the results obtained for these rocks may also be relevant for improving understanding of modern OIB systems with variable ^{182}W compositions.

2. Overview of Gorgona and Curaçao rocks

2.1. Age of the rocks

While there is general agreement that the dominant period of volcanism on Gorgona, Curaçao, and other CLIP locales was late Cretaceous, some variations in radiometric ages suggest either an extended period of volcanism, or possibly two or more discrete stages of volcanism. Several studies utilizing ^{40}Ar-^{39}Ar systematics reported ages for CLIP rocks, including for Gorgona and Curaçao, of ~89 Ma (e.g., Kerr et al., 1997; Sinton et al., 1998; Alvarado et al., 1997; Kerr et al., 2002). Walker et al. (1999) reported similar Re-Os isochron ages for Gorgona and Curaçao basalts

of 89.2 ± 5.2 Ma and 85.6 ± 8.1 Ma, respectively. Other studies utilizing ^{40}Ar-^{39}Ar have reported ages of CLIP volcanic rocks ranging from 99 Ma to as young as ~ 71 Ma (e.g., Hauff et al., 2000; Serrano et al., 2011; Dürkefälden et al., 2019a-b).

2.2. Characteristics of Gorgona rocks

Located ~ 35 km off the Pacific coast of Colombia (**Fig. 1**), Gorgona Island has been of special interest to petrologists since the discovery that it hosts Cretaceous komatiites (Gansser et al., 1979; Echeverría, 1980). These are the youngest known *bona fide* komatiites with spinifex textures. Studies of melt inclusions and host liquidus olivines have reported that the parental magmas of the komatiites contained < 0.9 wt. % H_2O and ~ 19 wt. % MgO (Révillon et al., 2000; Shimizu et al., 2009; Gurenko et al., 2016; Nicklas et al., 2019), implying that the komatiites were likely generated from anomalously hot and relatively dry mantle. In addition to the famous, heavily-studied Gorgona komatiites, other lithologies of the ~ 8 × 2.5 km Gorgona Island include gabbros, picrites and picritic tuff breccias, cumulate peridotites (wehrlites and dunites) and basalts. The Gorgona samples can be classified into two categories based on incompatible trace element patterns. The komatiites and picrites, as well as most of the gabbros and some of the peridotites and basalts, are strongly depleted in incompatible lithophile trace elements relative to the BSE (**Fig. S1**; e.g., Echeverría, 1980; Echeverría and Aitken, 1986; Révillon et al., 2000; Thompson et al., 2003; Kerr, 2005; Serrano et al., 2011). Other basalts, peridotites and gabbros, however, are characterized by minimal depletions and/or enrichments in incompatible lithophile trace elements relative to BSE (e.g., Aitken and Echeverría, 1984). These rocks have been interpreted to be derived from a mantle domain enriched in recycled crustal components (e.g., Arndt et al., 1997; Hauff et al., 2000; Révillon et al., 2002; Kerr 2005). Some prior studies have referred to the

chemically depleted and enriched basalts as D-type and E-type, respectively (Kerr et al., 1996a). This terminology will continue to be used here for the Gorgona samples.

The chemical differences among Gorgona rocks are complemented by a plethora of initial isotopic compositions of the long-lived radiogenic Sm-Nd, Rb-Sr, Lu-Hf, U-Th-Pb, Re-Os and Pt-Os systems (e.g., Echeverría, 1980; Aitken and Echeverría, 1984; Dupré and Echeverría, 1984; Walker et al., 1991; 1999; Révillon et al., 2000, 2002; Brandon et al., 2003; Thompson et al., 2003). Most Gorgona komatiites, picrites, peridotites, gabbros, and certain D-basalts are characterized by $^{143}Nd/^{144}Nd$, $^{176}Hf/^{177}Hf$ and Pb isotopic ratios that are similar to Pacific MORB, with initial εNd and εHf values (where ε values refer to the parts per 10,000 deviation in the $^{143}Nd/^{144}Nd$ and $^{176}Hf/^{177}Hf$ ratios relative to a chondritic reference at 89 Ma) ranging from ~ +8 to +12 (**Fig. 2**), and +15 to +18, respectively, and $^{206}Pb/^{204}Pb$ ratios ranging from ~ 18.3 to 19.0.

The isotopic compositions of the relatively chemically enriched Gorgona E-basalts are more similar to some ocean island basalts (OIB). These rocks are characterized by lower εNd and εHf values, and more radiogenic Pb, compared with the more chemically depleted Gorgona rocks and Pacific MORB (Echeverría, 1980; Aitken and Echeverría, 1984; Dupré and Echeverría, 1984; Arndt et al., 1997; Révillon et al., 2000; Thompson et al., 2003). Although chemically enriched relative to D-basalts, these rocks retain isotopic signatures of long-term chemical depletion relative to BSE, with initial εNd values ranging from ~ +5 to +8 (**Fig. 2**), initial εHf values averaging ~ +13, and $^{206}Pb/^{204}Pb$ ratios ranging from ~ 19.4 to 19.8 (Dupré and Echeverría, 1984; Thompson et al., 2003). Révillon et al. (2002) reported He isotopic data for three rocks, with $^{3}He/^{4}He$ ratios (R/R_A) ranging from 8.6 to 15.8 (where R/R_A refers to the $^{3}He/^{4}He$ ratio of a sample relative to the ratio in the present-day atmosphere). Hyung et al. (2023) reported $^{3}He/^{4}He$ ratios for Gorgona rocks ranging from 4.6 to as high as 39.5 in a whole rock sample.

Previously reported initial $^{187}Os/^{188}Os$ ratios of most komatiites and D-basalts are essentially uniform, with initial $\gamma^{187}Os$ values (where $\gamma^{187}Os$ is the percent difference between the $^{187}Os/^{188}Os$ of the sample and a chondritic reference calculated at 89 Ma) ranging between ~ 0 and +2, and averaging ~ +1 (Walker et al., 1991; 1999). Walker et al. (1999), however, reported that several komatiites and E-basalts are characterized by significantly more radiogenic initial $^{187}Os/^{188}Os$ ratios, with $\gamma^{187}Os$ values > +10. Further, Brandon et al. (2003) reported a correlation between initial $^{187}Os/^{188}Os$ and $^{186}Os/^{188}Os$ ratios, where ^{186}Os is the daughter product of the very long-lived ^{190}Pt ($t_{½}$ = 460 Ga). These authors suggested that the correlation resulted from mixing between mantle and an outer core component presumed to have high $^{187,186}Os/^{188}Os$.

2.3. Characteristics of Curaçao rocks

Most of the island of Curaçao, located ~ 70 km off the coast of Venezuela (**Fig. 1**), is composed of a volcanic succession that is at least 5 km thick (Klaver, 1987; Kerr et al., 1996b). The lavas exposed on the ~ 61 × 15 km island tend to be more evolved towards the top of the succession, with compositions varying from picrites lower in the sequence, to tholeiitic basalts toward the top. The modeling of Kerr et al. (1996b) led to the conclusion that the picrites and basalts can be related to a common magma by fractional crystallization involving olivine as the main liquidus phase.

The reported chemical and isotopic compositions of rocks from Curaçao are generally less-varied than for Gorgona. Basalts and picrites are enriched in incompatible lithophile trace elements compared to the D-type Gorgona rocks, and are only slightly less enriched than Gorgona E-basalts (**Fig. S1**). Prior studies have reported initial εNd values for Curaçao basalts and picrites that range from + 5.7 to +8.8, with most samples ranging only from ~ +6.5 to +7.5 (**Fig. 2**)(Kerr et al., 1996b;

Révillon et al., 1999; Hauff et al., 2000). Hence, the majority of basalts and picrites have long-term Sm-Nd isotopic systematics which, like the trace element abundances, are similar to the Gorgona E-basalts. Initial $^{187}Os/^{188}Os$ ratios for picrites, calculated for 89 Ma, are generally uniform with an average $\gamma^{187}Os$ value of +0.1 ± 1.1 (2SD) (Walker et al., 1999).

In general, for the entire CLIP system, indicators of lithophile trace element enrichment/depletion tend to correlate with long-lived lithophile radiogenic isotope systems. This is consistent with the long-term survival of chemical heterogeneities in the mantle sources of these rocks. For example, a compilation of Sm-Nd isotopic data from the literature for a variety of rocks comprising the CLIP shows that $^{147}Sm/^{144}Nd$ ratios are broadly positively correlated with initial εNd values (**Fig. 2**).

3. Samples

Sample locations from the islands of Gorgona and Curaçao are shown in **Fig. 1**. The GPS coordinates for sample collection sites, where available, are provided in **Table S1**. Most Gorgona samples examined here were collected on the island during a 2019 field trip. These samples are identified by the 19GOR-x notation. Sample GOR-1901 was also collected at this time. Some of the Gorgona Island samples analyzed for this study were obtained from the Smithsonian Institution, National Museum of Natural History. These rocks were originally collected by L.M. Echeverría during field work on the island in 1980 and 1981. Samples GOR152 through GOR160 come from the eastern-central coast of the island in the vicinity of "Punta Trinidad", whereas samples GOR23A, GOR23B, GOR47, and PC-5 were collected as float from the southwestern shore of the island (Echeverría, 1980). Samples GOR537 through GOR540 were collected from the beach at the "La Mancura" locale by S. Révillon and N.T. Arndt during a subsequent trip to

the island in the 1990's, and provided by N.T. Arndt (University of Grenoble). Two samples with elevated $^{3}He/^{4}He$ from the study of Révillon et al. (2002) (wehrlite GOR507 and olivine gabbro GOR509) were collected from the "Huanchinche" locality from the northwestern side of the island during the same 1990's trip. Dunite GOR503 with upper mantle-like $^{3}He/^{4}He$ was collected from the same site, while olivine gabbro GOR535 was collected from the Punta Trinidad site. Petrographic and compositional details regarding these samples can be found in Révillon et al. (2000).

The Gorgona samples are petrologically divided into komatiites, cumulate peridotites, picrites (and picritic tuffs), gabbros and basalts. As a result of their high MgO contents, wehrlite GOR507 and olivine gabbros GOR509 and 535 are grouped here as "peridotites". Sample 19GOR-8 is an unusual rock primarily consisting of olivine, clinopyroxene, and minor plagioclase. It is classified here as a plagioclase-bearing peridotite, and also grouped with the peridotites due to its high MgO abundance.

Finally, samples of picrite and basalt from Curaçao were collected during field trips to the island in 2013.

4. Analytical Methods

Samples were chemically and isotopically analyzed using previously described techniques. Detailed information regarding these techniques, including uncertainties, is provided in the **supplementary materials**. In brief, major and minor element abundances for most samples were obtained by X-ray fluorescence (XRF) analysis at Franklin and Marshall College, Lancaster, PA, USA. The abundances of lithophile trace elements in the whole-rock samples were determined at either the University of Maryland (UMd) using the standard addition inductively-coupled plasma

mass spectrometry (SA ICP-MS) method, or at Scripps Institution of Oceanography (SIO) using the standard-sample bracketing ICP-MS method following the protocols detailed in Puchtel et al. (2016) and Nicklas et al. (2018). One sample from Curaçao (CUR13-6) was analyzed for major and minor elements at Washington State University using XRF (see **supplementary materials** for details). Rocks standards data for major and trace elements are provided in **Table S2**.

Methods for determining HSE abundances and Os isotope ratios were described in Haller et al. (2021). In brief, approximately 2 g aliquots of whole-rock powders, appropriate quantities of isotopic spikes, and concentrated HCl and HNO_3 were sealed in *Pyrex* Carius tubes and heated to 270°C for ~72 hr. Osmium was extracted from the acid solution by CCl_4 solvent extraction (Cohen and Waters, 1996), then back-extracted into concentrated HBr and purified via micro-distillation using a method described by Birck et al. (1997). Osmium analysis was achieved using negative thermal ionization mass spectrometry (N-TIMS). Iridium, Ru, Pt, Pd, and Re were separated and purified using anion exchange chromatography modified after Rehkämper and Halliday (1997), then measured by multi-collector-ICP-MS (MC-ICP-MS). Average total analytical blanks during the analytical campaign were (in pg) for Os, Ir, Ru, Pt, Pd and Re: 0.8, 0.9, 2.8, 95, 6.4 and 1.1, respectively (n = 9). Blank corrections were negligible for most measurements. Estimated uncertainties for the concentration measurements of Ru, Pt, and Pd were ± 2%, ± 0.5% for Ir, ± 0.3% for Re and ± 0.1% for Os concentration. Uncertainty for $^{187}Re/^{188}Os$ is estimated to be ± 0.5%. Repeated analyses of $^{187}Os/^{188}Os$ in the UMd laboratory standard averaged ± 0.1% 2SD. Analytical uncertainties for $\gamma^{187}Os$ calculations for samples with $^{187}Re/^{188}Os < 10$ are therefore estimated to be ≤ 0.3 units (%). The effect of analytical uncertainties on $\gamma^{187}Os$ calculations are greater and more variable for samples with $^{187}Re/^{188}Os > 10$.

For ^{182}W analysis, between 20 and 85 grams of sample powder (based on W concentrations determined for the rocks), were digested in up to 500 mL of a mixture of HF:HNO_3 5:1 for five days at 145°C. The main dry down was followed by dissolution and repeated dry downs in 8M HCl to convert the samples into chloride form. Tungsten was separated and purified following a multi-step ion-exchange chromatography method described in Peters et al. (2019). During the final purification step, approximately 200 µL of a pre-filter resin (100-150 µm, *Triskem*) was added to the bottom of the column to remove organics. The final eluent was dried down and repeatedly treated with a mixture of concentrated HNO_3:HCl:H_2O_2 in the proportions 4:2:1 to remove the remaining organic residue before analysis. For isotopic analysis of most samples, approximately 700 to 1000 ng of W were dried onto a pure Re filament and coated with a electron emitter solution consisting of 15 µg La and 5 µg Gd. Tungsten isotope compositions were measured by N-TIMS using a *Thermo Fisher Triton* at the UMd and the Department of Lithospheric Research, University of Vienna (DLR), as well as a *Triton XT* thermal ionization mass spectrometer, also at the DLR, following slightly modified methods described in Archer et al. (2017) and Mundl-Petermeier et al., 2022). Samples for which < 500 ng of W were extracted (GOR-503, GOR-507, GOR-509; GOR-535) were analyzed using a *Neptune Plus* MC-ICP-MS at UMd (see **supplementary materials** for additional details regarding these analyses).

5. Results

5.1. General geochemical characteristics

Major, minor, and lithophile trace element concentration data for whole-rock samples from Gorgona Island and Curaçao are provided in **Table S1**. The major element data are re-calculated for loss on ignition (LOI). Major element concentrations for Gorgona rocks are in good agreement

with previously published data for instances where new and old data are available for the same rocks. Elements that are in lower concentrations, however, such as the alkalis and REE, vary by as much as ~50% between the new results and the literature values. For example, REE abundances are reported in the literature for samples GOR537, 538 and 539 (Révillon et al., 2000), GOR156 (Aitken and Echeverría, 1984) and GOR47 (Echeverría, 1980). Our REE concentrations agree with the literature values to within ~20%, whereas the La/Sm and Gd/Yb ratios replicate the literature values to within ~10%. The offsets between our new data and the literature data may reflect variations in chemical composition between separate pieces of rock processed for powders in the different studies.

The chemical trends revealed by the Gorgona suite are similar to those previously observed for other mafic-ultramafic suites (e.g., Puchtel et al., 1998; Puchtel and Humayun, 2001). For example, concentrations of the highly incompatible lithophile trace elements such as La, Nb and Th, are negatively correlated with MgO for most rocks of the Gorgona suite (**Fig. S2a-c**). The discrimination of Gorgona samples between D- and E- chemical types is achieved here through examination of REE patterns (e.g., Aitken and Echeverría, 1984). Bulk silicate Earth-normalized REE patterns for most rocks from Gorgona are characterized by strong depletions in the light REE (LREE), consistent with the D-type designation (**Figs. 3a-f**). Of the peridotitic rocks, wehrlite sample GOR507 and olivine gabbro sample GOR509 are the most strongly depleted in LREE. Conversely, four basalts (GOR23A, 19GOR22, 23 and 24), four peridotites (19GOR-7, 8, 13 and GOR535), and one gabbro (19GOR-19) are characterized by generally flat BSE-normalized REE patterns with comparatively high La/Sm (> 1) relative to the other rocks (**Fig. S2d**). Consequently, these nine rocks are considered to belong to the E-type.

It is important to note that the E- and D- type chemical designations do not necessarily reflect long-term chemical enrichment or depletion. For example, olivine gabbro sample GOR509 is characterized by strong depletion in LREE (**Fig. 3b**), yet Révillon et al. (2000) reported an initial εNd value of +6.6 for this sample, indicating long-term Sm/Nd similar to the E-type basalts. Sample GOR507 is similarly depleted in LREE, but has a significantly higher initial εNd value of +8.9 (Révillon et al., 2000).

Because of the more limited range of isotopic heterogeneity in rocks from Curaçao, as well as the extensive prior Re-Os isotopic analyses of these rocks (Walker et al., 1999), only five additional samples from Curaçao were examined here. The three picrites analyzed are characterized by > 20 wt. % MgO. In contrast to the Gorgona picrites and picritic tuffs, these picrites have relatively flat REE patterns and all have La/Sm ratios > 1 (**Fig. 3g; Fig. S2d**). The two basalts analyzed are typical Curaçao olivine tholeiites. Similar to the picrites, they are also enriched in La and Nb relative to most rocks of the Gorgona suite, and are comparable to the Gorgona E-type rocks in the degree of relative chemical enrichment (**Fig. S2a-b**).

5.2. Highly siderophile elements

Highly siderophile element concentrations and Re-Os isotopic data for the samples from Gorgona Island and Curaçao are provided in **Table 1**. Concentrations are reported as measured and not corrected for LOI. Loss on ignition corrected concentrations are provided in **Table S3**. The abundances of some HSE in samples GOR156, GOR159 and GOR160 were previously reported by Brügmann et al. (1987). The Os, Ir, Ru and Pd abundances measured in our samples are ~ 30 to 50% greater than those previously reported, most likely due to either differences in the digestion and chemical separation methods utilized, or sample heterogeneity. Relative abundances

of the elements, however, remain constant to within ± 10% between samples in this study, compared to prior work.

As is common for terrestrial igneous rocks, plots of MgO versus Os, Ir, and Ru for all Gorgona-Curaçao samples define diffuse inverse "J-shaped" arrays with highest concentrations in the higher MgO rocks, and lower concentrations with considerable variations in all three elements at the low-MgO end of the array (**Fig. 4a-c**). Abundances of Pt, Pd, and Re for most komatiite and peridotite samples plot along negatively sloping trends relative to MgO, with varying degrees of scatter (**Fig. 4d-f**). Abundance variations of Pt and Pd are modest, with nearly all samples having concentrations within a range of a factor of 10. The range of Re concentrations is higher than for Pt and Pd, with the highest MgO samples having the lowest Re concentrations.

The BSE normalized HSE patterns for the komatiites, peridotites, gabbros and basalts (**Fig. 5a-f**; normalizing values from Becker et al., 2006) are similar to patterns for rocks with comparable MgO worldwide (e.g., Walker, 2016). All Gorgona komatiites are enriched in Pt, Pd, and Re relative to BSE. Most peridotites have similar to higher abundances of Pt, Pd and Re, relative to the komatiites, and similar to lower abundances of Os, Ir and Ru. The plagioclase-bearing peridotite sample 19GOR-8 is characterized by a strong enrichment in Ir relative to Os and Ru. Wehrlite sample GOR507 is characterized by a notable depletion in Ir.

Most Gorgona picrites have generally uniform abundances of HSE. Picrite 19GOR-27, however, is characterized by much higher Os and Ir concentrations than the other picrites, while duplicate analyses of picrite 19GOR-11 show strong enrichment in Ir relative to Os and Ru. The magnitude of these enrichments is similar to that observed in the plagioclase-bearing peridotite 19GOR-8, although these rocks have very different major element compositions. These

enrichment spikes suggest the presence of unidentified trace phases that strongly concentrated Ir, and in some instances Os, from the melt.

All of the Gorgona basalts are depleted in Os, Ir, and Ru relative to the BSE, although the D-basalts have generally higher concentrations of these elements than the E-basalts. The incompatible HSE Pt, Pd and Re concentrations, by contrast, are similar to or higher than the abundances present in the komatiites. The Gorgona gabbros tend to have Os, Ir, and Ru concentrations that are intermediate between the komatiites/picrites/peridotites and basalts, and Pt, Pd, and Re concentrations that are similar to most other rocks of the suite. Poikilitic gabbro sample 19GOR-19 is characterized by substantially lower Os, Ir and Ru abundances compared with the other gabbros (**Fig. 5d**). This sample also has the lowest MgO (7.7 wt.%) of all the gabbros examined.

Bulk silicate Earth-normalized HSE patterns for basalts and picrites from Curaçao are generally similar to the patterns defined by Gorgona rocks with comparable MgO (**Fig. 5g**). The basalts are strongly depleted in Os, Ir, and Ru relative to Pt, Pd, and Re. The Curaçao picrites have similar HSE concentrations to the Gorgona komatiites.

5.3. Re-Os isotopic systematics

The new Re-Os isotopic data for the Gorgona rocks are similar to those previously reported in Walker et al. (1999). In **Fig. 6a-b** the Re-Os isotopic data for all Gorgona and Curaçao rocks examined here are plotted along with a "chondritic" reference isochron defined by a $^{187}Os/^{188}Os$ intercept of 0.1264 at 89 Ma, applying the reference parameters of Shirey and Walker (1998). In order to broadly characterize the isotopic systematics of the rocks with comparatively low Re/Os, the isotopic data for the komatiites, peridotites, picrites and gabbros are collectively regressed.

Komatiite basalt sample GOR4P and komatiite samples GOR23B and GOR47 plot significantly above the reference isochron. Poikilitic gabbro sample 19GOR-19 plots significantly below the reference isochron, and compared to the other gabbros is also characterized by an anomalously high $^{187}Re/^{188}Os$ (60.99). Data for these four samples are excluded from the regression calculations. The least squares regression of the remaining samples (n = 53 including duplicate analyses) using ISOPLOT 3.00 (Ludwig, 2003) yields a Model 3 best-fit slope of 0.001520 ± 0.000062 (2σ) (MSWD = 53) and an intercept of 0.12738 ± 0.00023 (2σ; initial $\gamma^{187}Os$ = +0.77 ± 0.19) (**Fig. S3a**). Applying a λ for ^{187}Re = $1.666 \times 10^{-11} yr^{-1}$ (Smoliar et al., 1996), the slope gives an age of 91.2 ± 3.7 Ma.

The regression age is within uncertainty of the 89 Ma age for Gorgona komatiites determined by prior studies using other methods, which is assumed to be the dominant crystallization age for these rocks (e.g., Sinton et al., 1998). The result of this regression, characterized by a high MSWD, should be interpreted with caution given the likelihood of minor isotopic heterogeneity and post-crystallization open-system behavior. Calculated individual initial $\gamma^{187}Os$ values for samples with $^{187}Re/^{188}Os$ ratios < 10, however, are not sensitive to age uncertainties on the order of several Ma. For example, the initial $\gamma^{187}Os$ value calculated for GOR23B, the komatiite with the highest $^{187}Re/^{188}Os$ of 7.264, would vary only from +10.8 to +10.3, applying age corrections of 86 and 92 Myr, respectively. When minor age uncertainty is combined with the analytical uncertainties, individual calculated initial $\gamma^{187}Os$ values for Gorgona komatiites, picrites, peridotites and gabbros (as well as Curaçao picrites), are conservatively estimated to be accurate to ± 0.4 γ units (%).

Accurately determining the initial $\gamma^{187}Os$ values of basaltic samples with $^{187}Re/^{188}Os$ ratios > 10 is more problematic than for the samples with low Re/Os. In addition, exposed contacts between different lithologic units on Gorgona are mainly fault-bounded, and many of the samples collected

are from float. Hence, the temporal relationships between the eruption ages of the relatively well-dated komatiites and the basalts cannot be safely based on field relations. Relatively small deviations from the assumed age for these rocks can lead to moderate differences in calculated initial γ^{187}Os. Further, increasingly higher Re/Os leads to increasingly larger error magnification in the calculation of initial isotopic composition, even when the system closure age is well constrained (e.g., Walker et al., 1994). Consequently, uncertainties for γ^{187}Os in the basaltic rocks are highly variable and are typically substantially larger than for low Re/Os ratio samples. For example, D-basalt 19GOR-16 has a comparatively low $^{187}Re/^{188}Os$ of 41.61. Its initial γ^{187}Os value varies moderately from -1.6 to +1.7 when calculated for 86 and 92 Ma, respectively, equating to a ~ ± 1.6% uncertainty. By comparison, initial γ^{187}Os values for E-basalt 19GOR-23, with a much higher $^{187}Re/^{188}Os$ of 418.8, vary from +38.6 to +5.5 when calculated for ages of 86 and 92 Ma, respectively. Given the age uncertainties for the basalts, as well as the variable $^{187}Re/^{188}Os$, initial γ^{187}Os values for basalts are calculated by combining replicate values where available, and estimating uncertainties by calculating variations between 86 and 92 Ma (**Table 1**). The data for each individual analysis, however, are plotted on the isochron.

Age uncertainties coupled with Re-Os isotopic data present similar issues for some of the Curaçao data. Least squares regression of the two new Re-Os isotopic data points for Curaçao basalts, combined with the basalt data from Walker et al. (1999) (n = 8), gives a Model 3 best fit slope of 0.001445 ± 0.000085 (2σ) (MSWD = 191), equating to an age of 86.7 ± 5.1 Ma, and an intercept of 0.138 ± 0.011 (2σ; initial γ^{187}Os = +9.09 ± 8.7) (**Fig. S3b**). When the new data for the picrites, as well as the picrite data from Walker et al. (1999) are incorporated into the regression (n = 19) a slope of 0.001511 ± 0.000037 (MSWD = 492), equivalent to an age of 90.6 ± 2.2 Ma, with an intercept of 0.1283±0.0032 is obtained (2σ; initial γ^{187}Os = +1.4 ± 2.6) (**Fig. S3c**). As with

the Gorgona regression, these regressions for the Curaçao rocks are problematic to equate to precise and accurate age and intercept values, given the previously reported strong evidence for variance in initial γ^{187}Os among the rocks included in both regressions. Walker et al. (1999) noted the substantial elevation of initial γ^{187}Os values for most Curaçao basalts compared with the picrites. Regardless, the resulting isochron ages for the Curaçao rocks, as with the Gorgona rocks, are generally consistent with the presumed 89 Ma emplacement age.

Initial γ^{187}Os values (calculated for 89 Ma) for all Gorgona and Curaçao rocks are plotted versus MgO in **Fig. 7**. Komatiite samples GOR23B and GOR47 plot more than 10% above the chondritic reference isochron, consistent with the results previously reported for these samples (Walker et al., 1991; 1999), three of the four E-basalts analyzed also plot significantly above the reference isochron, if a crystallization age of 89 Ma is assumed and the results for duplicate analyses are averaged.

The initial γ^{187}Os values for the three Curaçao picrites and one basalt (CUR-09) average +0.4, which overlaps within uncertainties of the intercept value for the Gorgona suite. This value is consistent with the average value of +0.1 previously reported for a larger number of picrite samples from Curaçao (Walker et al., 1999). Of note, basalt sample CUR13-6 has an initial γ^{187}Os value of +12.5, assuming a crystallization age at 89 Ma. This value is also comparable to the values reported for five Curaçao basalts in Walker et al. (1999) and likely reflects an enrichment of ^{187}Os in basalt CUR13-6 relative to the picrites.

5.4. ^{182}W isotopic systematics

The μ^{182}W values of the Gorgona suite range from +1.1 ± 4.5 for D-basalt 19GOR-25, to –53.1 ± 12.6 for the olivine gabbro GOR509 (**Table 1**) and are plotted versus initial γ^{187}Os values

in **Fig. 8**. The ^{182}W data do not correlate with groups related to lithophile or siderophile element characteristics. For example, although two D-basalts, one komatiite and one peridotite, all with strong LREE depletion, lack ^{182}W anomalies, other samples with depleted lithophile trace element characteristics (e.g., gabbro 19GOR-17; picrite 19GOR-10; olivine gabbro GOR509) are characterized by having negative anomalies. On the other hand, two of the three E-basalts, as well as gabbro 19GOR-19, all characterized as having La/Sm > 1, have small to moderate negative anomalies.

In addition to the large negative $\mu^{182}W$ value, olivine gabbro GOR509 is also characterized by elevated $^{3}He/^{4}He$ (with R/R_A averaging 15.8 ±4.1 2SD; Révillon et al., 2002). The $\mu^{182}W$ value for this sample is the largest negative anomaly yet reported for terrestrial rocks. This value was confirmed through the analysis of two aliquots of powder processed separately through chemistry coupled with 4 separate mass spectrometric analyses (**Table S4**). Dunite GOR503 and wehrlite GOR507, the Gorgona samples characterized by minimal to moderately elevated $^{3}He/^{4}He$, with R/R_A averaging 8.6 ± 1.6 and 12.7 ± 0.7, respectively, also have negative $\mu^{182}W$ values of -22.0 ± 14.2 and -18.8 ± 14.2, respectively. The uncertainties in $\mu^{182}W$ values for these rocks are larger than for other rocks because of the limited masses of the samples available for the analysis, combined with low W concentrations.

The $\mu^{182}W$ values for Curaçao rocks are also plotted versus $\gamma^{187}Os$ in **Fig. 8**. Of the 2 basalts and 3 picrites analyzed for $\mu^{182}W$, all are characterized by well-resolved negative anomalies, except for basalt sample CUR-09 which is lacking an anomaly with a $\mu^{182}W$ value of -0.9 ± 3.7. The three picrites have nearly identical $\mu^{182}W$ values that average -8.8 ± 1.6 (2SD). These results indicate that several of the rocks sampled from each island have negative $\mu^{182}W$ values that are well resolved from the *Alfa Aesar* laboratory standard.

6. Discussion

6.1. Chemical compositions

The major and lithophile trace element data for the Gorgona suite examined here are similar to those reported by prior studies. As concluded by earlier studies, these compositions are consistent with contributions from both chemically depleted and enriched, or less depleted mantle source components and discussed in the **supplementary materials**.

The absolute and relative abundances of HSE in the Gorgona and Curaçao suites are comparable to global data reported for both ancient and young rocks spanning similar major element compositions (e.g., MgO). With the exception of several of the Gorgona picrites that are strongly depleted in Re relative to the BSE estimates of Becker et al. (2006) and Fisher-Gödde et al. (2011), concentrations of Pt, Pd and Re in Gorgona and Curaçao suite rocks are similar to or moderately enriched relative to the BSE. The abundances of these elements are consistent with the observation that in mantle rocks these elements are primarily hosted by interstitial base metal sulfides that tend to be removed into the melt during relatively low degrees of partial melting of the mantle, and therefore, behave incompatibly (e.g., Barnes et al., 1985; Keays, 1995; Alard et al., 2000; Pearson, 2004; Bockrath et al., 2004). The abundances of Os, Ir and Ru in most of the Gorgona and Curaçao suite rocks are similar to or depleted relative to BSE abundances. This likely reflects the partial retention of these elements in refractory sulfides and alloys that tend to be sited within mantle silicates, and thus, are shielded from the immediate effects of partial melting of mantle rocks (e.g., Alard et al., 2000; Fonseca et al., 2012). Similar processes have been suggested to control HSE behavior during generalized mantle melting and crystallization scenarios (e.g., Barnes et al., 1985; Rehkämper et al., 1999; Brenan and Andrews, 2001; Pearson et al., 2004).

Precambrian komatiites, such as the 2.7 Ga Tony's Flow komatiite, Belingwe, southern Africa (Puchtel et al., 2009) and the 2.0 Ga Kevitsa and Jeesiörova komatiites, Finnish Lapland (Puchtel et al., 2020), are typified by well-defined linear trends between MgO or Ni and HSE. The trends are consistent with the compatibility/incompatibility of the HSE during crystal-liquid fractionation. For Gorgona komatiites and cumulate peridotites, only plots of MgO versus Pt, Pd and Re define negative trends, consistent with incompatible behavior with the fractionating mineral assemblage (olivine ± chromite) (**Fig. S4 a-f**). By contrast, no correlations are observed between Ni and the HSE abundances (**Fig. S5 a-f**). In comparison to the Archean systems, the lack of correlation and the more limited correlations for Gorgona samples could indicate minor redistribution of HSE subsequent to crystallization, but more likely reflects variable co-precipitation of HSE-bearing trace phases accompanying olivine precipitation. It also likely reflects the less extensive differentiation present in Gorgona komatiite flows compared with typical Precambrian komatiites (Echeverría, 1980).

In addition to olivine, chromite crystallization has been shown to fractionate some HSE, especially Ru, in komatiitic systems with <24 wt.% MgO (e.g., Barnes, 1998; Puchtel and Humayun, 2001; Locmelis et al., 2011). Chromite control appears to have been negligible on all HSE abundances for the komatiites and peridotites, except for Ru, which is characterized by a weak positive correlation with Cr (**Fig. S6a-f**). The correlation suggests preferential incorporation of Ru in crystallizing chromite, or trace phases that co-precipitated with chromite. The presence of small equant chromite grains in some of the komatiite samples is consistent with this interpretation.

The generally linear correlations between MgO versus Pt, Pd and Re means the concentrations of these elements in the dominant Gorgona komatiite source can be determined through projections

of the trends to an assumed source MgO concentration (**Fig. S7a-c**). Details regarding this calculation and an estimation of the concentrations of most HSE present in the dominant Gorgona komatiite source are provided in the **supplementary materials**. The comparatively flat BSE normalized HSE pattern of the inferred mantle source of the dominant Gorgona komatiites (**Fig. S8**) is well within the range of modern abyssal peridotites. This suggests that prior to the generation of the komatiites, the mantle source of the dominant Gorgona komatiites had not experienced melting events sufficient to significantly deplete or fractionate HSE, relative to the DMM or the BSE. Thus, the low degree partial melting that Arndt et al. (1997) inferred to have resulted in an initial depletion of incompatible lithophile trace elements prior to komatiite generation, evidently did not significantly affect the HSE. The inferred HSE abundances of the dominant komatiite source also effectively rule out significant direct contamination by outer core metal, as suggested by some prior studies (Brandon et al., 2003). Such a contribution would lead to substantially higher HSE abundances in the source. For example, a 1% addition of outer core metal (~ 1100 ppb Os) to ambient mantle (~ 3.5 ppb Os) would lead to a nearly fourfold increase in HSE abundances in the contaminated mantle material. In addition to the komatiites, these conclusions are likely valid for the petrogenetically related peridotites and gabbros.

Given the fractionated nature of HSE in the picrites, basalts, and the two komatiites with elevated γ^{187}Os from the Gorgona-Curaçao suite, comparable high-fidelity inferences regarding the HSE abundances in the mantle sources of these rocks cannot currently be made. As noted above, however, Pt and Pd abundances in these rocks are generally similar to BSE, displaying no evidence of significant overall depletions or enrichments of HSE in their mantle sources. This provides evidence that the mantle sources of these rocks also contained abundances of HSE broadly similar to those of the DMM.

Overall the new chemical results support the prior conclusions that two or more chemically distinct mantle source components contributed to the Gorgona-Curaçao suite. At least one source component was strongly depleted in incompatible trace elements, and the chemically enriched component was similar to the sources of some OIB. The HSE data suggest that the mantle sources were neither strongly enriched nor depleted in HSE relative to the upper mantle.

6.2. ^{187}Re-^{187}Os isotopic systematics

The average initial $\gamma^{187}Os$ value of +0.8 for the Gorgona suite, derived from the regression of the ultramafic rock data is a minimum of ~ 1% lower than estimates for BSE at 89 Ma (BSE = $\gamma^{187}Os \geq +2.0$; Meisel et al., 2001), but also nearly 3% higher than estimates for average DMM at 89 Ma (DMM= $\gamma^{187}Os = -1.9$; Snow and Reisberg, 1995; Brandon et al., 2000; Day et al., 2017) (**Fig. 6a**). Hence, the Os isotopic composition of the source of most of the Gorgona komatiites, peridotites and picrites is inconsistent with an origin solely from mantle domains with either average DMM or BSE isotopic compositions. The dominant composition could reflect mixing between DMM and an ^{187}Os enriched mantle reservoir, such as recycled oceanic crust (e.g., Walker et al., 1991; Thompson et al., 2003). Alternatively, the combined isotopic data may simply reflect modest heterogeneity in the Os isotopic composition of the DMM, as evidenced by Os isotopic heterogeneity among modern abyssal peridotites (e.g., Day et al., 2017).

The three Curaçao picrites examined here are characterized by a narrow range of initial $\gamma^{187}Os$ values that average 0.0 ± 1.5, essentially identical to the average value of +0.1 ± 1.1 reported for eight picrites by Walker et al. (1999). When all of the Curaçao picrite data are combined (n = 11) the average value of +0.1 ± 1.1 is only slightly less radiogenic than the dominant Gorgona composition, and also ~2% more radiogenic than estimates for the contemporaneous DMM (e.g.,

Walker, 2016). The ^{187}Os isotopic compositions of the dominant lavas on Gorgona and Curaçao, although not identical, are similar. Révillon et al. (1999) reported εNd values ranging from +5.7 to +7.2 for Curaçao picrites, consistent with the evidence for a long-term chemically enriched, or less depleted source, relative to DMM.

Gorgona komatiite samples GOR-23B and GOR-47 are characterized by high positive initial $\gamma^{187}Os$ values of +10.6 and +13.1, respectively. Both komatiites have initial εNd values of +9.8, within the same limited range as the other komatiites which are not characterized by elevated $\gamma^{187}Os$ (Walker et al., 1991). This indicates that Os and Nd isotopes in these rocks are not correlated. Three Gorgona E-basalts, and one Curaçao basalt are also characterized by high positive initial $\gamma^{187}Os$ values, with averages ranging from ~ +12.1 to +17.7, assuming a crystallization age of 89 Ma, albeit subject to uncertainties in their ages. In addition, five Curaçao basalts were reported to also have elevated initial $\gamma^{187}Os$ values ranging from +5.2 to +9.8 in Walker et al. (1999). The high apparent initial $\gamma^{187}Os$ values do not correlate with either lithophile element indicators of chemical enrichment, such as the La/Sm ratio (**Fig. 9a**), or with evidence for a source enriched or depleted in Pt (**Fig. 10a**).

Elevated $\gamma^{187}Os$ observed in some ocean island and flood basalt systems has previously been interpreted to provide evidence for: 1) the long-term presence of high-Re, recycled crust in the source (Walker et al., 1991; Hauri and Hart, 1993), 2) incorporation of material from a lower mantle domain that formed with elevated Re/Os as a result of early silicate-silicate or metal-silicate fractionation processes in a magma ocean (Walker et al., 1994), 3) incorporation of mantle that was modified by some form of core-mantle interaction (Walker et al., 1995; Brandon et al., 2003), or 4) incorporation of mantle that was modified as a result of sulfide metasomatism (Luguet et al., 2008). Detailed consideration of each of these options with respect to the CLIP rocks is provided

in the **supplementary materials**. In brief, the lack of correlation between γ^{187}Os and lithophile element indicators of silicate fractionation, such as Nd isotopes and enrichments in incompatible trace elements, lead us to discount the presence of a recycled crustal component, or early silicate fractionation in the mantle as the cause for the elevated γ^{187}Os. The lack of correlation leads to interpretations invoking either the presence of a mantle component characterized by an ancient HSE fractionation occurring in reaction products of interactions between the core and the mantle (e.g., Humayun et al., 2004), or as a result of sulfide metasomatism (e.g., Luguet et al., 2008). Such processes would only affect siderophile element abundances, and may be evidenced by the higher Re/Os for GOR23B and GOR47 than in the other komatiites.

Although core-mantle interaction and sulfide metasomatism are the most probable interpretations, each of these two possible explanations for the elevated γ^{187}Os values have potential weaknesses of their own. While chemical interactions between the core and mantle could result in the creation of a mantle domain characterized fractionated Re/Os, leading to long-term enrichments in ^{187}Os, as suggested by Humayun (2011), such interactions might also be expected to lead to correlations between ^{187}Os and ^{182}W, given the high W concentration and low μ^{182}W inferred for the core (e.g. Rizo et al., 2019). No such correlation is observed (**Fig. 8**). In addition to increasing Re/Os (and Pt/Os), sulfide metasomatism would likely lead to a corresponding overall enrichment in some of the HSE in the metasomatized source. This, in turn, could lead to enrichments in the products resulting from the melting of such materials. There are no obvious enrichments evident in the HSE patterns of the rocks with elevated γ^{187}Os (**Fig. 10a**), however, compared to the rocks with the lower γ^{187}Os.

6.3. ^{182}W isotopic systematics

Before seeking to interpret ^{182}W data for igneous rocks, it is important to assess whether the W isotopic compositions measured reflect the compositions of the rocks at the time they crystallized, and possibly their mantle sources. Many of the Precambrian komatiites, as well as younger igneous rocks examined to date have W concentrations that are considerably higher and more varied than would be expected to result from partial melting of mantle with the ~10 to 30 ppb W that has been estimated for the likely BSE and DMM type sources, and subsequent simple crystal-liquid fractionation during crystallization (e.g., Arevalo and McDonough, 2008; König et al., 2011; Peters et al., 2023). Higher than expected concentrations could be due to W mobility along with re-deposition within a volcanic pile, in which case the W isotopic composition would reflect that of the mantle source (Puchtel et al., 2022). Alternatively, exogenous W could be added to the rocks via fluids, such as from seawater, as may occur during serpentinization of komatiites. In this case, the isotopic composition of the W measured would not necessarily be representative of the mantle source of the rocks.

The pristine nature of W within such rocks can potentially be assessed by examining the abundance of W relative to an equally incompatible trace element, such as Th (e.g., Liu et al., 2016; Tusch et al., 2019). Both W and Th are highly incompatible trace elements in silicate systems, so moderate extents of crystal-liquid fractionation cannot normally be expected to lead to substantial modification of the W/Th ratio of ~ 0.19 estimated for the BSE (McDonough and Sun, 1995). Tungsten in contrast to Th, however, can be soluble in oxidizing aqueous solutions, so the most likely cause of substantial variations in W/Th among ultramafic and mafic rocks is fluid transport of W into and out of the rock (e.g., Liu et al., 2016; Tusch et al., 2019).

Gorgona rocks, for which W abundances have been measured, have generally low W concentrations, with the highest abundance of 77 ppb. Most of the komatiites, peridotites, gabbros

and basalts have concentrations between ~ 2 and 30 ppb, which are well within the range of what might be expected to result from moderate to high degrees of partial melting of BSE- or DMM-like source mantle, and subsequent, minor crystal-liquid fractionation processes. This conclusion extends to the E-type Gorgona rocks. The similarly low concentrations of W in Curaçao picrites and basalts are also permissive of primary melting/crystallization without subsequent open-system behavior (Th data are not available for these rocks). Despite the generally low W concentrations, W/Th ratios are variable, ranging from as high as 5.7 in komatiite 19GOR-1E, to as low as 0.12 in E-basalt 19GOR-22. There is no correlation between W/Th and either MgO or μ^{182}W (**Fig. 11a-b**). In most instances, this is because W concentrations are higher than expected for melts generated from variably melt-depleted mantle, as evidenced by positive concentration anomalies in the normalized incompatible element data for these rocks (**Fig. S1**). The lack of evidence for binary mixing between μ^{182}W and W/Th and suggests that upper level contamination of the parental melts by high W materials with μ^{182}W of 0 likely did not overprint negative values that may have been present in precursor melts. The consistency of W concentrations and the generally low concentrations of W in the Gorgona-Curaçao suite lead us to conclude that the W isotopic data recorded in these rocks is most likely reflective of those in their mantle sources. This in turn suggests that under certain conditions, such as high pressure-temperature melting in a rising plume, W may behave much less incompatibly than Th.

Of the Gorgona rocks, four peridotites, one gabbro, one picrite and two E-basalts have negative μ^{182}W values that are well resolved from the 2SE isotopic composition of the laboratory standard, assumed to record the composition of the modern upper mantle and the BSE (**Fig. 8**). Further, all three Curaçao picrites, and one of the two basalts from the island examined are also characterized by well-resolved negative anomalies.

Prior studies reporting negative $\mu^{182}W$ values in OIB and other mantle plume-derived systems interpreted the anomalous negative values as reflecting: 1) incorporation of material into plumes from a primordial mantle or recycled crustal domain that formed with low Hf/W compared to BSE while ^{182}Hf was extant (e.g., Tusch et al., 2022), 2) uneven distribution of late accreted materials within the silicate Earth, followed by incomplete homogenization within the mantle (i.e., grainy late accretion)(Marchi et al., 2018), or 3) incorporation of material from a lowermost mantle domain that chemically/isotopically exchanged W with the core (e.g., Mundl et al., 2017; Rizo et al., 2019; Mundl-Petermeier et al., 2020). The first two possibilities would require the retention of ^{182}W isotopic heterogeneity within the mantle for > 4.4 billion years. By contrast, core-mantle isotopic exchange could have occurred at any time in Earth history, given that the core has been characterized by a high W concentration (~ 500 ppb; McDonough and Sun, 1995) and a constant, low $\mu^{182}W$ value estimated to be ~ -210 since completion of its formation (Scherstén et al., 2004). The composition estimate for the core is based upon the assumption of a chondritic bulk Earth value and mass balance calculations, assuming that about 90% of Earth's W resides in the core. While there is strong evidence for ^{182}W isotopic heterogeneity surviving in the mantle through the Archean (e.g., Willbold et al., 2011), the anomalies observed in ancient rocks are mostly positive, and the positive anomalies in the upper mantle appear to have dissipated by the end of the Archean (Tusch et al., 2019; Nakanishi et al., 2023)

Prior studies of ^{182}W in modern OIB have been unsuccessful in correlating ^{182}W isotopic anomalies with most other geochemical parameters (e.g., Mundl-Petermeier et al., 2020). As noted above, variations in $\mu^{182}W$ for the Gorgona-Curaçao suite are correlated with neither variations in $\gamma^{187}Os$ (**Fig. 8**), nor with indicators of chemical enrichments, such as La/Sm (**Fig. 9b**). Although data are limited, there is also no evidence indicating a correlation between $\mu^{182}W$ and the long-

lived lithophile ^{147}Sm-^{143}Nd system (**Fig. S9**). Further, there is also no correlation between μ^{182}W and Pt concentration, which serves as a crude indicator of HSE abundances in the source (**Fig. 10b**). Thus, geochemical processes in the silicate portion of the Earth that led to elemental fractionations of either siderophile or lithophile elements were either not involved in the generation of the ^{182}W heterogeneities, or the effects upon the other elements were somehow overprinted while the ^{182}W heterogeneities were retained. Further, the absence of any indication of HSE enrichment, most importantly Pt, in the mantle source of the materials with negative μ^{182}W values argues against the long-term survival of mantle enriched in late accreted materials.

One geochemical parameter that has been shown to be negatively correlated with μ^{182}W in some plume-derived systems is ^{3}He/^{4}He (e.g., Mundl et al., 2017). For most OIB systems that include a high ^{3}He/^{4}He component, decreasing μ^{182}W is typically correlated with increasing ^{3}He/^{4}He, forming roughly linear trends on plots of ^{3}He/^{4}He (R/R_A) versus μ^{182}W (Mundl et al., 2017; Mundle-Petermeier et al., 2019; 2020). The slopes of these trends, however, vary for different OIB systems, and some high ^{3}He/^{4}He plume-derived rocks, such as those from West Greenland, have no ^{182}W anomaly (e.g., Mundl-Petermeier et al., 2019; Jansen et al., 2022). Although coupled He-W isotopic data are limited for Gorgona samples, the three samples previously characterized for ^{3}He/^{4}He indicate a possible correlation with a more steeply sloping trend than has been previously observed in OIB systems (**Fig. 12**).

Rocks with ^{3}He/^{4}He ratios higher than is typical for MORB are commonly interpreted to sample a less degassed, primitive portion of the mantle that has remained isolated from the convecting mantle for most of Earth history (e.g., Allègre, 1987). The less degassed source is often assumed to reside in the lower mantle. Given that ^{4}He is produced primarily from the decay of U and Th, it is also commonly assumed that mantle sources with high ^{3}He/^{4}He have not been strongly

enriched in U-Th through either crystal-liquid fractionation processes, or through the recycling of incompatible trace element-enriched crustal rocks (Allègre, 1987).

To explain the $^{3}He/^{4}He$-$\mu^{182}W$ correlations observed in OIBs, Mundl-Petermeier et al. (2020) modeled the mixing of three different mantle components in variable proportions. One component was proposed to be similar in composition to DMM with normal $\mu^{182}W$ and $^{3}He/^{4}He$. A second component is characterized by a negative $\mu^{182}W$ and high $^{3}He/^{4}He$. The third component is characterized by normal $\mu^{182}W$ but elevated $^{3}He/^{4}He$. The steep slope of the putative Gorgona trend may suggest incorporation of a component with greater enhancement of the $\mu^{182}W$ signal than the $^{3}He/^{4}He$ signal. This could result from the presence of higher W/He material in the component. As noted above, however, W concentrations in these rocks are not notably enriched.

The location in the mantle of the domain from which the isotopically anomalous component was derived remains unknown. Mundl-Petermeier et al. (2020) posited that the spatial association between OIB with negative ^{182}W anomalies and seismically-identified ultra-low velocity zones (ULVZ) at the core-mantle boundary suggests that these small features may be the ultimate source of the low $\mu^{182}W$ materials. The laterally more extensive large low shear-wave velocity provinces (LLSVP) have also been suggested to be the ultimate source of isotopically anomalous W (Tusch et al., 2022).

Overall, the Gorgona-Curaçao suite is characterized by the greatest range in $\mu^{182}W$ yet recorded. The variations in isotopic composition do not appear to be correlated with any accompanying lithophile or siderophile (including ^{187}Os) compositions. Very limited data suggest a possible negative correlation between $\mu^{182}W$ and $^{3}He/^{4}He$, as has been observed for other plume-derived systems.

6.4. Observations from data comparisons

At the outset of this study, it was anticipated that the relative youth of the Gorgona-Curaçao suite (allowing for precise age corrections of Re-Os isotopic data for rocks with high Re/Os), combined with the range of compositional variations from mafic to ultramafic rocks, would uniquely enable the cross comparison of lithophile and siderophile elemental and isotopic data obtained from a sizeable plume-derived system. Although ambiguities related to these comparisons remain, several important observations regarding the Gorgona-Curaçao suite can be made.

First, the lithophile element chemical and isotopic data, combined with siderophile element chemical and ^{187}Os and ^{182}W isotopic data for the Gorgona-Curaçao rocks supports the earlier contention of a heterogeneous plume, with the dominant component in the Gorgona suite characterized initially by ancient chemical depletion (e.g., Aitken and Echeverría, 1984; Révillon et al., 2002; Thompson et al., 2004; Serrano et al., 2011). This component likely became increasingly chemically depleted during the upward transit of the plume as a result of dynamic melting in the plume head (e.g., Arndt et al., 1997). The chemical compositions of the depleted components were similar to the DMM but differed in having somewhat higher $^{176}Hf/^{177}Hf$ (Thompson et al., 2004) and $^{187}Os/^{188}Os$ isotopic compositions. The HSE abundances estimated for this dominant component are similar to those estimated for the BSE and DMM. The most highly depleted component evident in the Gorgona suite does not appear to be significantly sampled by the Curaçao suite. Most rocks from Curaçao, and the volumetrically minor E-type rocks from Gorgona are characterized by either modest re-enrichment of a more depleted mantle domain, perhaps as a result of recycling, or a history of less depletion compared to the highly-depleted component.

Second, there is no discernable correlation between $\mu^{182}W$ and other siderophile element tracers including $\gamma^{187}Os$. The ^{187}Os enrichments (and presumably the accompanying, correlated ^{186}Os enrichments previously reported for some Gorgona samples) and negative ^{182}W anomalies for some CLIP rocks are either not related, or the isotopic signature of one element or the other in the mantle source has been overprinted by processes subsequent to the initiation of melting. Thus, processes that would be expected to generate correlations between the two siderophile element isotope systems, such as silicate-silicate or silicate-metal fractionation of Hf/W or Re/Os, occurring within the first ~60 Ma of Solar System history, are not directly implicated for generating the ^{187}Os and ^{182}W isotopic heterogeneities. This observation does not, however, rule out the possibility that such processes occurred subsequently to the extinction of ^{182}Hf, leading to the generation of ^{187}Os isotopic heterogeneities. Additionally, there are no correlations between either $\gamma^{187}Os$ or $\mu^{182}W$, and reported ^{143}Nd isotopic compositions. There is also no correlation between $\gamma^{187}Os$ or $\mu^{182}W$ and the elemental indicators of chemical enrichment and depletion, such as La/Sm. The sample with the lowest $\mu^{182}W$ value of -53 is from a long-term lithophile trace element depleted source, as evidenced by a comparatively low ε_{Nd} of +6.6 (Révillon et al., 2002). A similar correlation has been recognized for some OIB suites (Jackson et al., 2020), although other Gorgona and Curaçao samples with low ε_{Nd} also have negative ^{182}W anomalies.

Silicate fractionation during the lifetime of ^{182}Hf would likely have produced a positive correlation between ^{142}Nd and ^{182}W in the resulting chemically enriched or depleted reservoirs. No correlation was found between ^{142}Nd and ^{182}W for OIB from Samoa and Hawaii suites (Horan et al., 2018), which show strong $\mu^{182}W$ versus $^{3}He/^{4}He$ trends. The only modern OIB system for which a *negative* correlation between ^{142}Nd and ^{182}W has been reported is for Reunion Island (Peters et al., 2021). Hyung et al. (2023) reported normal $^{142}Nd/^{144}Nd$ ratios for a suite of Gorgona

rocks that included komatiite, picrite, as well as D- and E-basalts. None of the rocks from that study were the same as for this study, although sampling locations were similar. While it seems unlikely that a correlation between ^{142}Nd and ^{182}W for Gorgona rocks will be uncovered, future study should be directed to generating data for both systems on the same rocks. If it is confirmed that ^{142}Nd anomalies are absent from all Gorgona and Curaçao rocks, regardless of ^{182}W or ^{187}Os isotopic compositions, then it may be concluded either that early silicate fractionation did not cause the anomalous compositions, or that subsequent processes may have overprinted a correlation generated during early Earth history.

Third, direct incorporation of outer core metal into a rising plume would lead to a decrease in μ^{182}W of the metal-enriched mantle, but also to collateral enrichments in W and HSE abundances, for which there is no evidence in samples with negative μ^{182}W values. Unlike for the dominant komatiites, precise estimates of HSE abundances in the sources of samples with negative μ^{182}W values cannot be made. Nevertheless, the HSE abundances in all of the rocks examined, particularly the abundances of Pt and Pd, which are most diagnostic of mantle source concentrations, are broadly similar to those measured for rocks with similar major element compositions worldwide. Thus, direct physical incorporation of outer core metal into the CLIP plume was likely not a significant contributor to the isotopic heterogeneity of the Gorgona-Curaçao suite with respect to either ^{187}Os (and ^{186}Os) or ^{182}W.

The lack of a ^{187}Os-^{182}W correlation may also rule out reactive equilibration between the core and lowermost mantle, as proposed by Humayun (2011) and Rizo et al. (2019), since processes that might be expected to fractionate Re/Os leading to elevated ^{187}Os, could also plausibly lead to a correlation with negative μ^{182}W. The effects of such a process on these elements, however, is currently difficult to predict, given the limited data available for modeling their rates and nature of

exchange and fractionation, so reactive equilibration remains a plausible explanation for both anomalous ^{187}Os and ^{182}W.

Fourth, the small number of corresponding ^{182}W-^{3}He/^{4}He data reported here are broadly consistent with a limited correlation, albeit with a greater variance in ^{182}W relative to ^{3}He/^{4}He than has been previously observed in OIB. As noted, Rizo et al. (2019) and Mundl-Petermeier et al. (2020) favored models of core-mantle interaction to account for ^{182}W-^{3}He/^{4}He correlations in OIB. Although ^{3}He/^{4}He ratios measured in OIB that are elevated above the average upper mantle composition have commonly been attributed to contributions from less degassed mantle domains, it has also been postulated that primordial He has been transferred from the core to the mantle (e.g., Olson and Sharp, 2021). Consistent with this, Ferrick and Korenaga (2023) proposed a detailed model to explain the ^{182}W-^{3}He/^{4}He correlations. Their model invoked isotopic diffusion of both W and He across the core-mantle boundary and can potentially account for the observed correlations. An important aspect of this type of model is that retention of a less degassed mantle reservoir is not required, given that the isotopically anomalous He derives from the core. Alternatively, Fu et al. (2023) proposed that precipitation of FeSi in the outer core, and transfer of a small proportion of it into the overlying mantle led to the formation of ultra-low velocity zones. This is a potential mechanism for transporting low μ^{182}W from the core into a mantle domain that could ultimately contribute the low μ^{182}W signal to a plume rising from the core-mantle boundary.

Finally, the largest magnitude ^{187}Os and ^{182}W heterogeneities are observed in only a small fraction of the rocks examined. Neither type of heterogeneity is uniform, requiring mixing between components with higher γ^{187}Os on the one hand, and lower μ^{182}W on the other. Collectively, these requirements most likely implicate volumetrically minor streaks of isotopically anomalous material within the rising plume that produced the Gorgona and Curaçao rocks. Nevertheless,

observation that samples with negative $\mu^{182}W$ are also characterized by variable lithophile trace element compositions, e.g., both D- and E-type rocks, indicates a well-distributed component that was sufficiently enriched in W with low $\mu^{182}W$, but not sufficiently modified for other elements that correlations would be observed.

7. Conclusions

1. New data for lithophile major and trace elements are similar to prior studies and are consistent with contributions to the Gorgona and Curaçao magmatic rocks from a combination of chemically depleted and moderately enriched mantle source components.

2. The initial $^{187}Os/^{188}Os$ ratio for most rocks from both islands lies between average BSE and DMM values, and may reflect a dominant lower mantle composition. A minor proportion of the rocks are characterized by initial ratios > 10% higher, and indicate a small contribution to the magmatic systems from either mantle that has been modified by sulfide metasomatism or that experienced an ancient fractionation event. Accompanying HSE abundances are within the global range of compositions for rocks with equivalent MgO.

3. The $\mu^{182}W$ values vary substantially from normal (0) to strongly negative (-53). Although the data are limited, the $\mu^{182}W$ values may be negatively correlated with $^{3}He/^{4}He$, as has been observed in a number of modern ocean island basalt systems. The $\mu^{182}W$ values, however, do not correlate with any other geochemical parameter examined.

4. The negative $\mu^{182}W$ values are best explained as a result of a contribution from a mantle component that acquired a negative anomaly through either some form of core-mantle isotopic

exchange, or as a result of a mantle fractionation process that occurred within the first 60 Ma of solar system history and was then preserved for nearly all of Earth history.

Acknowledgements

We thank F. Albarède, M. Fischer-Gödde and an anonymous reviewer for providing valuable comments on the manuscript. We especially wish to thank the Parques Nacionales Naturales de Colombia for approval to visit Gorgona Island in 2019 (# 20182000069041) as well as for their assistance and support. The sampling expedition would not have been possible without this support. Support for this work was also provided by U.S. National Science Foundation grants EAR-1624587 (to RJW) and EAR-2220936 (to ISP). AM-P acknowledges FWF grant V659-N29 and CC acknowledges ERC grant No. 833632

Data Availability

Tables of all data presented and plotted are available through *Mendeley Data* at:

https://data.mendeley.com/datasets/8mh9y2tgzr/1

Appendix A. Supplementary Materials

The supplementary materials for this article include additional details regarding Sample preparation and analytical methods (**Section 1**), additional information providing an overview of

the origins of Gorgona rocks from prior studies (**Section 2**), calculations relating to the abundances of HSE in the mantle source of the dominant komatiites (**Section 3**), and some additional discussion of the ^{187}Re-^{187}Os isotopic systematics of rocks from the islands of Gorgona and Curaçao (**Section 4**). The supplementary materials for this article also include four tables (**Tables S1-S4**) and eleven figures (**Figs. S1-S11**). **Table S1** reports major and trace element data, as well as GPS coordinates for sample locations (where available) for all rocks studied. **Table S2** reports rock standards data for major and trace elements. **Table S3** reports LOI-corrected abundances of HSE. **Table S4** reports details regarding ^{182}W data obtained by MC-ICP-MS. **Figures S1** – **S2** are additional compositional and isotopic plots for Gorgona-Curaçao rocks. **Figures S3a-c** are *Isoplot* regression plots of Re-Os isotopic data. **Figures S4-S6** are plots of HSE abundances of Gorgona komatiites and peridotites versus MgO, Ni and Cr. **Figures S7a-c** are regressions of Re, Pt and Pd data for samples from a single komatiite flow to a projected olivine composition, used to constrain HSE abundances in the mantle source of the dominant Gorgona komatiites. **Figure S8** is a BSE normalized plot of the concentrations of HSE abundances projected for the dominant Gorgona mantle source. **Figure S9** is a plot of μ^{182}W versus εNd for four Gorgona peridotites. **Figure S10** is a plot of μ^{183}W(6/4) versus μ^{182}W(6/4) for samples measured by MC-ICP-MS. **Figure S11** is a plot of γ^{187}Os versus time (in Ga) for hybrid mantle reservoirs generated via the mixing model reported in Walker et al. (1999).

References

Aitken B.G. and Echeverría L.M. (1984) Petrology and geochemistry of komatiites and tholeiites from Gorgona island, Colombia. *Contrib. Mineral. Petrol.* **86**, 94–105.

Alard O., Griffin W.L., Lorand J-P., Jackson S.E. and O'Reilly S.Y. (2000) Non-chondritic distribution of the highly siderophile elements in mantle sulphides. *Nature* **407**, 891-894.

Allègre C.J. (1987) Isotope geodynamics. *Earth Planet. Sci. Lett.* **86** 175-203.

Alvarado G.E., Denyer P. and Sinton, C.W. (1997) The 89 Ma Tortugal komatiitic suite, Costa Rica: Implications for a common geological origin of the Caribbean and Eastern Pacific region from a mantle plume. *Geology* **25**, 439–442.

Archer G.J., Mundl A., Walker R.J., Worsham E.A. and Bermingham K.R. (2017) High-precision analysis of $^{182}W/^{184}W$ and $^{183}W/^{184}W$ by negative thermal ionization mass spectrometry: Per-integration oxide corrections using measured $^{18}O/^{16}O$. *Int. Journ. Mass Spectrom.* **414**, 80–86.

Arevalo Jr. R. and McDonough W.F. (2008) Tungsten geochemistry and implications for understanding the Earth's interior. *Earth Planet. Sci. Lett.* **272**, 656–665.

Arndt N. T., Kerr A. C., and Tarney J. (1997) Dynamic melting in plume heads: The formation of Gorgona komatiites and basalts. *Earth Planet. Sci. Lett.* **146**, 289-301.

Barnes S-J., Naldrett A.J. and Gorton M.P. (1985) The origin of the fractionation of platinum-group elements in terrestrial magmas. *Chem. Geol.* **53**, 303–323.

Barnes S.J. (1998) Chromite in komatiites, I. Magmatic controls on crystallization and composition. *Journ. Petrol.* **39**, 1689-1720.

Becker, H., Horan M.F., Walker R.J., Gao S., Lorand J.P. and Rudnick R.L. (2006) Highly siderophile element composition of the Earth's primitive upper mantle: Constraints from new data on peridotite massifs and xenoliths. *Geochim. Cosmochim. Acta* **70**, 4528-4550.

Birck J. L., Roy-Barman M. and Capmas F. (1997) Re–Os isotopic measurements at the femtomole level in natural samples. *Geostand. Geoanal. Res.* **21**, 19–27.

Bockrath C., Ballhaus C. and Holzheid A. (2004) Fractionation of the platinum-group elements during mantle melting. *Science* **305**, 1951-1953.

Brandon A.D., Snow J.E., Walker R.J., Morgan J.W. and Mock T.D. (2000) ^{190}Pt-^{186}Os and ^{187}Re-^{187}Os systematics of abyssal peridotites. *Earth Planet. Sci. Lett.* **177**, 319-335.

Brandon A.D., Walker R.J., Puchtel I.S., Becker H, Humayun M. and Révillon S. (2003) ^{186}Os-^{187}Os systematics of Gorgona Island komatiites: implications for early growth of the inner core. *Earth Planet. Sci. Lett.* **206**, 411-426.

Brenan J.M. and Andrews D. (2001) High temperature stability of laurite and Ru–Os–Ir alloy and their role in PGE fractionation in mafic magmas. *Can. Min.* **39**, 341−360.

Brügmann G.E., Arndt N.T., Hofmann A.W. and Tobschall H.J. (1987) Noble metal abundances in komatiite suites from Alexo, Ontario, and Gorgona Island, Colombia. *Geochim. Cosmochim. Acta* **51**, 2159-2169.

Cohen A. S. and Waters G. G. (1996) Separation of osmium from geological materials by solvent extraction for analysis by thermal ionization mass spectrometry. *Analyt. Chim. Acta* **332**, 269–275.

Day J.M.D., Walker R.J. and Warren J.M. (2017) ^{186}Os-^{187}Os and highly siderophile element abundance systematics of the mantle revealed by abyssal peridotites and Os-rich alloys. *Geochim. Cosmochim. Acta* **200**, 232-254.

Duncan R.A. and Hargraves R.B. (1984) Plate tectonic evolution of the Caribbean region in the mantle reference frame. In: Bonini R.B., Hargraves R.B., Shagam R. (eds.), The Geology of

North America. H. The Caribbean-South American plate boundary and regional tectonics. *Geol. Soc. Amer. Mem.* **162**, 81-94.

Dupré B. and Echeverría L.M. (1984) Pb isotopes of Gorgona island (Colombia): isotopic variations correlated with magma type. *Earth Planet. Sci. Lett.* **67**, 186–190.

Dürkefälden A., Hoernle K., Hauff F., Wartho J.-A., van den Bogaard P., and Werner R. (2019a) Age and geochemistry of the Beata Ridge: Primary formation during the main phase (~89 Ma) of the Caribbean Large Igneous Province. *Lithos* **328-329**, 69-87.

Dürkefälden A., Hoernle K., Hauff F., Werner R. and Garbe-Schönberg D. (2019b) Second-stage Caribbean Large Igneous Province volcanism: The depleted icing on the enriched cake. *Chem. Geol.* **509**, 45-63.

Echeverría L.M. (1980) Tertiary or Mesozoic komatiites from Gorgona Island, Colombia: Field relations and geochemistry. *Contrib. Min. Pet.* **73**, 253-266.

Echeverría L.M. and Aitken B.G. (1986) Pyroclastic rocks: another manifestation of ultramafic volcanism on Gorgona Island, Colombia. *Contrib. Min. Pet.* **92**, 428-436.

Ferrick A.L. and Korenaga J. (2023) Long-term core–mantle interaction explains W-He isotope heterogeneities. *Proc. Nat. Acad. Sci.* **120**, e2215903120.

Fonseca R.O.C., Laurenz V., Mallmann G., Luguet A., Hoehne N. and Jochum K.P. (2012) New constraints on the genesis and long-term stability of Os-rich allowys in the Earth's mantle. *Geochim. Cosmochim. Acta* **87**, 227-242.

Fu S., Chariton S., Prakapenka V.B. and Shim S-H. (2023) Core origin of seismic velocity anomalies at Earth's core-mantle boundary. *Nature* **615**, 646-651.

Gansser A., Dietrich V.J. and Cameron W.E. (1979) Paleogene komatiites from Gorgona Island. *Nature* **278**, 545-546.

Gazel E., Trela J., Bizimis M., Sobolev A., Batanova V., Class C. and Jicha B. (2018) Long lived source heterogeneities in the Galapagos mantle plume. *Geochem. Geophys. Geosyst.*, 10.1029/2017GC007338.

Gurenko A.A., Kamenetsky V.S. and Kerr A.C. (2016) Oxygen isotopes and volatile contents of the Gorgona komatiites, Colombia: A confirmation of the deep mantle origin of H_2O. *Earth Planet. Sci. Lett.* **454**, 154-165.

Haller M. B., O'Driscoll B., Day J.M.D., Daly J.S., Piccoli P.M. and Walker R.J. (2021) Meter-scale chemical and isotopic heterogeneities in the oceanic mantle, Leka Ophiolite Complex, Norway. *Journ. Petrol.* **62**, 1-29.

Hauff F., Hoernle K., Tilton G., Graham D.W. and Kerr A.C. (2000) Large volume recycling of oceanic lithosphere over short time scales: geochemical constraints from the Caribbean Large Igneous Province. *Earth Planet. Sci. Lett.* **174**, 247-263.

Hauri E.H. and Hart S.R. (1993) Re-Os isotope systematics of HIMU and EMII oceanic island basalts from the south Pacific Ocean. *Earth Planet. Sci. Lett*. **114**, 353-371.

Hoernle K., Hauff F. and van den Bogaard P. (2004) 70 m.y. history (139–69 Ma) for the Caribbean large igneous province. *Geology* **32**, 697-700.

Horan M.F., Carlson R.W., Walker R.J., Jackson M., Garçon M. and Norman M. (2018) Tracking Hadean processes in modern basalts. *Earth Planet. Sci. Lett.* **484**, 184-191.

Humayun M., Qin L. and Norman M.D. (2004) Geochemical evidence for excess iron in the mantle beneath Hawaii. *Science* **306**, 91-94.

Humayun M. (2011) A model for osmium isotopic evolution of metallic solids at the core-mantle boundary. *Geochem. Geophys. Geosyst.* **12**, doi:10.1029/2010GC003281.

Hyung E., Ibañez-Mejia M. and Rojas-Agramonte Y. (2023) The survival of primordial tracers of mantle heterogeneity investigated through $^{142}Nd/^{144}Nd$ and $^{3}He/^{4}He$ isotope decoupling in the Gorgona Island lavas. *Earth Planet. Sci.* **622**, 118409.

Jackson M.G., Blichert-Toft J., Halldórsson S.A., Mundl-Petermeier A., Bizimis M., Kurz M.D., Price A.A., Harðardóttir S., Willhite L.N., Breddam K., Becker T.W. and Fischer R.A. (2020) Ancient helium and tungsten isotopic signatures preserved in mantle domains least modified by crustal recycling. *Proc. Nat. Acad. Sci.* **117**, 30993-31001.

Jansen M.W., Tusch J., Münker C., Bragagni A., Avanzinelli R., Mastroianni F., Stuart F.M. and Kurzweil F. (2022) Upper mantle control on the W isotope record of shallow level plume and intraplate volcanic settings. *Earth Planet. Sci. Lett.* **585**, 117507.

Keays R. (1995) The role of komatiitic and picritic magmatism and S-saturation in the formation of ore deposits, *Lithos* **34**, 1-18.

Kerr A.C., Marriner G.F., Arndt N.T., Tarney J., Nivia A., Saunders A.D. and Duncan R.A. (1996a) The petrogenesis of Gorgona komatiites, picrites and basalts: new field, petrographic and geochemical constraints. *Lithos* **37**, 245-260.

Kerr A.C., Tarney, J., Marriner G.F., Klaver G.T., Saunders A.D. and Thirlwall M.F. (1996b) The geochemistry and petrogenesis of the late-Cretaceous picrites and basalts of Curaçao, Netherlands Antilles: A remnant of an oceanic plateau. *Contrib. Mineral. Petrol*. **124**, 29-43.

Kerr A.C., Tarney J., Marriner G.F., Nivia A. and Saunders A.D. (1997) The Caribbean-Colombian Cretaceous igneous province: the internal anatomy of an oceanic plateau. In. *Large Igneous Provinces: Continental, Oceanic, and Planetary Volcanism*. *Geophysical Mon*. 100 (eds. J.J. Mahoney and M.F. Coffin), pp. 123-144.

Kerr A.C., Tarney J., Kempton P.D., Spadea, P., Nivia A., Marriner G.F. and Duncan R.A. (2002) Pervasive mantle plume head heterogeneity: evidence from the late Cretaceous Caribbean-Colombian oceanic plateau. *Journ. Geophys. Res.* **107** (B7), 2140.

Kerr A.C. (2005) La Isla de Gorgona, Colombia: A petrological enigma? *Lithos* **84**, 77-101.

Klaver G.T. (1987) The Curaçao lava formation. An ophiolitic analogue of the anomalously thick layer 2B of the mid-Cretaceous oceanic plateaux in the Western Pacific and central Caribbean. PhD Thesis, U. Amsterdam, 168 pp.

König S., Münker C., Schuth S., and Garbe-Schönberg D. (2008) Mobility of tungsten in subduction zones. *Earth Planet. Sci. Lett.* **274**, 82-92.

Liu J., Touboul M., Ishikawa A., Walker R.J. and Pearson D.G. (2016) Widespread tungsten isotope anomalies and W mobility in crustal and mantle rocks of the Eoarchean Saglek Block, northern Labrador, Canada: implications for early Earth processes and W recycling. *Earth Planet. Sci. Lett.* **448**, 13-23.

Locmelis M., Pearson N.J., Barnes S.J. and Fiorentini M.L. (2011) Ruthenium in komatiitic chromite. *Geochim. Cosmochim. Acta* **75**, 3645-3661.

Ludwig K. R. (2003) ISOPLOT 3.00. A geochronological toolkit for Microsoft Excel, *Berkeley Geochronology Center Special Publication* **4**, 70 pp.

Luguet A., Pearson D.G., Nowell G.M., Dreher S.T., Coggon J.A., Spetsius Z.V. and Parman S.W. (2008) Enriched Pt-Re-Os isotope systematics in plume lavas explained by metasomatic sulphides. *Science* **319**, 453-456.

Madrigal P., Gazel E., Flores K.E., Bizimis M. and Jicha B. (2016) Record of massive upwellings from the Pacific large low shear velocity province. *Nature Comm.* **7**, 13309.

Marchi S., Canup R.M. and Walker R.J. (2018) Heterogeneous delivery of silicate and metal to the Earth by large planetesimals. *Nature Geosci.* **11**, 77-81.

McDonough W.F. and Sun S-S. (1995) The composition of the Earth. *Chem. Geol.* **120**, 223-253.

Meisel T., Walker R.J., Irving A.J., and Lorand J.-P. (2001) Osmium isotopic compositions of mantle xenoliths: a global perspective. *Geochim. Cosmochim. Acta* **65**, 1311-1323.

Mundl A., Touboul M., Jackson M. G., Day J. M. D., Kurz M. D., Lekic V., Helz R. T. and Walker R. J. (2017) Tungsten-182 heterogeneity in modern ocean island basalts. *Science* **69**, 66–69.

Mundl-Petermeier A., Walker R.J., Jackson M.G., Blichert-Toft J., Kurz M.D., and Halldórsson S.A. (2019) Temporal evolution of primordial tungsten-182 and $^{3}He/^{4}He$ signatures in the Iceland mantle plume. *Chem. Geol.* **525**, 245-259.

Mundl-Petermeier A., Walker R. J., Fischer R. A., Lekic V., Jackson M. G. and Kurz M. D. (2020) Anomalous ^{182}W in high $^{3}He/^{4}He$ ocean island basalts: Fingerprints of Earth's core? *Geochim. Cosmochim. Acta* **271**, 194–211.

Mundl-Petermeier A., Roberts J. and Vollstaedt H. (2022) High precision tungsten isotopes analyzed via thermal ionization mass spectrometry. *Thermo Fisher application note 000969*, 1-3.

Nakanishi N., Puchtel I.S., Walker R.J. and Nabelek P.I. (2023) Dissipation of tungsten-182 anomalies in the Archean upper mantle: evidence from the Black Hills, South Dakota, USA. *Chem. Geol.* **617**, 121255.

Nicklas R.W., Puchtel I.S., Ash R.D., Piccoli P., Hanski E., Nisbet E.G., Waterton P., Pearson D.G., and Anbar A.D. (2019) Secular Mantle Oxidation across the Archean-Proterozoic Boundary: Evidence from V partitioning in komatiites and picrites. *Geochimica et Cosmochimica Acta* **250**, 49-75.

Olson P.L. and Sharp Z.D. (2021) Primordial helium-3 exchange between Earth's core and mantle. *Geochem. Geophys. Geosys.* **23**, e2021GC009985.

Pearson D.G., Irvine G.L., Ionov D.A., Boyd F.R. and Dreibus G.E. (2004) Re–Os isotope systematics and platinum group element fractionation during mantle melt extraction: a study of massif and xenolith peridotite suites. *Chem. Geol.* **208**, 29-59.

Peters B.J., Mundl-Petermeier A., Horan M.F., Carlson R.W. and Walker R.J. (2019) Chemical separation of tungsten and other trace elements for TIMS isotope ratio measurements using organic acids. *Geostand. Geoanalyt. Res.* **43**, 245–259.

Peters B.J., Mundl-Petermeier A., Carlson R.W., Walker R.J. and J.M.D. Day (2021) Combined lithophile-siderophile isotopic constraints on Hadean processes preserved in ocean island basalt sources. *Geochem. Geophys. Geosys.* **22**, e2020GC009479.

Peters D., Rizo H., Carlson R.W., Walker R.J., Rudnick R.L. and Luguet A. (2023) Tungsten in the (upper) mantle: less incompatible and more abundant. *Geochim. Cosmochim. Acta* **351**, 167-180.

Puchtel I. S., Hofmann A. W., Mezger K., Jochum K. P., Shchipansky A. A., and Samsonov A. V. (1998) Oceanic plateau model for continental crustal growth in the Archaean: A case study from the Kostomuksha greenstone belt, NW Baltic Shield. *Earth Planet. Sci. Lett.* **155**, 57–74.

Puchtel I.S. and Humayun M. (2000) Platinum group elements in Kostomuksha komatiites and basalts: Implications for oceanic crust recycling and core-mantle interaction. *Geochim. Cosmochim. Acta* **64**, 4223-4238.

Puchtel I.S. and Humayun M. (2001) Platinum group element fractionation in a komatiitic basalt lava lake. *Geochim. Cosmochim. Acta* **65**, 2979-2993.

Puchtel I.S., Walker R.J., Brandon A.D., and Nisbet E.G. (2009) Pt–Re–Os and Sm–Nd isotope and HSE and REE systematics of the 2.7 Ga Belingwe and Abitibi komatiites. *Geochim. Cosmochim. Acta* **73**, 6357-6389.

Puchtel I.S., Touboul M., Blichert-Toft J., Walker R.J., Brandon A.D., Nicklas R.W., Kulikov V.S., and Samsonov A.V. (2016) Lithophile and siderophile element systematics of the Earth's mantle at the Archean-Proterozoic boundary: Evidence from 2.4 Ga komatiites. *Geochim. Cosmochim. Acta* **180**, 227–255.

Puchtel I.S., Mundl-Petermeier A., Horan M.F., Hanski E., Blichert-Toft J., Walker R.J. (2020) Ultra-depleted 2.05 Ga komatiites of Finnish Lapland: Products of grainy late accretion or core-mantle interaction? *Chem. Geol*. **554**, 119801.

Puchtel I.S., Blichert-Toft J., Horan M.F., Touboul M. and Walker R.J. (2022) The komatiite testimony to ancient mantle heterogeneity. *Chem. Geol.* **594**, 120776.

Révillon S., Arndt N.T., Hallot E., Kerr A.C. and Tarney J. (1999) Petrogenesis of picrites from the Caibbean plateau and the North Atlantic magmatic province. *Lithos* **49**, 1-21.

Révillon S., Arndt N.T., Chauvel C. and Hallot E. (2000) Geochemical study of ultramafic volcanic and plutonic rocks from Gorgona island, Colombia: the plumbing system of an oceanic plateau. *Journ. Petrol.* **41**, 1127–1153.

Révillon S., Chauvel C., Arndt N.T., Pik R., Martineau F., Fourcade S. and Marty B. (2002) Heterogeneity of the Caribbean plateau mantle source: Sr, O and He isotopic compositions of olivine and clinopyroxene from Gorgona Island. *Earth Planet. Sci. Lett.* **205**, 91– 106.

Rehkämper M. and Halliday A.N. (1997) Development and application of new ion-exchange techniques for the separation of the platinum group and other siderophile elements from geological samples. *Talanta* **44**, 663–672.

Rehkämper M., Halliday A.N., Alt J., Fitton J.G., Zipfel J. and Takazawa E. (1999) Non-chondritic platinum-group element ratios in oceanic mantle lithosphere: petrogenetic signature of metl percolation? *Earth Planet. Sci. Lett.* **172**, 65-81.

Rizo H., Andrault D., Bennett N. R., Humayun M., Brandon A.D., Vlastelic I., Moine B., Poirier A., Bouhifd M.A. and Murphy D.T. (2019) ^{182}W evidence for core-mantle interaction in the source of mantle plumes. *Geochem. Perspect. Lett.* **11**, 6–11.

Scherstén A., Elliott T. Hawkesworth C. and Norman M. (2004) Tungsten isotope evidence that mantle plumes contain no contribution from the Earth's core. *Nature* **427**, 234-237.

Sen G., Hickey-Vargas R., Waggoner D.G. and Maurrasse F. (1988) Geochemistry of basalts from the Dumisseau Formation, southern Haiti: implications for the origin of the Caribbean Sea crust. *Earth Planet. Sci. Lett.* **87**, 423–437.

Serrano L., Ferrari L., Martinez M.L., Petrone C.M. and Jaramillo C. (2011) An integrative geologic, geochronologic and geochemical study of Gorgona Island, Colombia: Implications for the formation of the Caribbean Large Igneous Province. *Earth Planet. Sci. Lett.* **309**, 324–336.

Shimizu K., Shimizu N., Komiya K., Suzuki K., Maruyama S. and Tatsumi, Y. (2009) CO_2-rich komatiitic melt inclusions in Cr-spinels within beach sand from Gorgona Island, Colombia. *Earth Planet. Sci. Lett.* **288**, 33-43.

Shirey S.B. and Walker R.J. (1998) Re-Os isotopes in cosmochemistry and high-temperature geochemistry. *Ann. Rev. Earth Planet. Sci.* **26**, 423-500.

Sinton C.W., Duncan R.A., Storey M., Lewis J. and Estrada J.J. (1998) An oceanic flood basalt province within the Caribbean plate. *Earth Planet. Sci. Lett.* **155**, 221– 235.

Smoliar M.I., Walker R.J. and Morgan J.W. (1996) Re-Os ages of group IIA, IIIA, IVA and IVB iron meteorites. *Science* **271**, 1099-1102.

Snow J. and Reisberg L. (1995) Os isotopic systematics of the MORB mantle: results from altered abyssal peridotites. *Earth Planet. Sci. Lett.* **133**, 411-421.

Thompson P. M. E., Kempton P. D., White R. V., Kerr A. C., Tarney J., Saunders A. D., Fitton J. G. and McBirney A. (2003) Hf–Nd isotope constraints on the origin of the Cretaceous Caribbean plateau and its relationship to the Galapagos plume. *Earth Planet. Sci. Lett.* **217**, 59–75.

Tusch J., Sprung P., van de Löcht, Hoffmann J. E., Boyd A.J., Rosing M.T. and Münker C. (2019) Uniform ^{182}W isotope compositions in Eoarchean rocks from the Isua region, SW Greenland: The role of early silicate differentiation and missing late veneer. *Geochim. Cosmochim. Acta* **257**, 284-310.

Tusch J., Hoffmann J. E., Hasenstab E., Fischer-Gödde M., Marien C. S., Wilson A. H. and Münker C. (2022) Long-term preservation of Hadean protocrust in Earth's mantle. *Proc. Nat. Acad. Sci.* **119**, 1–12.

Vockenhuber C., Oberli F., Bichler M., Ahmad I., Quittem G., Meier M., Halliday A. N., Lee D.-C., Kutschera W., Steier P., Gehrke R. J. and Helmer R. G. (2004) New half-life measurement of ^{182}Hf: Improved chronometer for the early solar system. *Phys. Rev. Lett.* **93**, 172501-1–172501-4.

Walker R.J., Echeverría L.M., Shirey S.B. and Horan M.F. (1991) Re - Os isotopic constraints on the origin of volcanic rocks, Gorgona Island, Colombia: Os isotopic evidence for ancient heterogeneities in the mantle. *Contrib. Mineral. Petrol.* **107**, 150-162.

Walker R.J., Morgan J.W., Horan M.F., Czamanske G.F., Krogstad E.J., Fedorenko V. and Kunilov V.E. (1994) Re-Os isotopic evidence for an enriched-mantle source for the Noril'sk-type ore-bearing intrusions, Siberia. *Geochim. Cosmochim. Acta* **58**, 4179-4197.

Walker R.J., Morgan J.W. and Horan M.F. (1995) ^{187}Os enrichment in some mantle plume sources: Evidence for core-mantle interaction? *Science* **269**, 819-822.

Walker, R.J., Storey M., Kerr A. C., Tarney J. and Arndt N.T. (1999) Implications of ^{187}Os isotopic heterogeneities in a mantle plume: Evidence from Gorgona Island and Curaçao. *Geochim. Cosmochim. Acta* **63**, 713-728.

Walker R.J. (2016) Siderophile elements in tracing planetary formation and evolution. *Geochem. Persp.* **5-1**, 1-143.

Willbold M., Elliott T. and Moorbath S. (2011) The tungsten isotopic composition of the Earth's mantle before the terminal bombardment. *Nature* **477**, 195-198.

Figure Captions

Figure 1. Maps of Gorgona Island and Curaçao. Approximate sampling locations of all rocks are shown on each. The maps are modified after Kerr *et al*. (1996a-b). Where available, GPS coordinates are provided in **Table S1**.

Figure 2. Plot of $^{147}Sm/^{144}Nd$ versus εNd (calculated for 89 Ma) for Gorgona, Curaçao and other CLIP rocks. Plot shows a generally positive correlation between $^{147}Sm/^{144}Nd$ versus εNd. Data for Gorgona rocks are from Echeverría (1980), Aitken and Echeverría (1984), Echeverría and Aitken (1986), Walker et al. (1991), Révillon et al. (2000; 2002) and Kerr (2005). Data for Curaçao and other CLIP locations are from Kerr et al. (1996b), Révillon et al. (1999) and Hauff et al. (2000).

Figure 3. Abundances of rare earth elements normalized to bulk silicate Earth (normalizing concentrations from McDonough and Sun, 1996). Plots are of: a) Gorgona komatiites, where komatiites GOR-23B and GOR-47 with elevated $\gamma^{187}Os$ are shown as circles with crosses), b) Gorgona peridotites, c) Gorgona picrites, d) Gorgona gabbros, e) Gorgona enriched basalts (E-basalts), f) Gorgona depleted basalts (D-basalts), and g) Curaçao basalts (squares) and picrites (triangles). Analytical uncertainties are the size of the symbols or smaller. The gray fields in b-g outline the range of compositions defined by the Gorgona komatiites in a.

Figure 4. Plots of: a) Os, b) Ir, c) Ru, d) Pt, f) Pd and g) Re (all in ppb) versus MgO (in wt.%) of whole rock samples. Note that the Os, Ir, Ru and Re axes are logarithmic scale, while the axes for Pt and Pd are linear. There are broad positive correlations between Os, Ir, Ru and Re relative to MgO. Platinum and Pd show negative correlations with MgO for the komatiites and peridotites. Analytical uncertainties are the size of the symbols or smaller. Note that replicate analyses are included in these plots. The symbols are the same as in **Fig. 3**, and as shown in the legend.

Figure 5. Abundances of highly siderophile elements present in a) Gorgona komatiites, b) Gorgona peridotites, c) Gorgona picrites, d) Gorgona gabbros, e) Gorgona enriched E-basalts, f)

Gorgona D-basalts, and g) Curaçao basalts and picrites, all normalized to Primitive Mantle values from Becker et al. (2006). Analytical uncertainties are the size of the symbols or smaller. Note that for clarity replicate analyses are not included in these plots. The symbols are the same as in **Fig. 3**, and shown in the legend. The gray field in each figure shows the range of compositions defined 95% of modern abyssal peridotites, with data compiled by Walker (2016).

Figure 6a-b. $^{187}Re/^{188}Os$ versus $^{187}Os/^{188}Os$ isochron diagrams for Gorgona and Curaçao rocks. Note that Figure 5a is an enlargement of a portion of Figure 5b. Reference isochrons for 89 Ma are defined by an initial ratio of 0.1264, based on the chondritic evolution model of Shirey and Walker (1998). A 91.2 Ma isochron obtained by regression of data for most komatiites, peridotites, picrites and gabbros is also shown for comparison. Analytical uncertainties are the size of the symbols or smaller. The symbols are the same as in **Fig. 3**, and shown in the legend. Estimates of the average isotopic composition of bulk silicate Earth (BSE), from Becker et al. (2006) and the depleted mid-ocean ridge basalt mantle (DMM), from Snow and Reisburg (1995) are shown as orange and black stars, respectively, in **Fig. 6a**. Note that replicate analyses are included in these plots.

Figure 7. Plot of MgO (in wt.%) versus $\gamma^{187}Os$ (calculated for 89 Ma) for Gorgona and Curaçao rocks. The gray dashed line is the chondritic reference for 89 Ma, as defined by the chondritic evolution model of Shirey and Walker (1998). Uncertainties in $\gamma^{187}Os$ resulting from analytical uncertainties combined with error expansion from projections to initial isotopic compositions from the assumed 89 Ma crystallization age are reflected by the size of accompanying error bars, or the size of the symbols. The symbols are the same as in **Fig. 3**, and shown in the legend. Note that duplicate Os isotopic analyses of E-basalts and D-basalts are averaged, with error bars sized as per discussion in the text.

Figure 8. Plot of $\mu^{182}W$ versus $\gamma^{187}Os$ (calculated for 89 Ma) for Gorgona and Curaçao rocks. The gray dashed line is the chondritic reference for 89 Ma, as defined by the chondritic evolution model of Shirey and Walker (1998). The gray fields reflect the 2SD (light gray) and 2SE (dark gray) uncertainties determined for repeated measurements of the *Alfa Aesar* laboratory W standard during the analytical campaigns for the Gorgona and Curaçao rocks. Uncertainties in γOs resulting from

analytical uncertainties combined with error expansion from projections to initial isotopic compositions from the assumed 89 Ma crystallization age are reflected by the size of accompanying error bars, or the size of the symbols. Note that replicate Os isotopic analyses of E-basalts and D-basalts are averaged, with error bars sized as per discussion in the text. The error bars for $\mu^{182}W$ reflect either the 2SD of repeated analyses of the standard, or the run statistics in 2SE – whichever was larger. The symbols are the same as in **Fig. 3**, and shown in the legend.

Figure 9a-b. Plots of: a) initial $\gamma^{187}Os$ (calculated for 89 Ma) and b) $\mu^{182}W$ versus La/Sm ratio for Gorgona and Curaçao rocks. No correlations are noted for $\gamma^{187}Os$ or $\mu^{182}W$ vs. La/Sm ratio. The symbols are the same as in **Fig. 3**, and shown in the legend.

Figure 10a-b. Plots of: a) initial $\gamma^{187}Os$ (calculated for 89 Ma) and b) $\mu^{182}W$ versus Pt (in ppb) for Gorgona and Curaçao rocks. No correlation is noted for either comparison.

Figure 11a-b. Plots of: a) MgO (in wt.%) versus W/Th ratio, and b) $\mu^{182}W$ versus W/Th ratio for Gorgona and Curaçao rocks. The dashed horizontal lines reflects the approximate W/Th estimated for the primitive mantle (e.g. Tusch et al., 2019).

Figure 12. Plot of $^{3}He/^{4}He$ (R/R_A) versus $\mu^{182}W$ for Gorgona peridotites (green diamonds) and the global database for ocean island basalts reported in Mundl-Petermeier et al. (2020) (gray symbols). Helium isotopic data are from Révillon et al. (2022). The gray arrow highlights a possible trend between the two isotopic systems.

Figures

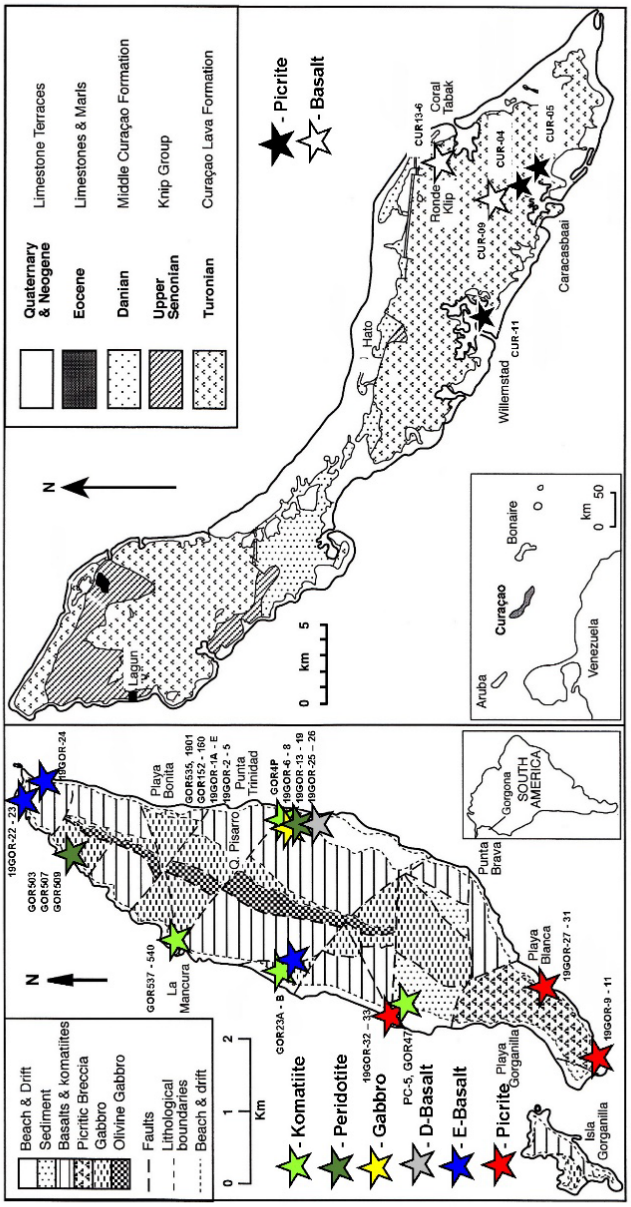
Quaternary & Neogene
Limestone Terraces
Eocene
Limestones & Marls
Danian
Middle Curaçao Formation
Upper Senonian
Knip Group
Turonian
Curaçao Lava Formation
Picrite
Basalt
Hato
Willemstad
Ronde Klip
Coral Tabak
Caracasbaai
CUR-11
CUR-09
CUR-04
CUR-05
CUR13-6
Lagun
0 km 5
Aruba
Curaçao
Bonaire
Venezuela
0 50 km
Gorgona
SOUTH AMERICA
Beach & Drift
Sediment
Basalts & komatiites
Picritic Breccia
Gabbro
Olivine Gabbro
Faults
Lithological boundaries
Beach & drift
0 1 2 Km
Komatiite
Peridotite
Gabbro
D-Basalt
E-Basalt
Picrite
19GOR-22 - 23
19GOR-24
GOR503
GOR507
GOR509
Playa Bonita
GOR535, 1901
GOR152 - 160
19GOR-1A - E
19GOR-2 - 5
Punta Trinidad
GOR4P
19GOR-6 - 8
19GOR-13 - 19
19GOR-25 - 26
Cr. Pisarro
GOR537 - 540
La Mancura
GOR23A - B
PC-5, GOR47
19GOR-32 - 33
Punta Brava
Playa Blanca
19GOR-27 - 31
Playa Gorganilla
Isla Gorganilla
19GOR-9 - 11

Figure 1.

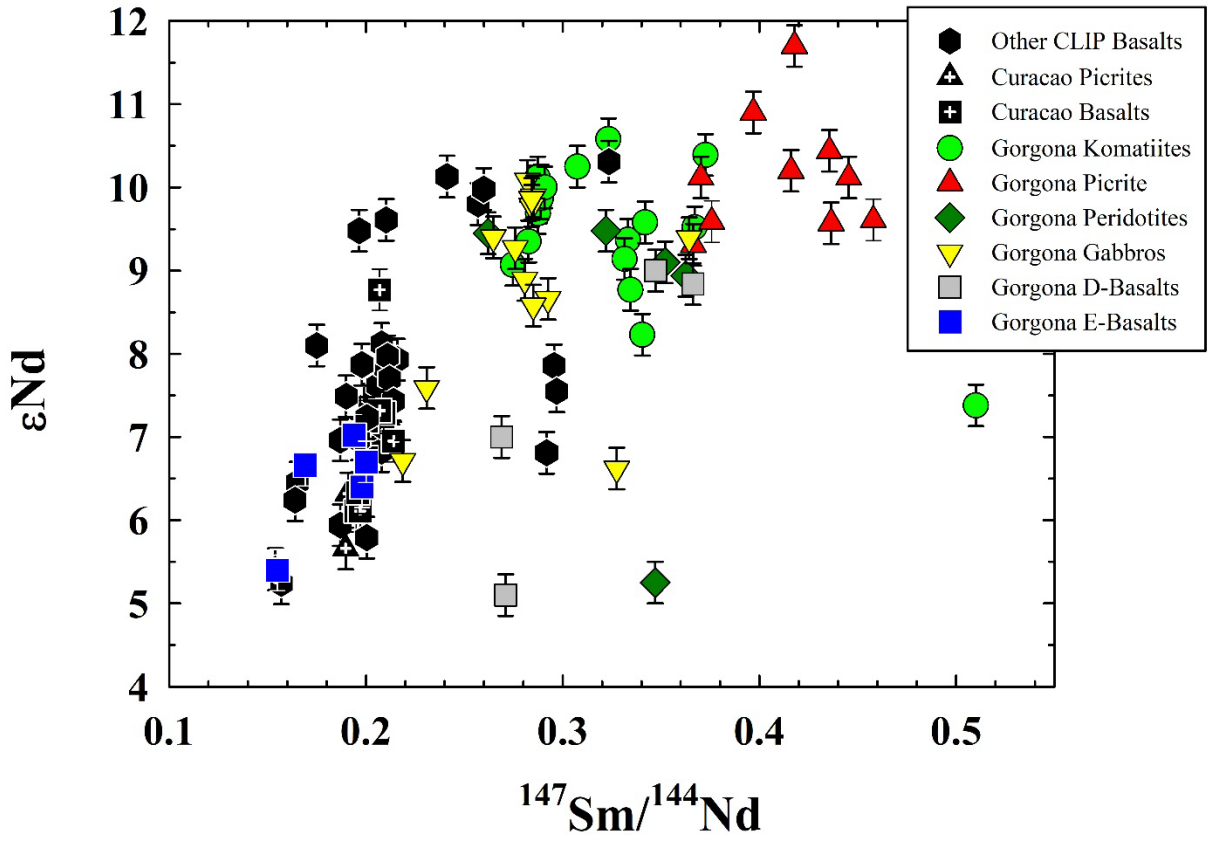

Figure 2.

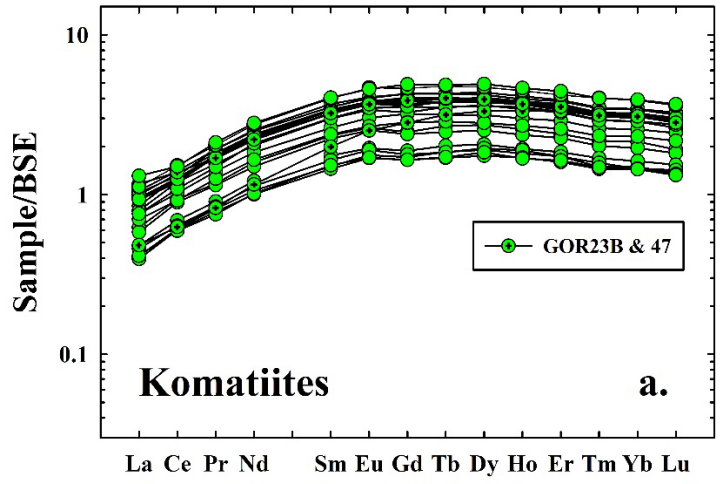
10
1
0.1
Sample/BSE
GOR23B & 47
Komatiites
a.
La Ce Pr Nd Sm Eu Gd Tb Dy Ho Er Tm Yb Lu

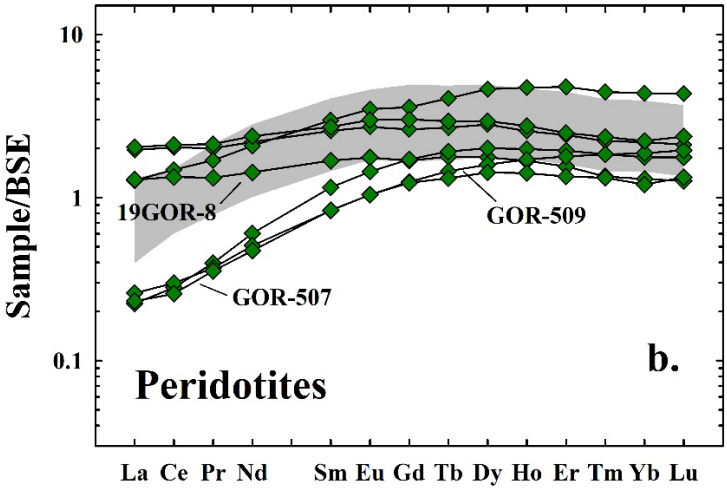
10
1
0.1
Sample/BSE
19GOR-8
GOR-509
GOR-507
Peridotites
b.
La Ce Pr Nd Sm Eu Gd Tb Dy Ho Er Tm Yb Lu

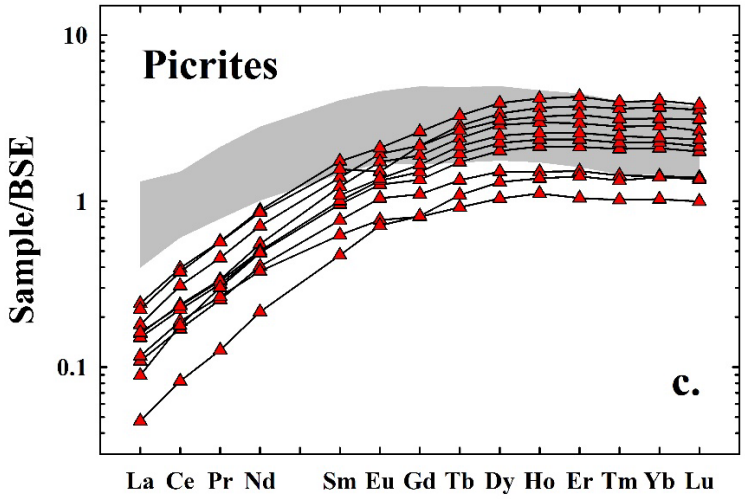
Picrites
Sample/BSE
10
1
0.1
c.
La Ce Pr Nd Sm Eu Gd Tb Dy Ho Er Tm Yb Lu

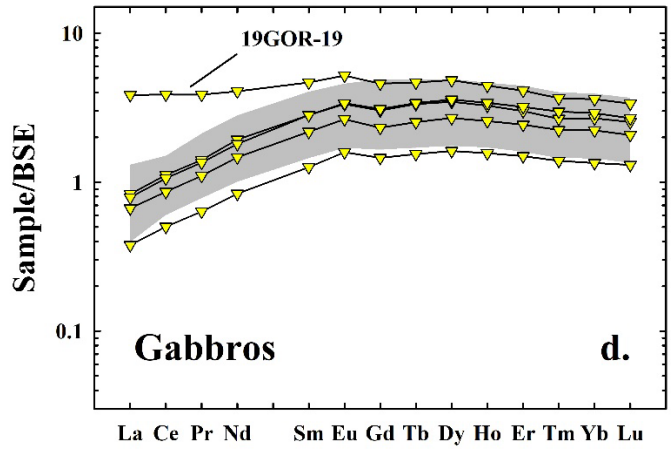
19GOR-19
10
1
0.1
Sample/BSE
Gabbros
d.
La Ce Pr Nd Sm Eu Gd Tb Dy Ho Er Tm Yb Lu

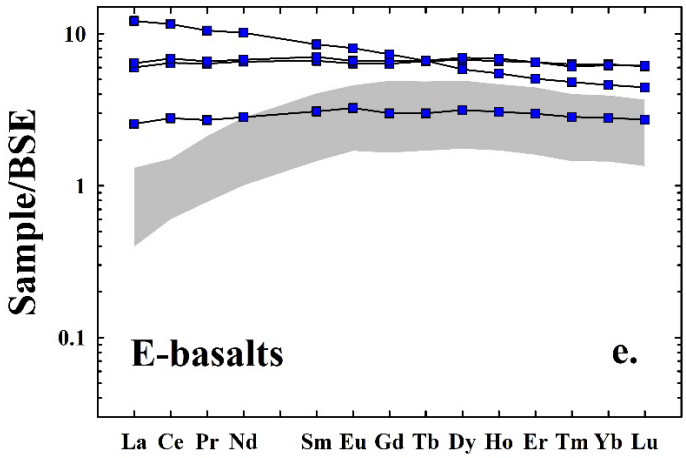
10
1
0.1
Sample/BSE
E-basalts
e.
La Ce Pr Nd Sm Eu Gd Tb Dy Ho Er Tm Yb Lu

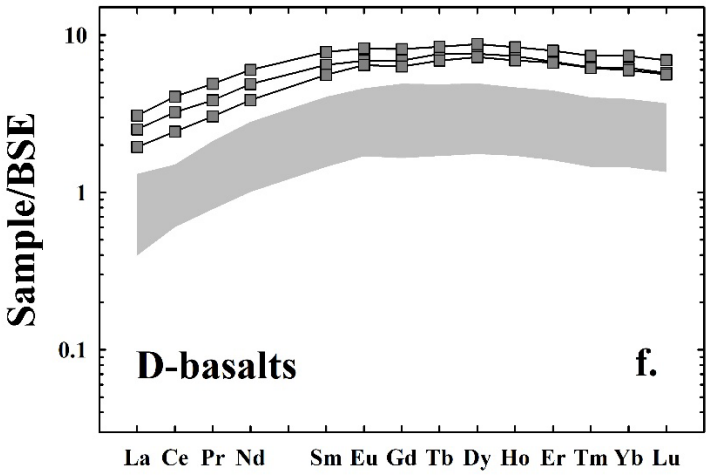
10
1
0.1
Sample/BSE
D-basalts
f.
La Ce Pr Nd Sm Eu Gd Tb Dy Ho Er Tm Yb Lu

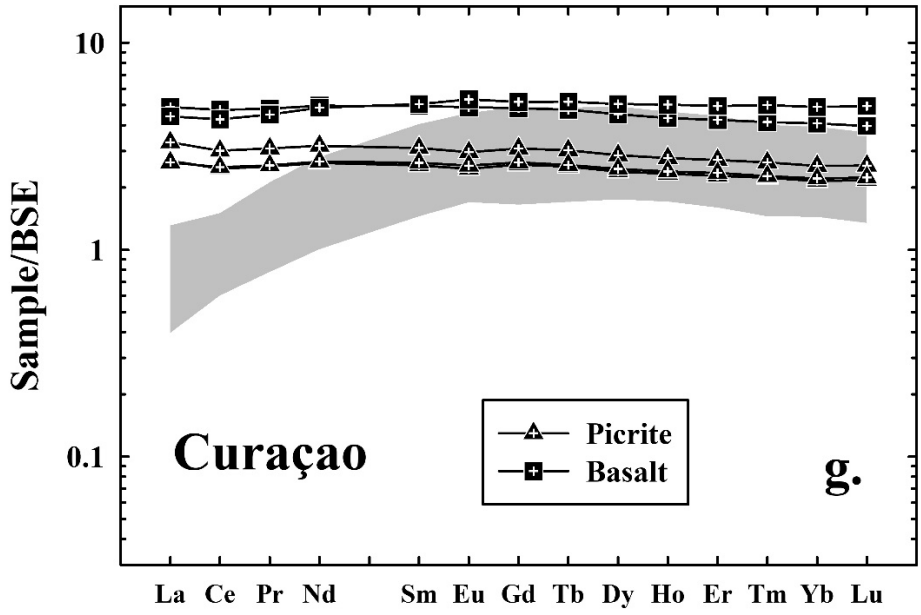
10
1
0.1
Sample/BSE
Curaçao
Picrite
Basalt
g.
La Ce Pr Nd Sm Eu Gd Tb Dy Ho Er Tm Yb Lu

Figure 3a-g.

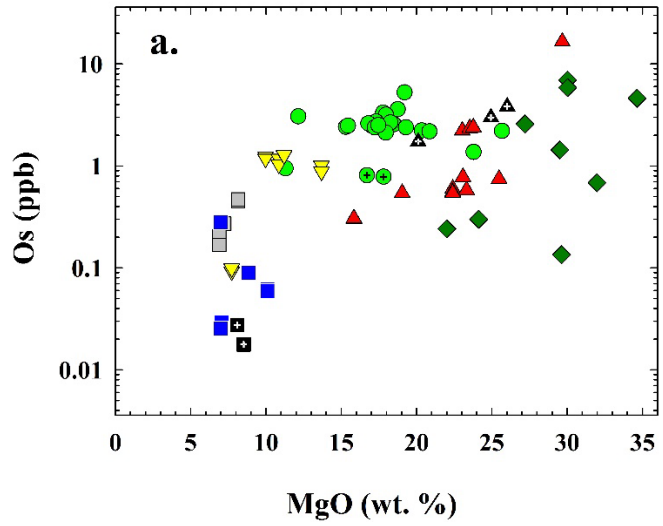
a.
Os (ppb)
10
1
0.1
0.01
0
5
10
15
20
25
30
35
MgO (wt. %)

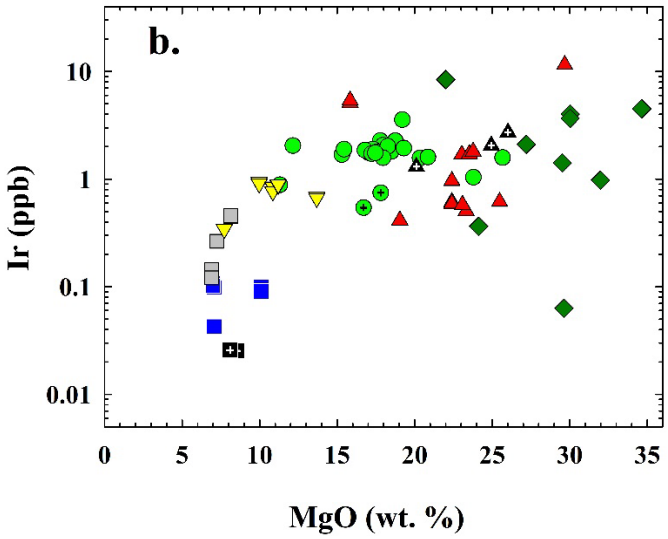
b.
Ir (ppb)
10
1
0.1
0.01
0
5
10
15
20
25
30
35
MgO (wt. %)

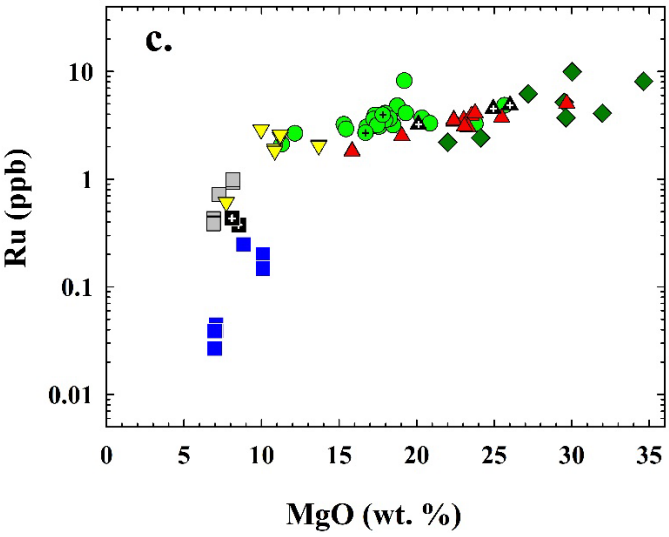
c.
Ru (ppb)
10
1
0.1
0.01
0
5
10
15
20
25
30
35
MgO (wt. %)

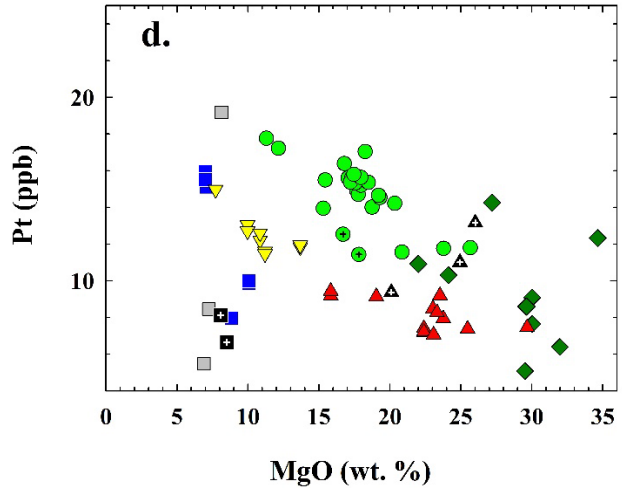
d.
Pt (ppb)
20
10
0
5
10
15
20
25
30
35
MgO (wt. %)

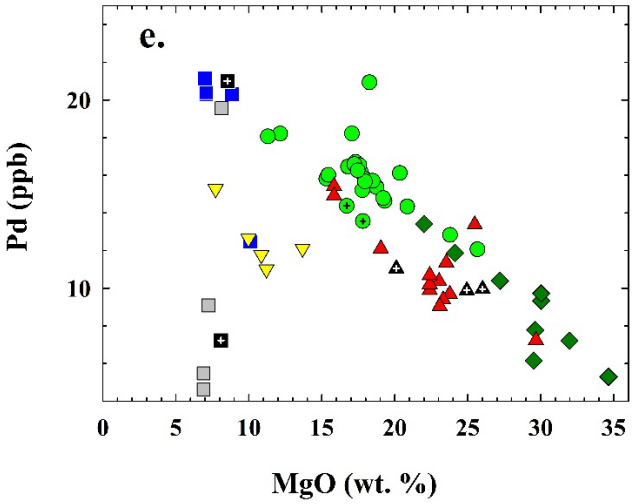
e.
Pd (ppb)
20
10
0
5
10
15
20
25
30
35
MgO (wt. %)

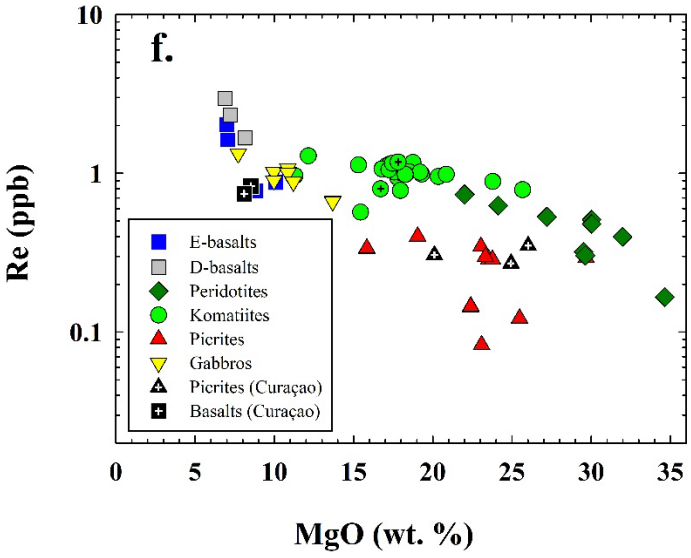
f.
Re (ppb)
10
1
0.1
E-basalts
D-basalts
Peridotites
Komatiites
Picrites
Gabbros
Picrites (Curaçao)
Basalts (Curaçao)
0
5
10
15
20
25
30
35
MgO (wt. %)

Figure 4a-f.

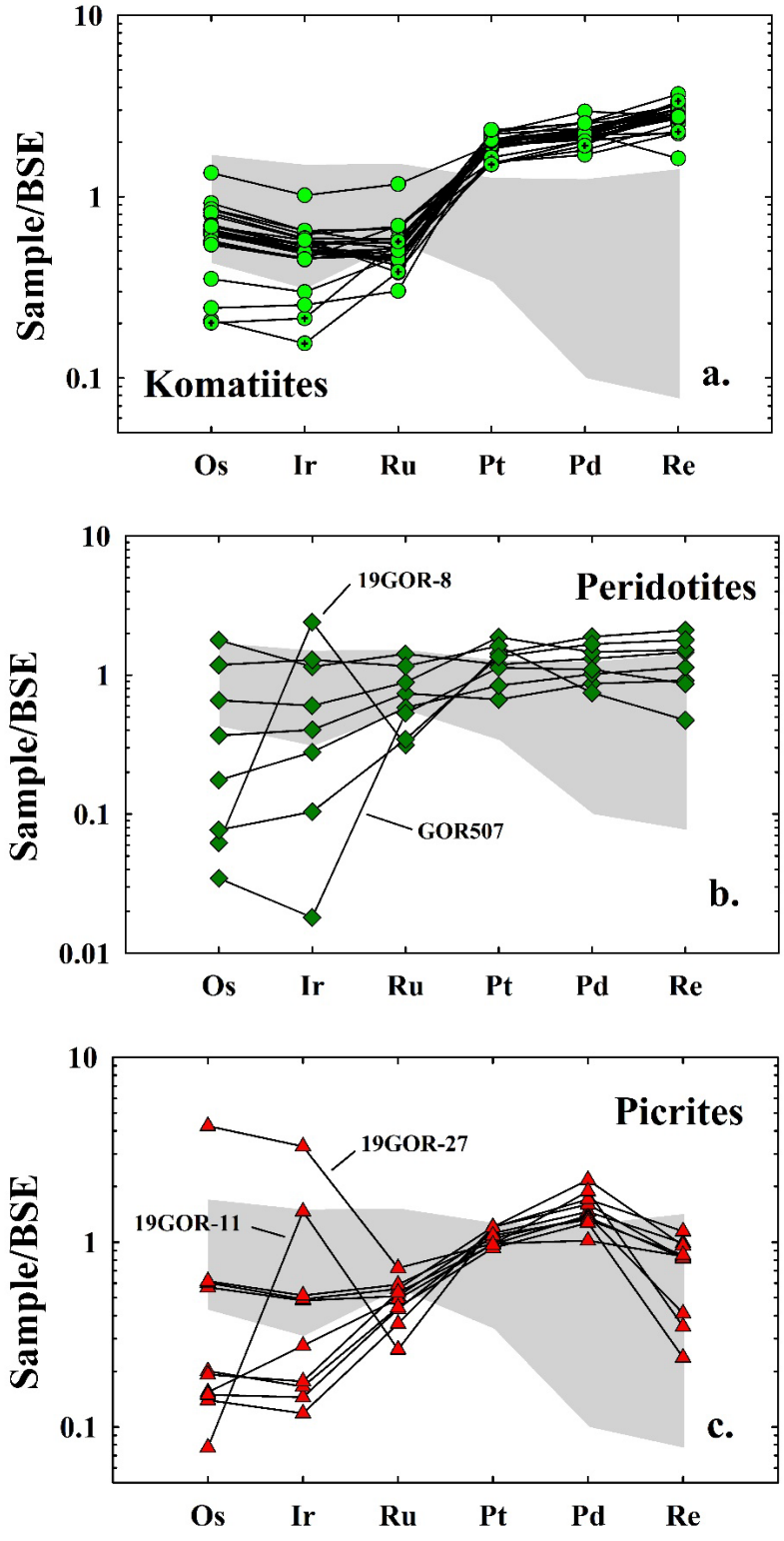
10
1
0.1
Sample/BSE
Komatiites
a.
Os
Ir
Ru
Pt
Pd
Re
10
1
0.1
0.01
Sample/BSE
19GOR-8
Peridotites
GOR507
b.
Os
Ir
Ru
Pt
Pd
Re
10
1
0.1
Sample/BSE
19GOR-27
19GOR-11
Picrites
c.
Os
Ir
Ru
Pt
Pd
Re

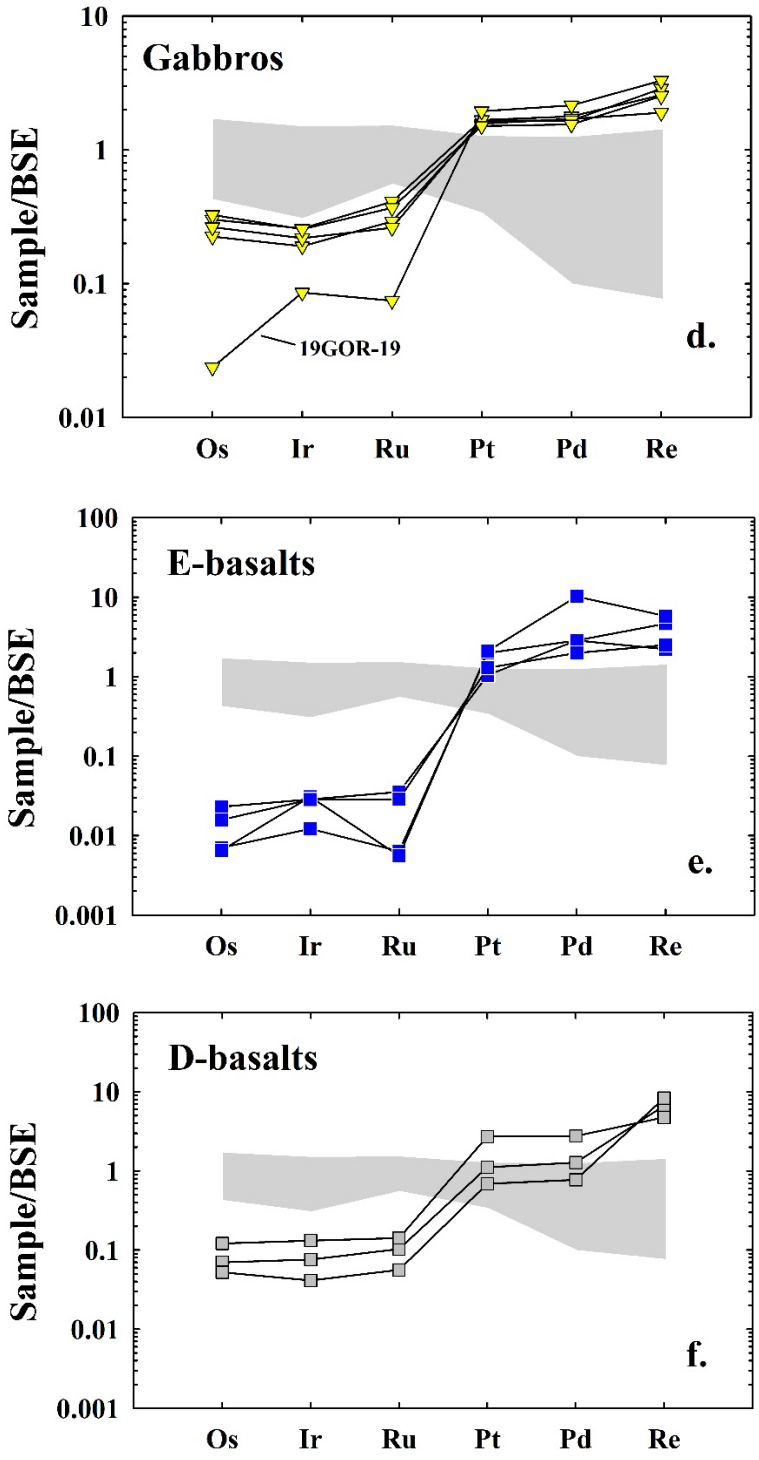
Gabbros
Sample/BSE
10
1
0.1
0.01
19GOR-19
d.
Os
Ir
Ru
Pt
Pd
Re
E-basalts
Sample/BSE
100
10
1
0.1
0.01
0.001
e.
Os
Ir
Ru
Pt
Pd
Re
D-basalts
Sample/BSE
100
10
1
0.1
0.01
0.001
f.
Os
Ir
Ru
Pt
Pd
Re

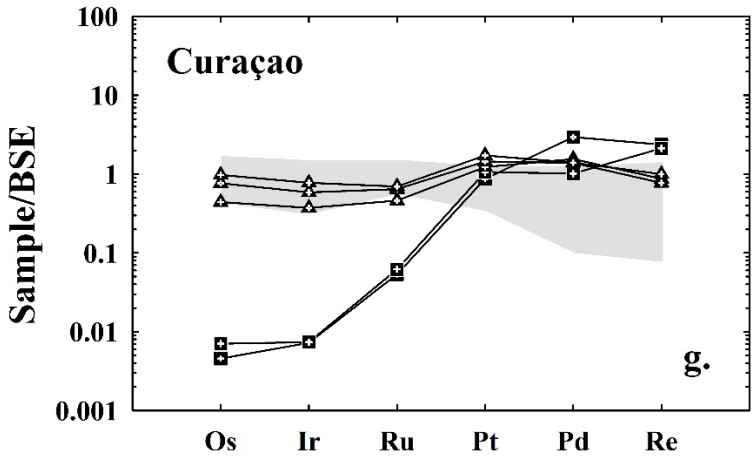

Figure 5a-g.

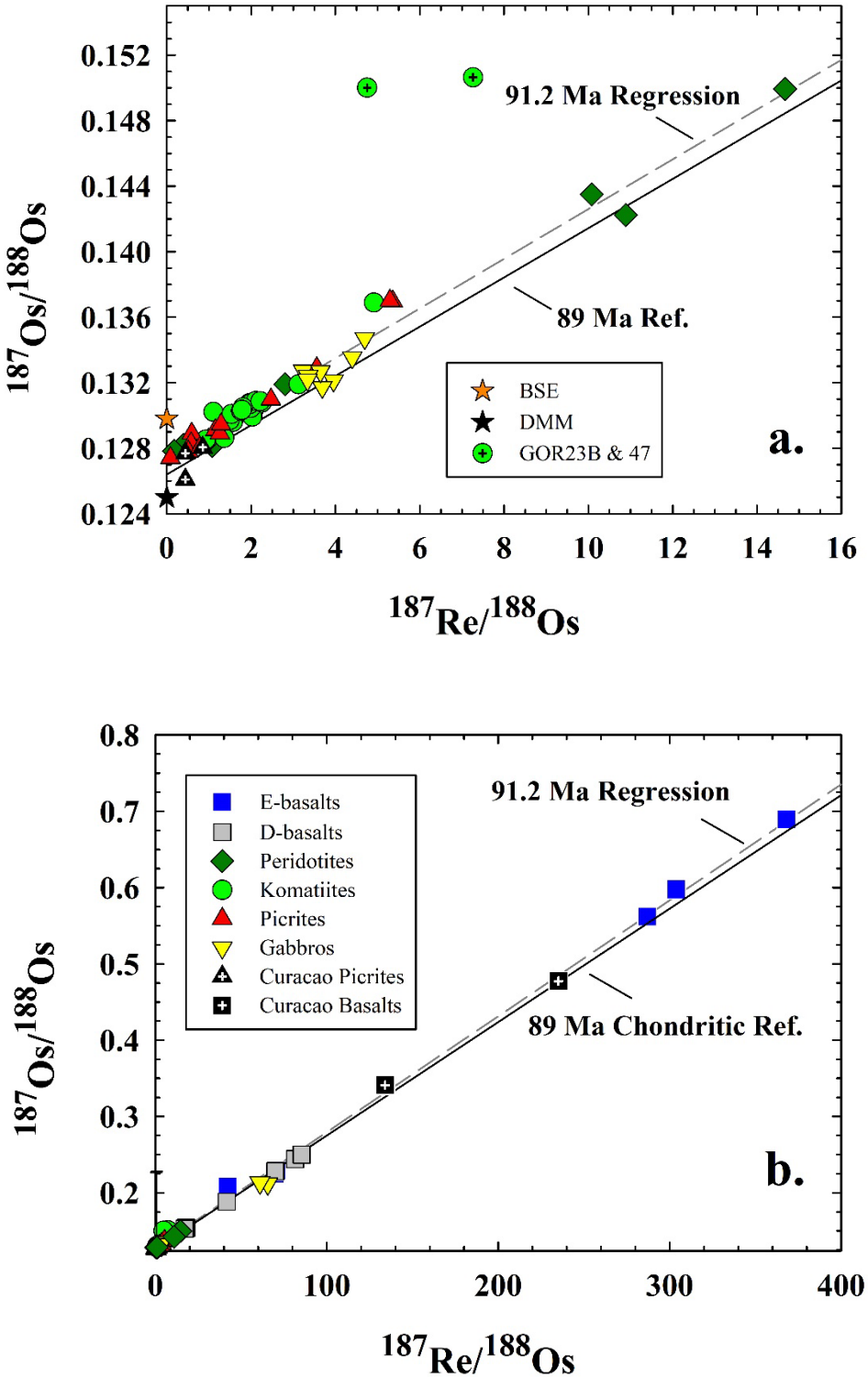
0.152
0.148
0.144
0.140
0.136
0.132
0.128
0.124
$^{187}Os/^{188}Os$
0
2
4
6
8
10
12
14
16
$^{187}Re/^{188}Os$
91.2 Ma Regression
89 Ma Ref.
BSE
DMM
GOR23B & 47
a.
0.8
0.7
0.6
0.5
0.4
0.3
0.2
$^{187}Os/^{188}Os$
0
100
200
300
400
$^{187}Re/^{188}Os$
E-basalts
D-basalts
Peridotites
Komatiites
Picrites
Gabbros
Curacao Picrites
Curacao Basalts
91.2 Ma Regression
89 Ma Chondritic Ref.
b.

Figure 6a-b.

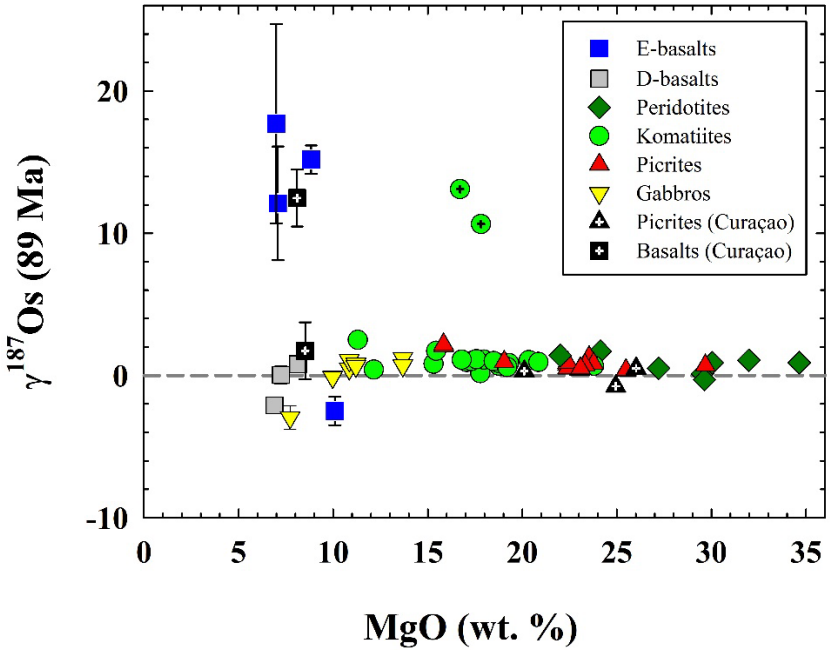

Figure 7.

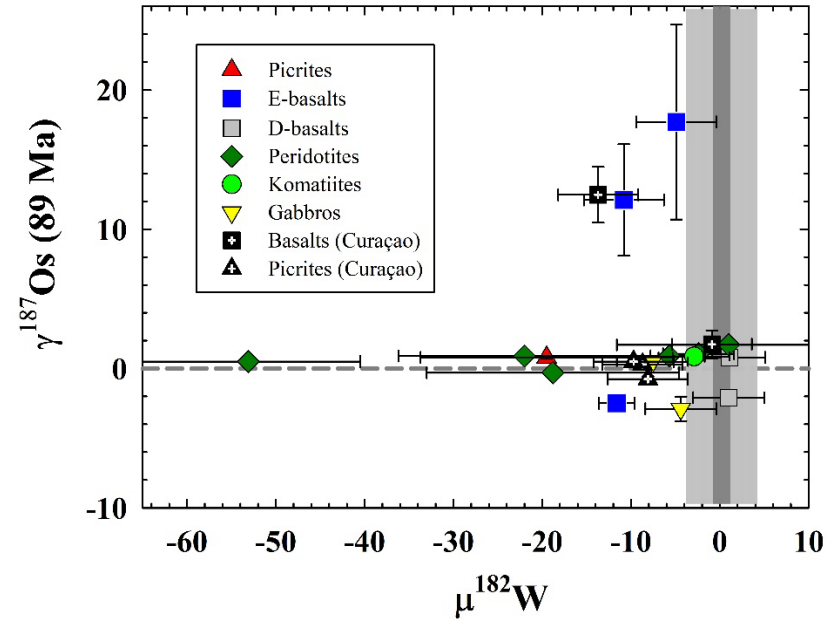

Figure 8.

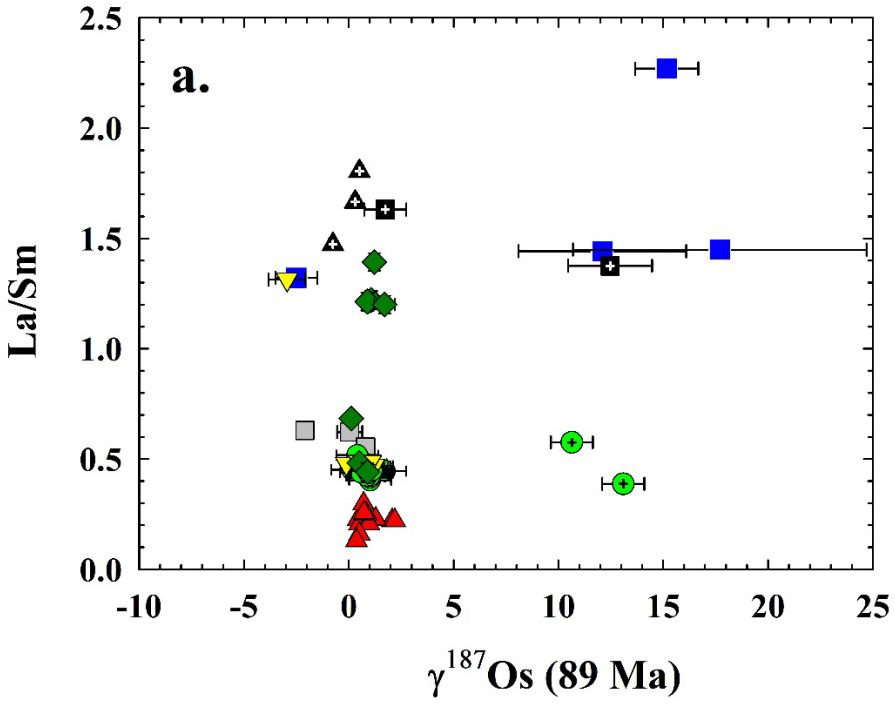
a.
La/Sm
γ^{187}Os (89 Ma)
2.5
2.0
1.5
1.0
0.5
0.0
-10
-5
0
5
10
15
20
25

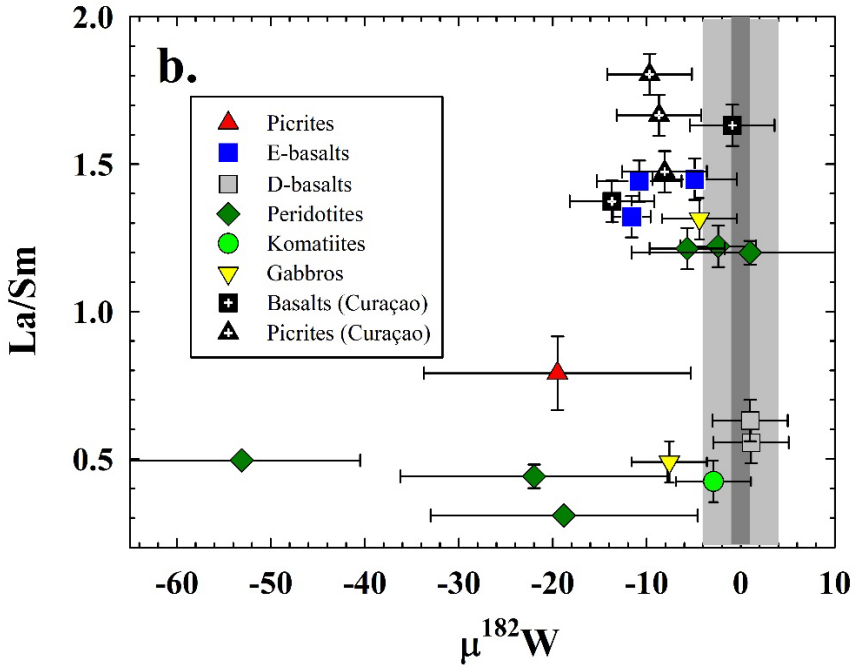
b.
Picrites
E-basalts
D-basalts
Peridotites
Komatiites
Gabbros
Basalts (Curaçao)
Picrites (Curaçao)
La/Sm
μ^{182}W
2.0
1.5
1.0
0.5
-60
-50
-40
-30
-20
-10
0
10

Figure 9a-b.

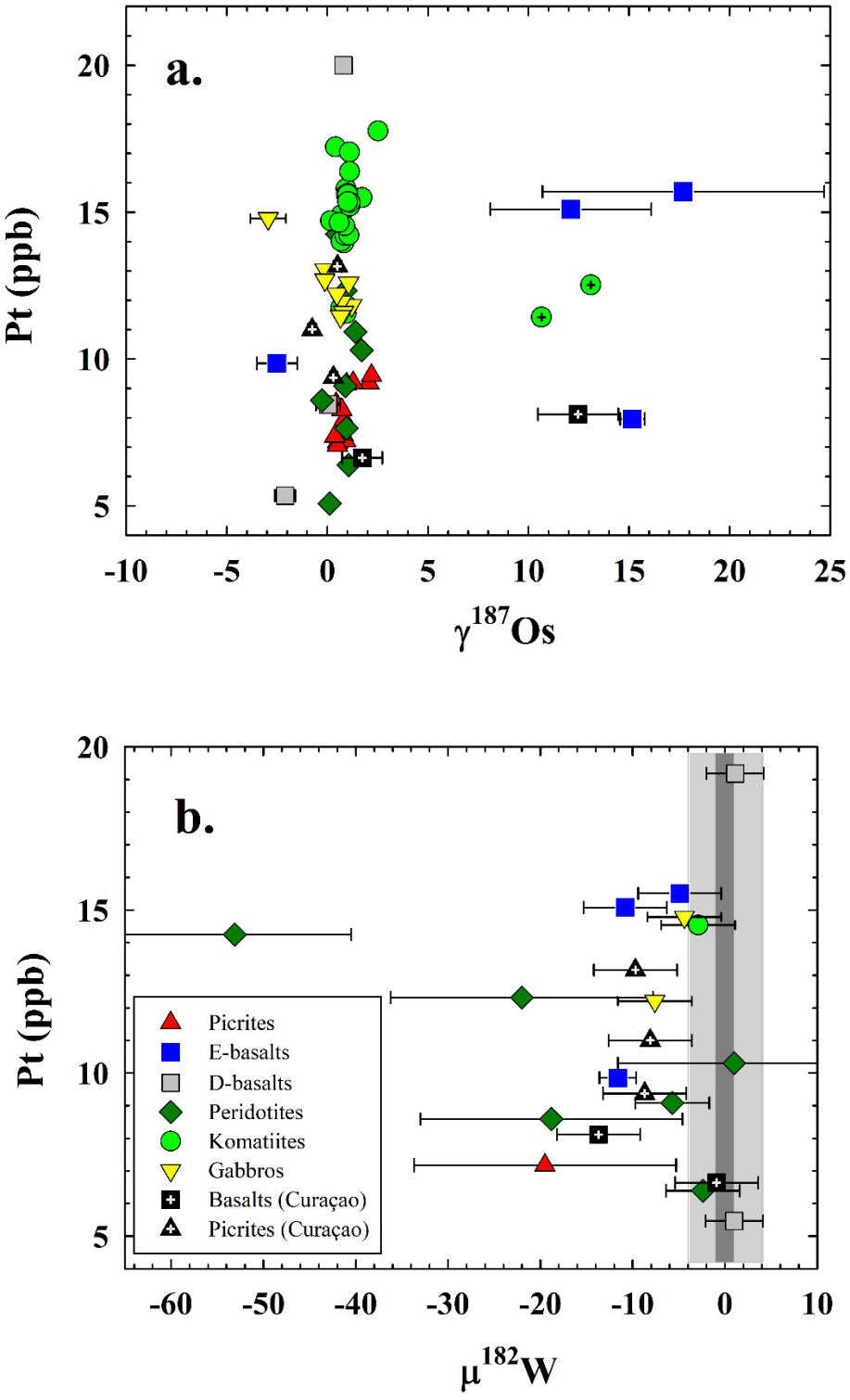
a.
Pt (ppb)
20
15
10
5
-10
-5
0
5
10
15
20
25
γ187Os
b.
Pt (ppb)
20
15
10
5
-60
-50
-40
-30
-20
-10
0
10
μ182W
Picrites
E-basalts
D-basalts
Peridotites
Komatiites
Gabbros
Basalts (Curaçao)
Picrites (Curaçao)

Figure 10a-b.

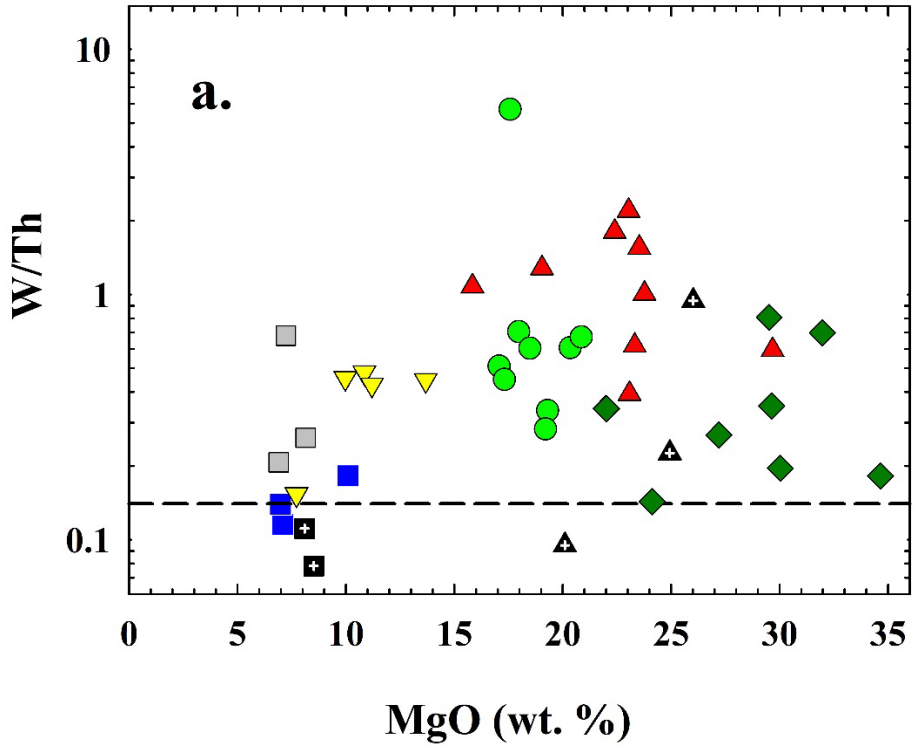
a.
W/Th
10
1
0.1
0
5
10
15
20
25
30
35
MgO (wt. %)

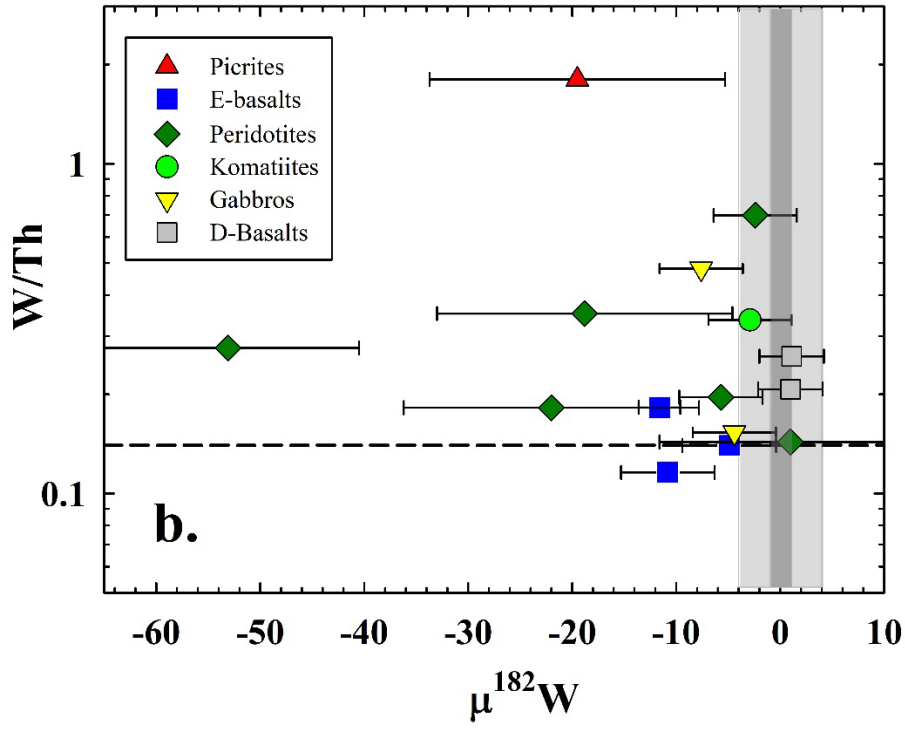
Picrites
E-basalts
Peridotites
Komatiites
Gabbros
D-Basalts
b.
W/Th
1
0.1
-60
-50
-40
-30
-20
-10
0
10
μ182W

Figure 11a-b.

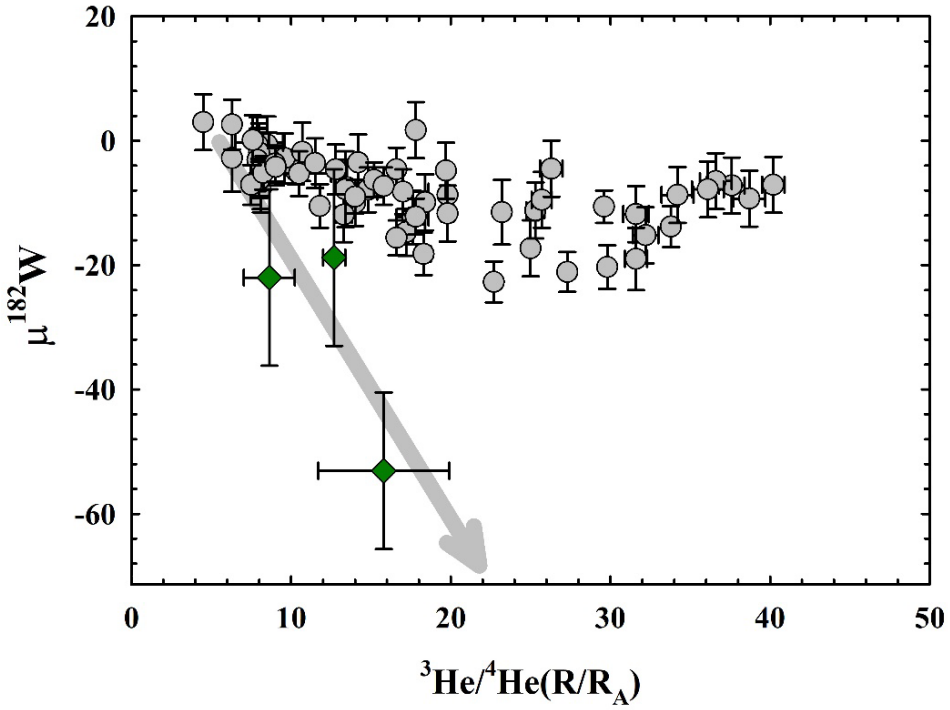

Figure 12.

Appendix A. Supplementary Material

^{182}W and ^{187}Os Constraints on the Origin of Siderophile Isotopic Heterogeneity in the Mantle

Richard J. Walker[a], Andrea Mundl-Petermeier[a,b], Igor S. Puchtel[a], Robert W. Nicklas[c], Jan L. Hellmann[a], Lina M. Echeverría [d], Kyle D. Ludwig[a], Katherine R. Bermingham[e], Esteban Gazel[f], Charlotte L. Devitre[f], Matthew G. Jackson[g], Catherine Chauvel[h]

a - Department of Geology, University of Maryland, College Park, MD, USA
b - University of Vienna, Department of Lithospheric Research, 1090 Vienna, Austria
c - Department of Earth and Environmental Sciences, Boston College, Chestnut Hill, MA, USA
d - Corning Inc. retired.
e - Department of Earth and Planetary Science, Rutgers University, Piscataway, NJ, USA
f - Department of Earth and Atmospheric Sciences, Cornell University, Ithaca, NY, USA
g - Department of Earth Science, University of California Santa Barbara, Santa Barbara, CA, USA
h - Université Paris Cité, Institut de Physique du Globe de Paris, CNRS, F-75005 Paris, France

email addresses for authors:
Richard Walker: rjwalker@umd.edu
Andrea Mundl-Petermeier: andrea.mundl@univie.ac.at
Igor Puchtel: puchtel@umd.edu
Robert Nicklas: nicklasr@bc.edu
Jan Hellmann: hellmann@umd.edu
Lina Echeverría: lina.echeverria2@gmail.com
Kyle Ludwig: kyle.ludwig.kl@gmail.com
Katherine Bermingham: kb1012@eps.rutgers.edu
Esteban Gazel: egazel@cornell.edu
Charlotte L. Devitre: cld243@cornell.edu
Matthew G. Jackson: jackson@geol.ucsb.edu
Catherine Chauvel: chauvel@ipgp.fr

Corresponding Author: Richard J. Walker: rjwalker@umd.edu

Submitted to *Geochimica et Cosmochimica Acta:* June 28, 2023

October 20, 2023 Revision

1. Sample Preparation and Analytical Methods

Picrite and basalt samples from both islands range from fresh, with minimal alteration, to highly serpentinized. Because of the known presence of W contamination in the Gorgona powders produced during the 1980's, presumably as a result of the use of metal-rich processing equipment, pieces of the remaining bulk rock samples from the earlier sample collection campaigns were reprocessed into new sample powders using metal-free equipment. Powders were prepared from each sample via a multi-step process. First, altered outer portions of the rocks were cut off using a diamond rock saw. The cut surfaces were then abraded using SiC sandpaper to remove possible saw blade contamination. The abraded chunks were then crushed using a jaw crusher armed with alumina ceramic jaw plates, and then ground to fine consistency powders using first a shatterbox armed with an alumina ceramic grinding container and puck, and then an alumina ceramic disk mill.

Whole-rock major element concentrations for most samples were commercially determined by X-ray fluorescence (XRF) analysis at Franklin and Marshall College, Lancaster, PA, USA. The measurements were made using a *PANalytical 2404* XRF vacuum spectrometer, as per methods detailed in Boyd and Mertzman (1987) and Mertzman (2000). Sample powders were initially heated to determine loss on ignition (LOI), then mixed with lithium tetraborate, added to a Pt crucible, and heated until molten. The molten material was then transferred to a Pt casting dish and rapidly cooled, resulting in a glass disk that was then used for XRF analysis. The working curves for each element were determined by analyzing geochemical rock standards (Abbey, 1983; Govindaraju, 1994; Mertzman, 2000). For major elements with concentrations >0.5%, the typical accuracy of the analyses was ±1%, as estimated by repeated mesurements of USGS GRM BCR-1, BHVO-1, and BIR-1 (see **Table S2**). Accuracy of ± 5% was typically obtained for minor elements in concentrations <0.5%. The total measured Fe_2O_3 compositions were used to calculate Fe^{3+} and Fe^{2+}, based on stoichiometry (Droop, 1987). Based on repeated analyses of some samples, the 2SD reproducibility of major elements for Gorgona- Curaçao samples was typically: 1.3% for SiO_2, 1.8% for Al_2O_3, 0.9% for Fe_2O_{3Total}, 1.0% for MgO and 0.10% for CaO (in relative % terms).

The abundances of lithophile trace elements in the whole-rock samples were determined at either the University of Maryland (UMd) using the standard addition solution inductively-coupled plasma mass spectrometry (SA ICP-MS) method, or at Scripps Institution of Oceanography (SIO) using the standard sample bracketing ICP-MS method, following the protocols detailed in Puchtel et al. (2016) and Nicklas et al. (2019). The sample solutions were analyzed on either a *Thermo Finnigan Element 2* sector field ICP-MS at the UMd *Plasma Laboratory* (*PL*), or using a *Thermo iCAP* ICP-MS at SIO. The external precision and accuracy (2SD) of the procedures were previously determined to be ~5% for all the elements of interest based on replicate analyses of USGS GRM BIR-1 and BCR-1 (Puchtel et al., 2016; Nicklas et al., 2019)(**Table S2**).

Major element abundances for sample CUR13-6 were obtained using XRF at the *GeoAnalytical Lab* at Washington State University (WSU) (Johnson et al., 1999). To provide a measure of the accuracy of the method, a USGS reference material BCR2 was processed as a powder with the sample unknown and characterized for major during the same analytical session.

Trace element concentrations for this rock were obtained at UMd using the methods described above.

Highly siderophile element concentrations were determined by isotope dilution combined with Carius tube digestion. The blank corrections were negligible for all elements (<0.2%), except for Os and Ir in certain basalts with low concentrations. Osmium and Ir blank corrections ranged to as high as 3 and 6%, respectively, for basalt 19GOR-22. Osmium concentration and isotopic measurements were obtained using negative thermal ionization mass-spectrometry (NTIMS). All Os samples were analyzed using a secondary electron multiplier detector of a *Thermo Fisher Triton Plus* mass spectrometer at the *Isotope Geochemistry Laboratory* (IGL), UMd. The measured isotopic ratios were corrected for mass-fractionation using $^{192}Os/^{188}Os = 3.083$. The internal precision of measured $^{187}Os/^{188}Os$ for all samples was between 0.05-0.2% relative (2SE). The $^{187}Os/^{188}Os$ ratio of 300–500 pg loads of the in-house *Johnson-Matthey* Os standard measured during the period of data collection averaged 0.11367 ± 11 (2SD, N = 10). This value characterizes the external precision of the isotopic analysis (~0.10%). Given the good agreement (better than 0.10%) between ratios measured for the standard and the absolute ratio previously determined for the standard, no corrections were made for instrumental bias.

The isotope dilution measurements of Re, Ir, Ru, Pt, and Pd were performed at the *PL* via multi-collector inductively-coupled plasma mass-spectrometry (MC-ICP-MS) using either a *Nu Instruments Nu Plasma* mass spectrometer and a triple electron multiplier configuration in static mode, or a *Thermo Fisher Neptune Plus* with multiple faraday cup detectors, also in static mode. Isotopic mass fractionation was monitored and corrected for by interspersing samples and standards. The results from these runs agreed within 0.5% for Re and Ir, and within 2% for Ru, Pt, and Pd, with fractionation-corrected values obtained from measurements of undiluted solutions of iron meteorites using Faraday cups of the same instrument with a signal of >100 mV for the measured isotopes. Therefore, we cite ±2% as the uncertainty on the concentrations of Ru, Pt, and Pd, ±0.5% for Ir, ±0.3% for Re, and ±0.1% as the uncertainty on the concentrations of Os obtained using NTIMS. The uncertainty on the Re concentration was the main source of uncertainty for the Re/Os ratio, which is conservatively estimated to be ±0.5%. The uncertainty on the $^{187}Os/^{188}Os$ ratio used for isochron calculations was either the external reproducibility of the *Johnson-Matthey* Os laboratory standard run during the analytical campaign, or the in-run precision of the individual analyses, whichever was greater, typically 0.10%. The initial $\gamma^{187}Os$ values for individual samples were calculated as the percent deviation of their isotopic composition at 89 Ma relative to the chondritic reference model of Shirey and Walker (1998).

High-precision W concentrations were determined by the isotope dilution method for samples destined for ^{182}W analysis. Approximately 100 mg of powdered sample was digested in 6 mL concentrated $HF:HNO_3$ (5:1) for five days at 160°C, together with appropriate amounts of a ^{182}W spike. After complete dissolution, the samples were dried down and subsequently converted to chloride form by repeated dry downs in 8M HCl. After evaporation to dryness, residues were picked up in a loading solution (0.5M HCl-0.5M HF) and W was separated using an anion-exchange column chemistry similar to that discussed in Kleine et al. (2004). Tungsten

concentrations were measured using a *Thermo Fisher iCap RQ* quadrupole ICP-MS at the Department of Lithospheric Research, University of Vienna, or at the PL using a *Thermo Fisher Neptune Plus* MC ICP-MS.

Tungsten isotope compositions were measured in negative thermal ionization mode (N-TIMS) using a *Thermo Fisher Triton* at the UMd and a *Triton XT* Thermal Ionization Mass Spectrometers at the Department of Lithospheric Research, University of Vienna. The analytical method comprises two acquisition lines with 34 s integration and 10 s idle time. Amplifiers equipped with 10^{11} Ω resistors were rotated after each block. A 360 s baseline measurement was performed before every block each consisting of 20 cycles. Source lens focus and peak centers were done before every second and sixth block, respectively. A total of 28 blocks of data were collected during each measurement. To correct for per-integration oxide interferences, $^{186}W^{16}O_2{}^{18}O$ and $^{187}Re^{16}O_2{}^{18}O$ were measured with every run using amplifiers equipped with 10^{12} Ω (Triton) and 10^{13} Ω (Triton XT) resistors. Isotope ratios were corrected for instrumental mass bias by normalizing to $^{186}W/^{183}W=1.98594$ or $^{186}W/^{184}W=0.92767$ (Völkening et al., 1991). All data are reported as $\mu^{182}W$ and $\mu^{183}W$ notations, which represent the deviations of $^{182}W/^{184}W$ and $^{183}W/^{184}W$, respectively, of a given sample from that of repeated measurements of the UMd and Vienna *Alfa Aesar* laboratory W standard solutions within a sample campaign. The average $\mu^{183}W$ of all samples analyzed in this study is identical within uncertainties to the average *Alfa Aesar* W standard data (0.6 ±5.0, 2SD, n=14).

For the low W abundance samples for which we had limited quantities of sample (GOR-503, GOR-507, GOR-509, GOR-535, and 19GOR-7 duplicate; ~2 to 14 ppb W), W isotopic compositions were measured using MC-ICPMS, allowing accurate measurements, albeit with less precision, with only ~30 ng of W. Sample powders were dissolved in a 5:1 HF–HNO_3 mixture for five days at 140 °C, followed by 3:1 HCl–HNO_3 for 24 h at 130 °C. After repeated dry downs in 6 M HCl–0.06 M HF samples were re-dissolved in concentrated HF for 24 h at 100 °C. Fluorides were removed from the sample solution by centrifugation, followed by repeated rinsing in HF and H_2O. Combined sample solution and rinses were dried down and converted to chloride form using 6 M HCl–0.06 M HF. Tungsten purification followed a two-stage anion exchange chromatography described in Hellmann et al. (2019), where each samples was divided over three to five aliquots for column separation. Following the second stage, W cuts were recombined and the clean-up stage was repeated using a single column. After each stage, organics were removed from the eluents by repeated dried downs in HNO_3–H_2O_2 and then final W cuts were dissolved in 0.56 M HNO_3–0.24 M HF.

The low abundance W isotope measurements were performed using a *Thermo Fisher Neptune Plus* MC-ICPMS at UMd. Samples were introduced using a *Cetac Aridus* 3 desolvator and a *Savillex* C-flow nebulizer at an uptake rate of 50 µL/min. Total ion beam intensities of ~2×10^{-10} A were obtained for a ~30 ppb W solution, using Jet sampler and X skimmer cones. Each measurement consisted of 60 s baseline integrations, followed by 200 isotope ratio measurements of 4.2 s each. Each sample analysis was bracketed by measurements of an *Alfa Aesar* W standard solution, and sample and standards were analyzed at similar ion beam intensities.

Isobaric Os interferences on ^{184}W and ^{186}W were monitored on mass ^{188}Os and were negligible for all samples. Instrumental mass bias was corrected relative to $^{186}W/^{183}W = 1.98594$ or $^{186}W/^{184}W = 0.92767$ using the exponential law. In this study, we used $^{186}W/^{184}W$-normalized ^{182}W data to avoid normalizations involving ^{183}W, which can be biased by a small analytical artifact resulting from odd-even isotope effects (Willbold et al., 2011; Kruijer et al., 2012; Cook and Schönbächler, 2016; Budde et al., 2022). This effect, in the form of ^{183}W deficits, is present in all the samples analyzed by ICP-MS in the present study (**Table S4**). The extent of the ^{183}W deficits (i.e., $\mu^{183}W$ (6/4) of –3 to –20) is consistent with that obtained for *e.g.,* Samoan and Hawaiian ocean island basalts analyzed using MC-ICP-MS (Archer et al., 2023). Note that ^{183}W deficits could also be of nucleosynthetic origin and would be accompanied by negative $\mu^{182}W$ values. In a plot of $\mu^{182}W$ versus $\mu^{183}W$ (**Fig. S10**), however, samples do not plot along a theoretical *s*-process line (Bisterzo et al., 2011), suggesting that the variation in ^{182}W is purely radiogenic in origin.

The accuracy of the analytical procedure was assessed through measurements of 19GOR-7, which was also analyzed by N-TIMS. The $\mu^{182}W$ of -3.0 ± 13.0 determined using MC-ICPMS is indistinguishable from -2.4 ± 4.5 obtained by N-TIMS, indicating accurate sample analyses for samples with limited W.

2. Overview of the Origins of Gorgona Rocks from Prior Studies

Several studies have concluded that the Gorgona suite was produced by dynamic melting of a chemically and isotopically heterogeneous mantle plume at various depths within and above the garnet stability field (Arndt e al., 1997; Révillon et al. 2000; 2002; Kerr, 2005). Arndt et al. (1997) reasoned that an incompatible trace element depleted plume component initially produced an incompatible trace element-enriched melt through low degrees of partial melting at high pressures, and that this stage of melting led to further chemical depletion in the residual plume materials. Subsequent dynamic melting of the rising plume sequentially generated the komatiites and picrites characterized by increasingly greater chemical depletion. Arndt et al. (1997) concluded that at the stage the picritic melts were produced, the source mantle was considerably more depleted in incompatible trace elements than the present source of mid-ocean ridge basalts (MORB). Because there is no physical evidence of rocks that crystallized from the putative initial enriched melts, it was inferred that these melts did not reach the surface. Chemical similarities between the komatiites, peridotites, and gabbros have led to the interpretation that some of the peridotites and gabbros formed by crystallization in magma chambers that fed the eruption of the komatiites (e.g., Révillon et al., 2000).

3. Lithophile Element Compositions.

The major and lithophile trace element data for Gorgona and Curaçao are consistent with previous studies and indicate contributions from both chemically depleted and enriched, or less depleted mantle source components (e.g., Echeverría, 1980; Aitken and Echeverría, 1984; Révillon et al., 1999, 2000, 2002; Kerr, 2005; Serrano et al., 2011). The incompatible trace element depleted

characteristics of the komatiites and related intrusive rocks require derivation from a chemically strongly depleted source component (e.g., Révillon et al., 2000). Picrites with MgO concentrations that overlap with the komatiite suite are characterized by the greatest depletions in the LREE and other incompatible lithophile trace elements in the suite, consistent with derivation from the most depleted mantle source component sampled by the Gorgona suite. The mantle sources of all these rocks are also characterized by long-term geochemical depletion evidenced by positive ε_{Nd} and ε_{Hf} values. Arndt et al. (1997) concluded that the source(s) of these rocks underwent dynamic melting in a rising plume. Conversely, the chemical and modest isotopic enrichments of the E-type rocks, relative to the depleted rocks, indicate derivation from a separate mantle source component. Most prior studies have attributed this presumed enrichment to the presence of a recycled lithospheric component (e.g., Révillon et al., 2002; Thompson et al., 2003), but the compositions could also reflect a source with less long-term chemical depletion, rather than re-enrichment.

The Curaçao basalts of this study have incompatible lithophile trace elements compositions broadly similar to the Gorgona E-basalts. The Curaçao picrites are chemically enriched relative to any rocks in the Gorgona suite with similar MgO (**Fig. S2a-d**). As with the Gorgona E-type rocks, these relative enrichments may indicate a recycled lithospheric component in their mantle source, or more limited prior depletion (e.g., Klaver, 1987; Révillon et al., 1999).

4. Abundances of HSE in the Mantle Source of the Dominant Komatiites

In order to estimate the absolute and relative abundances of HSE in the dominant Gorgona komatiite mantle source, the approach of Puchtel et al. (2004) is applied. This method combines HSE abundance and Re-Os isotopic data for a suite of komatiitic lavas believed to be derived from a common primary magma that are related by fractional crystallization of olivine after lava emplacement.

Given the strongly chalcophile nature of HSE, the sulfide saturation status of the primary magma to the Gorgona komatiites during both separation from the mantle melting source region, and during emplacement must be established before the HSE abundances in the mantle source can be estimated. Towards this end, Steenstra et al. (2020) presented a refined parameterization model for calculating S concentration at sulfide saturation (SCSS) in silicate liquids as a function of *P*, *T*, and major and trace element abundances. This model is applied here to determine the sulfide saturation status of the parental magma to the Gorgona komatiites.

In order to calculate the *P*-*T* parameters of the magma generation of the komatiites, the mantle melting parameterization models of McKenzie and Bickle (1988), Herzberg and Asimow (2008), Herzberg and Gazel (2009), and Herzberg et al. (2010), and the major element composition of a Gorgona emplaced komatiite lava flow from Nicklas et al. (2019) were used. These calculations suggest that the mantle potential temperature, T_{pot} at melting initiation, was ~1600°C, the liquidus temperature T_{liq} at magma emplacement was ~1420°C, and the depth of melting initiation D_{init} was ~140 km, which translates into a pressure of 4.4 GPa. This estimate of the depth of melting initiation defines the maximum depth of the komatiite magma separation from its mantle source, and is broadly consistent with prior estimates (e.g., Herzberg, 1995; Arndt et al.,

1997). Because SCSS of a silicate liquid increases with decreasing pressure as silicate liquid rises towards the surface, this depth is conservatively accepted here as the depth of melting termination and separation of the komatiite magma from its source. The temperature at which melting terminated for the Gorgona komatiite system is then assumed to be equal to the temperature of melting initiation (1600°C). Further, using these parameters, the compositions of the emplaced komatiite magma from Nicklas et al. (2019), and Eq. (4) from Steenstra et al. (2020), the SCSS of the Gorgona komatiite magma upon separation from the mantle source, and upon emplacement, are calculated to be 1170 and 1660 ppm S, respectively.

In order to evaluate the sulfide saturation status of the Gorgona komatiite magma, knowledge of its S content is required. To estimate this, the S content in its mantle source, S partition coefficient, and the degree of melting must first be estimated. The average S content of the BSE is estimated to be 250 ±50 ppm (McDonough and Sun, 1995), and that of the modern DMM to be 195 ±45 to 206 ±25 ppm (Nielsen et al., 2014; Sun et al., 2020). The mantle source of the Gorgona komatiites is at least as depleted in highly incompatible lithophile trace elements as modern DMM, therefore, most likely had a S content similar to that of the DMM, i.e., ~200 ppm, or lower.

To estimate the degree of partial melting that produced the Gorgona parental komatiite magma, a batch melting model and the abundances of the moderately incompatible lithophile trace elements (e.g., Nd, Sm, Lu, Hf) in this magma and its mantle source obtained via utilizing the projection technique of Puchtel et al. (2004) and trace element partition coefficients between the major mantle phases and silicate liquid from Green (2004), were used. The degree of partial melting is calculated to be 34%. Assuming that S was moderately incompatible during the partial melting that produced the Gorgona komatiites, with the degree of incompatibility similar to that of Sm (e.g., McDonough and Sun, 1995), the primary Gorgona komatiite magma is then calculated to have contained 553 ppm S. This S content in the komatiite magma is significantly lower than the calculated SCSS of the Gorgona komatiite magma upon separation from the melting residue, and provides strong evidence for the sulfide-undersaturated nature of the Gorgona primary komatiite magma.

Given the sulfide undersaturated nature of the primary komatiite magma, least-squares linear regressions of Re, Pt, and Pd concentrations versus MgO, using ISOPLOT 3.00 (Ludwig, 2003), are used to project to source concentrations. For these calculations, we focus on samples collected from a single continuous outcrop that likely accessed different portions of the same lava flow (GOR-152 to 160). Sample GOR152 was excluded from the regressions, as it plots well off the regression lines, indicating that this sample likely experienced post-emplacement mobility of Re, Pt, and Pd. In order to better constrain the slope in the MgO versus HSE diagrams, a theoretical HSE composition of liquidus olivine in equilibrium with the emplaced komatiite lava was used for each regression calculation. The theoretical olivine is assumed to have had 0.00349 ppb Re, 0.193 ppb Pt, and 0.132 ppb Pd, based on the data for an olivine separate from the similarly well-preserved Belingwe komatiites (Puchtel et al., 2009), combined with the observation that Re, Pt, and Pd concentrations in olivine are typically very low and vary little between komatiite flows.

The MgO content for the liquidus olivine was adopted to be 49.1±0.5% MgO, based on data from Nicklas et al. (2019). The Pt and Pd regressions (**Fig. S7a-b**) have MSWD values ≤2.5, indicating strongly linear behavior, whereas the Re regression (**Fig. S7c**) has a MSWD value of ~10. The Re, Pt, and Pd abundances in the projected mantle source with a BSE MgO content of 38 wt.% (Hofmann, 1988) are calculated to be 0.396±0.038, 5.42±0.16 and 5.84±0.26 ppb, respectively. The total Re, Pt, and Pd concentrations in the Gorgona source are 78±4% of the BSE values estimated by Becker et al. (2006).

The observation that the Re-Os isotope systematics of the komatiites evidently remained undisturbed since soon after crystallization permits the application of the initial $^{187}Os/^{188}Os$ ratio of 0.12738 ±23, derived from the Re-Os isochron, to calculate a time-integrated Re/Os ratio in this mantle source. Evolution of the dominant komatiite mantle source from an early Solar System $^{187}Os/^{188}Os$ ratio of 0.09531 at 4558 Ma (Shirey and Walker, 1998) to the initial $^{187}Os/^{188}Os$ of the Gorgona komatiites at 89 Ma requires a $^{187}Re/^{188}Os$ ratio of 0.415±0.006. This time-integrated $^{187}Re/^{188}Os$ ratio is well within the range of chondritic meteorites (e.g., Walker et al., 2002). From the calculated time-integrated Re/Os ratio and estimated Re source concentration, an Os concentration of 4.51±0.43 ppb is calculated. The Os/Ir ratios of the Gorgona komatiites are very consistent, averaging 1.4±0.2 (2SD), and do not correlate with the MgO contents, indicating that the Os/Ir ratio did not notably fractionate during komatiite lava differentiation. This in turn suggests that Os and Ir also did not significantly fractionate from one another during mantle melting. Using the average Os/Ir of the samples and the Os abundance estimated for the source, the komatiite source Ir abundance is calculated to be 3.22±0.86 ppb. The Ru concentration of the mantle source, unfortunately, cannot be reliably estimated due to the complicating effect of possible chromite fractionation during the komatiite differentiation (e.g., **Fig. S6c**).

The total abundance of all the estimated HSE in the source of the Gorgona komatiites, except for Ru, is calculated to be 86±9% of those in the BSE estimates of Becker et al. (2006). The calculated HSE abundances of the komatiite source region normalized to the BSE estimate of Becker et al. (2006) are plotted in **Fig. S8**. Previous studies have reported the abundances of HSE in various upper mantle reservoirs, such as modern abyssal peridotites (Luguet et al. 2001; Alard et al. 2005; Becker et al. 2006; Liu et al. 2009), and the peridotite sections of ophiolites (Schulte et al. 2009; O'Driscoll et al. 2012; Haller et al., 2021). For comparison with Gorgona, the range of HSE abundances of abyssal peridotites (95%) is plotted on the same BSE-normalized plot**.** Except for a slight depletion in Pt, relative to the other HSE, these results show that the komatiite source region underwent little fractionation of the HSE during its history prior to their creation.

5. Additional Discussion of ^{187}Re-^{187}Os Isotopic Systematics

The presence of recycled continental crust has commonly been cited as the cause of incompatible trace element enrichment and high $^{87}Sr/^{86}Sr$ and low $^{143}Nd/^{144}Nd$ and $^{176}Hf/^{177}Hf$ in the sources of some OIB, compared with DMM, whereas elevated $^{187}Os/^{188}Os$ and $^{206}Pb/^{204}Pb$ has commonly been attributed to recycled oceanic crust (e.g., Hofmann and White, 1982; Allègre, 1982; Hauri and Hart, 1993). Contamination of intraplate magmas ascending through ancient crust can

also lead to enrichments in ^{187}Os and ^{186}Os (e.g., Day and O'Driscoll, 2019). Given that the Gorgona and Curaçao lavas did not traverse ancient crust, the latter possibility appears unlikely to explain the more radiogenic Os isotopic compositions present in some komatiites and basalts. Walker et al. (1999) showed that in order to generate the magnitude of the ^{187}Os enrichments observed in the two Gorgona komatiites by means of incorporation of a recycled oceanic crustal component, the recycled component would either have to comprise a substantial portion of the source (e.g., >30%) if the recycled component was <2 Ga, or was very old (>4 Ga) if the component comprised <15% of the source (**Fig. S11**). The presence of a substantial portion of recycled mafic (or especially felsic) crust in the source of the ^{187}Os-rich komatiites, however, was considered petrologically unlikely by Walker et al. (1999), given the komatiitic composition of the parental melt. Further, the two komatiites characterized by high $\gamma^{187}Os$ are as strongly depleted in incompatible lithophile trace elements as the dominant komatiites, as reflected in their, e.g., La/Sm ratios and initial εNd values averaging ~ +9.8. Conversely, several of the chemically enriched rocks (La/Sm>1) including three peridotites are characterized by comparatively low initial $\gamma^{187}Os$ values (**Fig. 9a**). Consequently, other geochemical data do not support an interpretation of recycled crust as the cause of the radiogenic Os compositions in the high $\gamma^{187}Os$ komatiites.

Contrary to the komatiite source, however, the presence of a recycled component remains a possible explanation to account for the elevated initial $\gamma^{187}Os$ and incompatible trace element enrichments in the Gorgona (E-type) and Curaçao basalts with elevated $\gamma^{187}Os$. Although the mixing relationships regarding the age of the recycled component remain the same as for the komatiites, the fact these rocks are mafic relaxes the limit on the proportion of the recycled component permissible in the source of these rocks. If the sources of these basalts were strongly enriched in a recycled component, in contrast to the source of the komatiites, then at least two different ^{187}Os-rich mantle sources would be implicated to explain elevated $\gamma^{187}Os$ in both suites. This seems unlikely given that the raised initial $\gamma^{187}Os$ values for both the ^{187}Os-enriched komatiites and the basalts would need to have resulted from two different processes. This possibility, nevertheless, requires further study.

The generation of a long-term high-Re/Os domain within the mantle as the result of early Earth processes, such as magma ocean crystallization, or metal-silicate segregation at high pressures, remains a plausible explanation for the ^{187}Os isotopic enrichments. Assessing the viability of such processes based solely on Os isotopic data, however, is problematic at present because of the limited information available regarding the partitioning characteristics of Re and Os at high pressures and temperatures as a result of either silicate fractionation, or metal-silicate interactions. Given that Re is a moderately incompatible trace element in silicate systems, while Os is typically compatible, it is likely that silicate fractionation would have led to the creation of high and low Re/Os ratio mantle domains, if repeated magma oceans formed and crystallized during Earth's accretion, as well as in much smaller mantle domains. As with the recycling scenario, however, collateral enrichments in incompatible lithophile elements would also be expected. For example, an incompatible element enriched (high Re/Os) mantle domain produced by silicate crystal-liquid fractionation would also be expected to result in a low Sm/Nd ratio,

relative to BSE, therefore evolving to a lowered εNd value with time. However, the two high γ^{187}Os komatiites are characterized by εNd values that are essentially identical to those of the dominant komatiites (Walker et al., 1991), consistent with strong, long-term LREE depletion. Conversely, enrichments in lithophile trace elements and lower ε^{143}Nd values are observed in the E-basalts, providing permissive evidence for early incompatible trace element enrichment in their source.

Preferential removal of Os, relative to Re, as a result of metal sinking through lower mantle assemblages during final stages of core segregation, might also have led to the formation of a lower mantle domain with elevated Re/Os ratio, compared to BSE (e.g., Touboul et al., 2012). The nature and extent of this type of fractionation, however, is poorly constrained for high pressure and temperature conditions. Metal-silicate interaction would not have significantly affected lithophile trace elements, and thus, remains a permissive process for the generation of Re/Os heterogeneities and subsequent heterogeneities in ^{187}Os/^{188}Os, without collateral effects on lithophile trace elements or isotopic systematics. Such processes occurring subsequent to the approximately 60 Ma lifetime of ^{182}Hf would also have had no impact on μ^{182}W.

Core-mantle interaction scenarios are also potentially appealing to account for the isotopic compositions of certain siderophile elements, such as Os (and W), especially where no accompanying complementary lithophile elemental or isotopic effects are observed. Core-mantle interactions have been proposed to account for geochemical observations for certain OIB including those characterized by high ^{3}He/^{4}He (Bouhifd et al., 2020), negative μ^{182}W values (Rizo et al., 2019), and elevated γ^{187}Os (Walker et al., 1997). The presumption of elevated γ^{187}Os contributed from the outer core was initially based upon the assumption that solid metal-liquid metal partitioning under the conditions of Earth's core are similar to those observed for asteroidal cores, which are sampled in the form of iron meteorites. It also requires that the inner core has been present through much of Earth history, given that the limited mass of the inner core could only sparingly raise the Re/Os ratio of the outer core. Because the crystallization of solid metal also leads to an increase in Pt/Os ratio in the fractionated liquid, the concept was subsequently advanced to include a prediction of coupled ^{186,187}Os enrichment in mantle that incorporated outer core metal, with possible examples associated with putative Siberian and Hawaiian plumes (Walker et al., 1997; Brandon et al., 1998). Coupling the ^{187}Re-^{187}Os and ^{190}Pt-^{186}Os systems, Brandon et al. (2003) reported that certain Gorgona komatiites plot along a postulated mixing curve between ambient upper mantle and a high ^{186,187}Os/^{188}Os component that was suggested to be the outer core.

The interpretation of coupled ^{186,187}Os enrichments resulting from direct core-mantle interactions has subsequently been criticized, as more recent studies of the thermal modeling of the Earth and magnetic studies have concluded that the inner core started forming only within the last 1 Ga (e.g., Labrosse, 2018; Bono et al., 2019; Zhou et al., 2022). The application of low pressure partition coefficients (e.g., Chabot et al., 2008) for the Re-Pt-Os systems suggests that such late crystallization of the inner core would not allow sufficient enrichment in Re and Pt, relative to Os, to account for the Gorgona rocks with elevated initial ^{186,187}Os. Further, the abundances of HSE in the mantle source of Gorgona rocks inferred here (86 ± 9% BSE) from Pt

and Pd abundances, including the two komatiites with elevated γ^{187}Os, are similar to BSE. Consequently, there is no supporting evidence for the physical incorporation of HSE-rich, outer core metal into the Gorgona source mantle, as might occur via metal entrainment into a plume rising from the core-mantle boundary. Alternatively, reactions between FeO-FeS-Fe liquids at the core-mantle boundary, with accompanying fractionation of Re/Pt/Os, have also been proposed as a possible means of generating coupled Os isotopic enrichments in some plume-derived systems, without appreciable accompanying HSE enrichment (Humayun et al., 2004; Humayun, 2011). Subsequent studies of ^{186}Os in the mantle have also suggested that intra-mantle sulfide metasomatism can potentially generate domains with coupled high Re/Os and Pt/Os ratios that, with time, could lead to the observed coupled isotopic enrichments of ^{187}Os and ^{186}Os (e.g., Luguet et al., 2008). These possibilities remain valid with respect to the Os isotopic enrichments observed.

The new HSE data reveal that the two komatiites characterized by the highly radiogenic γ^{187}Os values (GOR-23B, GOR-47) also have the most fractionated patterns of the komatiite suite, with the most depleted Os and Ir concentrations, relative to Re and Pt (**Fig. 5a**). If the high Re/Os ratio is a long-term characteristic of a mantle source component, rather than having been produced by crystal-liquid fractionation, or other processes at or near the time of mantle melting to produce the parental melt, the fractionated ratio could explain the high initial γ^{187}Os values. The initial ^{186}Os/^{188}Os ratios of these komatiites have not been determined because of limited amount of material available, so it remains unknown whether the mantle sources of these rocks were characterized by coupled ^{187,186}Os enrichment. Walker et al. (1991) reported initial εNd values for the two komatiites to be ~ +9.8, consistent with long term depletion in incompatible elements comparable to DMM, and similar to the other Gorgona komatiites.

References

Abbey S. (1983) Studies in "standard samples" of silicate rocks and minerals 1969-1982. *Papers – Geol. Surv. Can.* **83–15**, 1–114.

Aitken B.G. and Echeverría L.M. (1984) Petrology and geochemistry of komatiites and tholeiites from Gorgona island, Colombia. *Contrib. Mineral. Petrol.* **86**, 94–105.

Alard O., Luguet A., Pearson N.J., Griffin W.L., Lorand J-P., Gannoun A., Burton K.W. and O'Reilly S.Y. (2005) *In situ* Os isotopes in abyssal peridotites bridge the isotopic gap between MORBs and their source mantle. *Nature* **436**, 1005-1008.

Allègre C.J. (1982) Chemical geodynamics. *Tectonophysics* **81**, 109-132.

Archer G.J., Budde G., Worsham E.A., Stracke A., Jackson M.G. and Kleine T. (2023) Origin of ^{182}W anomalies in ocean island basalts. *Geochem. Geophys. Geosyst.* **24**, e2022GC010688.

Arevalo Jr. R. and McDonough W.F (2008) Tungsten geochemistry and implications for understanding the Earth's interior. *Earth Planet. Sci. Lett.* **272**, 656-665.

Arndt N. T., Kerr A. C., and Tarney J. (1997) Dynamic melting in plume heads: The formation of Gorgona komatiites and basalts. *Earth Planet. Sci. Lett.* **146**, 289-301.

Becker, H., Horan M.F., Walker R.J., Gao S., Lorand J.P. and Rudnick R.L. (2006) Highly siderophile element composition of the Earth's primitive upper mantle: Constraints from new data on peridotite massifs and xenoliths. *Geochim. Cosmochim. Acta* **70**, 4528-4550.

Bisterzo S., Gallino R., Straniero O., Cristallo S. and Käppeler F. (2011) The *s*-process in low-metallicity stars–II. Interpretation of high-resolution spectroscopic observations with asymptotic giant branch models. *Month. Not. Royal Astron. Soc.* **418**, 284-319.

Bono R. K., Tarduno J. A., Nimmo F. and Cottrell R. D. (2019) Young inner core inferred from Ediacaran ultra-low geomagnetic field intensity. *Nature Geosci.* **12**, 143–147.

Bouhifd M.A., Jephcoat A.P., Porcelli D., Kelley S.P. and Marty B. (2020) Potential of Earth's core as a reservoir for noble gases: Case for helium and neon. *Geochem. Persp. Lett.* **15**, 15–18.

Boyd F. R. and Mertzman S. A. (1987). Composition of structure of the Kaapvaal lithosphere, southern Africa. *Geochem. Soc. Spec. Pub.* **1**, 13–24.

Brandon A., Walker R.J., Morgan J.W., Norman M.D. and Prichard H.M. (1998) Coupled ^{186}Os and ^{187}Os evidence for core-mantle interaction. *Science* **280**, 1570-1573.

Brandon A.D., Walker R.J., Puchtel I.S., Becker H, Humayun M. and Revillon S. (2003) ^{186}Os-^{187}Os systematics of Gorgona Island komatiites: implications for early growth of the inner core. *Earth Planet. Sci. Lett.* **206**, 411-426.

Budde G., Archer G.J., Tissot F.L., Kleine T. and Tappe, S. (2022) Origin of the analytical ^{183}W effect and its implications for tungsten isotope analyses. *Journ. Anal. Atom. Spect.* **37**, 2005-2021.

Chabot N.L., Campbell A.J., McDonough W.F., Draper D.S., Agee C.B., Humayun M., Watson H.C., Cottrell E. and Saslow S.A. (2008) The Fe–C system at 5 GPa and implications for Earth's core. *Geochim. Cosmochim. Acta* **72**, 4146-4158.

Cook D.L. and Schönbächler M. (2016) High-precision measurement of W isotopes in Fe–Ni alloy and the effects from the nuclear field shift. *Journ. Anal. Atom. Spect.* **31**, 1400-1405.

Day J.M.D. and O'Driscoll B. (2019) Ancient high Pt/Os crustal contaminants can explain radiogenic ^{186}Os in some intraplate magmas. *Earth Planet. Sci. Lett.* **519**, 101-108.

Droop G.T.R. (1987) A general equation for estimating Fe^{3+} concentrations in ferromagnesian silicates and oxides from microprobe analyses, using stoichiometric criteria. *Min. Mag.* **51**, 431–435.

Echeverría L.M. (1980) Tertiary or Mesozoic komatiites from Gorgona Island, Colombia: Field relations and geochemistry. *Contrib. Min. Pet.* **73**, 253-266.

Govindaraju K. (1994). Compilation of working values and sample description for 383 geostandards. *Geostand. Geoanal. Res.* **18**, 1.

Green T.H., Blundy J.D., Adam J. and Yaxley G.M. (2004). SIMS determination of trace element partition coefficients between garnet, clinopyroxene and hydrous basaltic liquids at 2–7.5 GPa and 1080–1200◦C. *Lithos* **53**, 165-187.

Haller M. B., O'Driscoll B., Day J.M.D., Daly J.S., Piccoli P.M. and Walker R.J. (2021) Meter-scale chemical and isotopic heterogeneities in the oceanic mantle, Leka Ophiolite Complex, Norway. *Journ. Pet.* **62**, 1-29.

Hauri E.H. and Hart S.R. (1993) Re-Os isotope systematics of HIMU and EMII oceanic island basalts from the south Pacific Ocean. *Earth Planet. Sci. Lett*. **114**, 353-371.

Hellmann J.L., Kruijer T.S., Van Orman J.A., Metzler K. and Kleine T. (2019) Hf-W chronology of ordinary chondrites. *Geochim. Cosmochim. Acta* **258**, 290-309.

Herzberg C.T. (1995) Generation of plume magmas through time: an experimental perspective. *Chem. Geol.* **126**, 1-16.

Herzberg C.T. and Asimow P.D. (2008) Petrology of some oceanic island basalts: PRIMELT2.XLS software for primary magma calculation. *Geochem. Geophys. Geosyst.* **9**, Q09001.

Herzberg C.T. and Gazel E. (2009). Petrological evidence for secular cooling in mantle plumes. *Nature* **458**, 619-622.

Herzberg C.T., Condie K., and Korenaga J. (2010) Thermal history of the Earth and its petrological expression. *Earth Planet. Sci. Lett.* **292**, 79-88.

Hofmann A.W. and White W.M. (1982) Mantle plumes from ancient oceanic crust. *Contrib. Mineral. Petrol.* **57**, 421-436.

Hofmann A.W. (1988) Chemical differentiation of the Earth: The relationship between mantle, continental crust and oceanic crust. *Earth Planet. Sci. Lett.* **90**, 297-314.

Humayun M., Qin L. and Norman M.D. (2004) Geochemical evidence for excess iron in the mantle beneath Hawaii. *Science* **306**, 91-94.

Humayun M. (2011) A model for osmium isotopic evolution of metallic solids at the core-mantle boundary. *Geochem. Geophys. Geosyst.* **12**, doi:10.1029/2010GC003281.

Johnson D., Hooper P. and R. Conrey (1999) XRF analysis of rocks and minerals for major and trace elements on a single low dilution Li-tetraborate fused bead. *Advan. X-Ray Anal.* **41**, 843-867.

Kerr A.C. (2005) La Isla de Gorgona, Colombia: A petrological enigma? *Lithos* **84**, 77-101.

Klaver G.T. (1987) The Curaçao lava formation. An ophiolitic analogue of the anomalously thick layer 2B of the mid-Cretaceous oceanic plateaux in the Western Pacific and central Caribbean. PhD Thesis, U. Amsterdam, 168 pp.

Kleine T., Mezger K., Münker C., Palme H. and Bischoff A. (2004) ^{182}Hf-^{182}W isotope systematics of chondrites, eucrites, and martian meteorites: Chronology of core formation and early mantle differentiation in Vesta and Mars. *Geochim. Cosmochim. Acta* **68**, 2935-2946.

Knaack, C., Cornelius, S., and Hooper, P., 1994. Trace element analyses of rocks and minerals by ICP-MS. Washington State University., Open-File Rep.

Kruijer T.S., Sprung P., Kleine T., Leya I., Burkhardt C. and Wieler R. (2012) Hf–W chronometry of core formation in planetesimals inferred from weakly irradiated iron meteorites. *Geochim. Cosmochim. Acta* **99**, 287-304.

Labrosse S. (2018) Thermal evolution of the core with a high thermal conductivity. *Phys. Earth Planet. Inter.* **247**, 36-55.

Liu C-Z., Snow J.E., Brügmann G., Hellebradn E. and Hofmann A.W. (2009) *Earth Planet. Sci. Lett.* **283**, 122-132.

Ludwig K.R. (2003) ISOPLOT 3.00. A geochronological toolkit for Microsoft Excel, *Berkeley Geochron. Cent. Spec. Pub.* **4**, 70 pp.

Luguet A., Alard O., Lorand J.P., Pearson N.J., Ryab C. and O'Reilly S.Y. (2001) Laser-ablation microprobe (LAM)-ICPMS unravels the highly siderophile element geochemistry of the oceanic mantle. *Earth Planet. Sci. Lett.* **189**, 285-294.

Luguet A., Pearson D.G., Nowell G.M., Dreher S.T., Coggon J.A., Spetsius Z.V. and Parman S.W. (2008) Enriched Pt-Re-Os isotope systematics in plume lavas explained by metasomatic sulphides. *Science* **319**, 453-456.

McDonough W.F. and Sun S-S. (1995) The composition of the Earth. *Chem. Geol.* **120**, 223-253.

McKenzie D. and Bickle M.J. (1988) The volume and composition of melt generated by extension of the lithosphere. *Journ. Petrol.* **29**, 625-679.

Mertzman S.A. (2000) K-Ar results from the southern Oregon-northern California Cascade Range. *Oregon Geol.* **62**, 99–122.

Nicklas R.W., Puchtel I.S., Ash R.D., Piccoli P., Hanski E., Nisbet E.G., Waterton P., Pearson D.G. and Anbar A.D. (2019) Secular Mantle Oxidation across the Archean-Proterozoic Boundary: Evidence from V partitioning in komatiites and picrites. *Geochim. Cosmochim. Acta* **250**, 49-75.

Nielsen S.G., Shimizu N., Lee C.T.A., and Behn M.D. (2014). Chalcophile behavior of thallium during MORB melting and implications for the sulfur content of the mantle. *Geochem. Geophys. Geosyst.* **15**, 4905-4919.

O'Driscoll B., Day J.M.D., Walker R.J., Daly S., McDonough W.F. and Piccoli P.M. (2012) Chemical heterogeneity in the upper mantle recorded by peridotites and chromitites from the Shetland Ophiolite Complex, Scotland. *Earth Planet. Sci. Lett.* **333-334**, 226-237.

Puchtel I.S., Humayun M., Campbell A.J., Sproule R.A., Lesher C.M. (2004) Platinum group element geochemistry of komatiites from the Alexo and Pyke Hill areas, Ontario, Canada. *Geochim. Cosmochim. Acta* **68**, 1361-1383.

Puchtel I.S., Walker R.J., Brandon A.D., and Nisbet E.G. (2009) Pt–Re–Os and Sm–Nd isotope and HSE and REE systematics of the 2.7 Ga Belingwe and Abitibi komatiites. *Geochim. Cosmochim. Acta* **73**, 6357-6389.

Puchtel I.S., Touboul M., Blichert-Toft J., Walker R.J., Brandon A.D., Nicklas R.W., Kulikov V.S., and Samsonov A.V. (2016) Lithophile and siderophile element systematics of the Earth's mantle at the Archean-Proterozoic boundary: Evidence from 2.4 Ga komatiites. *Geochim. Cosmochim. Acta* **180**, 227–255.

Révillon S., Arndt N.T., Hallot E., Kerr A.C. and Tarney J. (1999) Petrogenesis of picrites from the Caibbean plateau and the North Atlantic magmatic province. *Lithos* **49**, 1-21.

Révillon S., Arndt N.T., Chauvel C. and Hallot E. (2000) Geochemical study of ultramafic volcanic and plutonic rocks from Gorgona Island, Colombia: the plumbing system of an oceanic plateau. *Journ. Petrol.* **41**, 1127–1153.

Révillon S., Chauvel C., Arndt N.T., Pik R., Martineau F., Fourcade S. and Marty B. (2002) Heterogeneity of the Caribbean plateau mantle source: Sr, O and He isotopic compositions of olivine and clinopyroxene from Gorgona Island. *Earth Planet. Sci. Lett.* **205**, 91– 106.

Rizo H., Andrault D., Bennett N. R., Humayun M., Brandon A.D., Vlastelic I., Moine B., Poirier A., Bouhifd M.A. and Murphy D.T. (2019) ^{182}W evidence for core-mantle interaction in the source of mantle plumes. *Geochem. Persp. Lett.* **11**, 6–11.

Schulte R.F., Schilling M., Horan M.F., Anma R., Komiya T., Farquhar J., Piccoli P.M., Pitcher L. and Walker R.J. (2009) Chemical and chronologic complexity in the convecting upper mantle: evidence from the Taitao Ophiolite, southern Chile. *Geochim. Cosmochim. Acta* **73**, 5793-5819.

Serrano L., Ferrari L., Martinez M.L., Petrone C.M. and Jaramillo C. (2011) An integrative geologic, geochronologic and geochemical study of Gorgona Island, Colombia: Implications for the formation of the Caribbean Large Igneous Province. *Earth Planet. Sci. Lett.* **309**, 324–336.

Shirey S.B. and Walker R.J. (1998) Re-Os isotopes in cosmochemistry and high-temperature geochemistry. *Ann. Rev. Earth Planet. Sci.* **26**, 423-500.

Steenstra E.S., Berndt J., Klemme S., Rohrbach A., Bullock E.S., and van Westrenen W. (2020) An experimental assessment of the potential of sulfide saturation of the source regions of eucrites and angrites: Implications for asteroidal models of core formation, late accretion and volatile element depletions. *Geochim. Cosmochim. Acta* **269**, 39-62.

Sun Z., Xiong X., Wang J., Liu X., Li L., Ruan M., Zhang L., and Takahashi E. (2020). Sulfur abundance and heterogeneity in the MORB mantle estimated by copper partitioning and sulfur solubility modelling. *Earth Planet. Sci. Lett.* **538**, 116169.

Thompson P. M. E., Kempton P. D., White R. V., Kerr A. C., Tarney J., Saunders A. D., Fitton J. G. and McBirney A. (2003) Hf–Nd isotope constraints on the origin of the Cretaceous Caribbean plateau and its relationship to the Galapagos plume. *Earth Planet. Sci. Lett.* **217**, 59–75.

Touboul M., Puchtel I.S. and Walker R.J. (2012) ^{182}W evidence for long-term preservation of early mantle differentiation products. *Science* **335**, 1065-1069, DOI: 10.1126/science.1216351.

Völkening J., Köppe M. and Heumann K. G. (1991) Tungsten isotope ratio determinations by negative thermal ionization mass spectrometry. *Internat. Journ. Mass Spectrom. Ion Proc.* **107**, 361–368.

Walker R.J., Echeverría L.M., Shirey S.B. and Horan M.F. (1991) Re - Os isotopic constraints on the origin of volcanic rocks, Gorgona Island, Colombia: Os isotopic evidence for ancient heterogeneities in the mantle. *Contrib. Mineral. Petrol.* **107**, 150-162.

Walker R.J., Morgan J.W., Beary E., Smoliar M.I., Czamanske G.K. and Horan M.F. (1997) Applications of the ^{190}Pt-^{186}Os isotope system to geochemistry and cosmochemistry. *Geochim. Cosmochim. Acta* **61**, 4799-4808.

Walker, R.J., Storey M., Kerr A. C., Tarney J. and Arndt N.T. (1999) Implications of ^{187}Os isotopic heterogeneities in a mantle plume: Evidence from Gorgona Island and Curaçao. *Geochim. Cosmochim. Acta* **63**, 713-728.

Walker R.J., Horan M.F., Morgan J.W., Becker H., Grossman J.N. and Rubin A. (2002) Comparative ^{187}Re-^{187}Os systematics of chondrites: Implications regarding early solar system processes. *Geochim. Cosmochim. Acta* **66**, 4187-4201.

Wang Z. and Becker H. (2014) Abundances of sulfur, selenium, tellurium, rhenium and platinum-group elements in eighteen reference materials by isotope dilution sector-field ICP-MS and negative TIMS. *Geostandards and Geoanalytical Research* **38**, 189-209.

Willbold M., Elliott T. and Moorbath S. (2011) The tungsten isotopic composition of the Earth's mantle before the terminal bombardment. *Nature* **477**, 195-199.

Zhou T., Tarduno J.A., Nimmo F., Cottrell R.D., Bono R.K., Ibanez-Mejia M., Huang W., Hamilton M., Kodama K., Smirnov A.V., Crummins B. and Padgett III F. (2022) Early Cambrian renewal of the geodynamo and the origin of inner core structure. *Nature Comm.*, doi.org/10.1038/s41467-022-31677-7.

Data Availability

Tables of all data presented and plotted are available through Mendeley Data at:

https://doi.org/10.17632/8mh9y2tgzr.1

Table S1. Major and trace element abundances of Gorgona Island - Curaçao rocks. Oxides are in wt.%. All other elements in ppm. * - from Echeverría (1980). ** - from Révillon et al. (2000). *+ - Major elements from Révillon et al. (2000), trace elements measured at UMd. n.d. - not determined.

	Gorgona																								
Latitude (N)					2°58.653'											2°58.567'					2°58.604'	2°58.653'			
Longitude (W)					78°10.273'											78°10.300'					78°10.252'	78°10.273'			
	Komatiites																								
Number	**GOR4P***	**GOR23B**	**GOR47**	**PC-5**	**GOR152**	**GOR153**	**GOR155**	**GOR156**	**GOR157**	**GOR159**	**GOR160**	**GOR537**	**GOR538**	**GOR539**	**GOR540**	**19GOR-1A**	**19GOR-1B**	**19GOR-1C**	**19GOR-1D**	**19GOR-1E**	**19GOR 2**	**19GOR 3**	**19GOR 4**	**19GOR 5**	**GOR1901**
SiO_2	46.90	43.24	46.33	45.49	45.25	44.10	46.33	45.03	45.69	44.46	45.13	44.30	42.90	43.90	43.50	45.75	45.12	44.88	45.48	45.63	45.27	44.60	44.80	44.40	45.67
TiO_2	0.73	0.65	0.40	0.64	0.68	0.51	0.69	0.63	0.77	0.61	0.65	0.64	0.52	0.65	0.66	0.66	0.63	0.58	0.65	0.65	0.63	0.59	0.58	0.61	0.66
Al_2O_3	14.20	11.86	12.07	11.92	12.49	9.66	12.57	11.80	13.95	11.56	11.78	12.00	9.30	12.20	12.20	11.94	11.58	10.63	11.91	11.69	11.44	11.12	10.48	11.41	12.01
Fe_2O_{3T}	11.10	14.39	11.72	12.63	12.88	12.21	12.78	12.69	13.14	12.74	12.72	12.80	12.00	12.20	12.80	12.73	12.49	12.64	12.66	12.89	12.49	12.91	12.50	12.48	12.70
MnO	0.25	0.22	0.20	0.18	0.21	0.20	0.18	0.21	0.21	0.20	0.19	0.18	0.19	0.19	0.19	0.19	0.19	0.19	0.19	0.19	0.19	0.20	0.18	0.19	0.19
MgO	11.30	17.81	16.70	17.48	15.31	23.79	15.45	17.67	12.15	18.75	17.77	17.20	25.70	18.30	18.00	17.06	17.97	20.35	17.31	17.57	18.48	19.30	20.86	19.20	16.76
CaO	12.90	10.14	10.86	10.33	11.18	8.22	10.31	10.26	12.19	9.80	10.13	10.70	8.05	11.00	10.80	10.24	10.30	9.27	10.23	10.18	9.78	9.58	9.31	9.56	10.52
Na_2O	1.80	1.12	1.29	1.22	1.62	0.93	1.33	1.27	1.59	1.23	1.18	1.63	0.69	1.03	1.40	1.16	1.08	0.98	1.22	1.09	1.23	1.00	0.96	0.97	1.20
K_2O	0.030	0.064	0.019	0.050	0.021	0.005	0.066	0.021	0.042	0.020	0.044	0.041	0.031	0.083	0.021	0.039	0.033	0.027	0.037	0.047	0.048	0.026	0.043	0.032	0.035
P_2O_5	n.d.	0.046	0.039	0.040	0.039	0.032	0.041	0.038	0.044	0.036	0.036	0.040	0.051	0.063	0.053	0.043	0.045	0.039	0.044	0.043	0.049	0.044	0.040	0.043	0.045
Total	**99.21**	**99.54**	**99.64**	**99.98**	**99.68**	**99.66**	**99.73**	**99.63**	**99.77**	**99.40**	**99.64**	**99.53**	**99.43**	**99.61**	**99.62**	**99.82**	**99.44**	**99.58**	**99.73**	**99.98**	**99.60**	**99.37**	**99.75**	**98.89**	**99.78**
LOI	4.32	4.61	3.68	2.68	2.80	3.29	5.97	3.09	3.15	2.69	5.07	1.83	2.88	4.21	4.64	3.51	3.17	3.12	2.73	3.90	4.13	3.31	3.58	3.06	2.74
Sc	33.9	29.3	31.8	n.d.	37.7	29.3	38.9	35.0	42.0	34.2	35.7	35.2	27.3	33.3	36.6	18.5	17.8	15.3	13.6	16.7	32.8	28.5	14.1	14.7	n.d.
V	265	258	234	266	328	251	329	312	342	301	305	260	210	266	298	191	131	118	186	130	259	241	122	121	275
Cr	691	1759	1394	1250	1304	1244	990	1303	867	2840	1472	1444	2805	1004	1404	814	1155	854	1174	548	1199	2123	650	2981	1181
Co	51.8	109	65.5	n.d.	54.9	101	61.0	96.1	68.0	94.9	87.1	80.2	82.2	60.5	67.2	55.9	40.5	45.5	57.7	39.8	81.3	84.4	44.8	40.8	n.d.
Ni	177	1158	872	n.d.	474	827	478	871	286	929	657	1001	1610	939	1103	459	368	437	484	341	706	871	490	407	n.d.
Cu	118	158	114	n.d.	146	107	155	134	158	133	132	137	99.5	135	123	84.4	57.6	54.1	85.4	57.2	117	106	53.6	53.0	n.d.
Zn	58.7	n.d.	n.d.	n.d.	n.d.	n.d.	n.d.	n.d.	n.d.	n.d.	n.d.	n.d.	n.d.	n.d.	n.d.	46.8	30.4	29.1	42.5	28.2	60.7	58.5	30.1	29.9	n.d.
Ga	13.2	14.22	12.3	n.d.	14.6	10.9	14.4	13.6	16.3	13.4	14.0	13.8	10.1	13.0	13.2	8.81	6.61	5.69	8.14	6.21	12.7	11.6	5.87	6.30	n.d.
Sr	90.2	n.d.	n.d.	n.d.	n.d.	n.d.	n.d.	n.d.	n.d.	n.d.	n.d.	n.d.	n.d.	n.d.	n.d.	36.4	41.0	26.1	34.1	34.5	55.5	47.3	30.1	30.1	n.d.
Y	15.5	14.0	12.5	n.d.	15.3	11.4	15.6	14.3	17.3	13.8	14.4	14.5	10.4	13.4	13.2	10.2	8.05	6.92	8.88	7.85	14.9	13.5	6.77	7.08	n.d.
Zr	31.9	29.5	16.0	n.d.	33.1	24.8	31.9	30.9	36.5	29.2	30.9	29.9	21.8	28.2	26.4	22.8	15.7	13.9	21.2	15.6	30.7	28.3	14.1	14.7	n.d.
Nb	0.425	0.692	0.304	0.414	0.404	0.313	0.409	0.384	0.444	0.367	0.371	0.383	0.300	0.367	0.328	0.270	0.193	0.158	0.259	0.178	0.355	0.320	0.164	0.165	0.3948
Ba	7.77	n.d.	n.d.	n.d.	n.d.	n.d.	n.d.	n.d.	n.d.	n.d.	n.d.	n.d.	n.d.	n.d.	n.d.	n.d.	n.d.	n.d.	n.d.	n.d.	n.d.	n.d.	n.d.	n.d.	n.d.
La	0.687	0.756	0.313	0.644	0.685	0.490	0.666	0.618	0.849	0.599	0.611	0.610	0.453	0.616	0.491	0.403	0.311	0.269	0.377	0.297	0.551	0.514	0.256	0.267	0.607
Ce	2.43	2.31	1.05	2.26	2.35	1.71	2.19	2.13	2.51	2.00	2.02	2.06	1.54	2.09	1.82	1.56	1.15	0.993	1.50	1.07	2.15	2.01	1.01	1.03	2.10
Pr	0.493	0.431	0.210	0.461	0.487	0.355	0.489	0.446	0.538	0.440	0.455	0.444	0.319	0.435	0.378	0.298	0.230	0.191	0.291	0.214	0.427	0.396	0.198	0.206	0.435
Nd	3.26	2.76	1.44	2.98	3.12	2.30	3.18	2.92	3.50	2.84	2.97	2.85	2.06	2.85	2.62	1.99	1.52	1.27	1.87	1.42	2.75	2.54	1.26	1.33	2.89
Sm	1.54	1.31	0.81	1.38	1.43	1.06	1.50	1.37	1.64	1.30	1.35	1.37	0.967	1.31	1.22	0.950	0.713	0.619	0.908	0.666	1.30	1.21	0.588	0.610	1.36
Eu	0.679	0.565	0.388	0.587	0.619	0.466	0.627	0.588	0.705	0.563	0.577	0.586	0.412	0.572	0.535	0.403	0.301	0.262	0.389	0.292	0.572	0.522	0.261	0.271	0.577
Gd	2.37	2.11	1.53	2.15	2.33	1.74	2.32	2.20	2.67	2.08	2.21	2.11	1.54	2.00	1.93	1.34	1.02	0.898	1.30	0.968	1.95	1.78	0.896	0.934	2.10
Tb	0.449	0.398	0.313	0.399	0.423	0.313	0.426	0.398	0.481	0.375	0.389	0.390	0.283	0.375	0.347	0.266	0.200	0.170	0.244	0.182	0.379	0.350	0.168	0.183	0.393
Dy	3.00	2.66	2.24	2.68	2.84	2.12	2.94	2.69	3.31	2.58	2.73	2.61	1.89	2.55	2.45	1.84	1.39	1.24	1.70	1.31	2.67	2.42	1.18	1.28	2.67
Ho	0.635	0.550	0.497	0.552	0.590	0.446	0.615	0.564	0.692	0.545	0.572	0.559	0.402	0.548	0.509	0.383	0.288	0.250	0.352	0.282	0.547	0.525	0.254	0.270	0.551
Er	1.75	1.55	1.46	1.55	1.68	1.27	1.71	1.60	1.94	1.53	1.61	1.55	1.13	1.52	1.43	1.05	0.807	0.716	0.991	0.758	1.48	1.45	0.699	0.759	1.54
Tm	0.258	0.213	0.213	0.220	0.235	0.177	0.238	0.222	0.272	0.212	0.222	0.219	0.158	0.209	0.198	0.147	0.115	0.101	0.137	0.107	0.209	0.200	0.0986	0.102	0.220
Yb	1.61	1.36	1.40	1.43	1.50	1.13	1.52	1.42	1.73	1.36	1.41	1.39	1.02	1.34	1.27	0.945	0.714	0.636	0.862	0.641	1.33	1.26	0.635	0.659	1.41
Lu	0.230	0.190	0.203	0.201	0.213	0.164	0.220	0.204	0.249	0.194	0.204	0.201	0.146	0.198	0.185	0.129	0.104	0.0893	0.123	0.0961	0.196	0.177	0.0907	0.0913	0.201
Hf	1.06	0.917	0.545	0.900	0.998	0.751	0.997	0.956	1.131	0.888	0.947	0.921	0.684	0.899	0.876	0.673	0.474	0.432	0.696	0.463	0.939	0.880	0.439	0.475	0.950
W	0.0353	n.d.	n.d.	n.d.	n.d.	n.d.	n.d.	n.d.	n.d.	n.d.	n.d.	n.d.	n.d.	n.d.	n.d.	0.00929	0.0106	0.00753	0.00808	0.0766	0.0188	0.00925	0.0115	0.00469	n.d.
Pb	0.0620	n.d.	n.d.	n.d.	n.d.	n.d.	n.d.	n.d.	n.d.	n.d.	n.d.	n.d.	n.d.	n.d.	n.d.	0.0496	0.0580	0.0371	0.0508	0.0269	0.110	0.0750	0.0296	0.0391	n.d.
Th	0.0387	0.0602	0.0218	0.0275	0.0369	0.0235	0.0311	0.0289	0.0343	0.0279	0.0315	0.0273	0.0200	0.0282	0.0233	0.0182	0.0151	0.0124	0.0180	0.0135	0.0311	0.0275	0.0171	0.0166	0.0257
U	0.0132	0.0332	0.0129	0.0120	0.0116	0.00871	0.0126	0.0104	0.0123	0.00983	0.0254	0.0110	0.00736	0.0156	0.0104	0.00723	0.00593	0.00429	0.00624	0.00870	0.0114	0.00887	0.00551	0.00502	0.0102
W/Th	0.914	n.d.	n.d.	n.d.	n.d.	n.d.	n.d.	n.d.	n.d.	n.d.	n.d.	n.d.	n.d.	n.d.	n.d.	0.510	0.706	0.607	0.450	5.69	0.604	0.336	0.671	0.283	n.d.
U/Th	0.342	0.552	0.592	0.438	0.315	0.371	0.405	0.359	0.357	0.352	0.804	0.401	0.368	0.552	0.447	0.397	0.394	0.346	0.347	0.646	0.366	0.322	0.322	0.302	0.397

Table S1 cont.

	Gorgona																			
Latitude (N)	2˚58.318'	2˚58.271'		2˚58.167'					2˚58.167'		02˚58.246'			2˚56.064'				2˚56.207'		
Longitude (W)	78˚10.259'	78˚10.271'		78˚10.314'					078◦10.314'		78˚10.274'			78˚12.195'				78˚11.849'		
	Peridotites								*Gabbros*					*Picrites*						
Number	**19GOR 6**	**19GOR 7**	**19GOR-8**	**19GOR 13**	**GOR503****	**GOR507****	**GOR509****	**GOR535****	**19GOR-14**	**19GOR-15**	**19GOR-17**	**19GOR-18**	**19GOR-19**	**19GOR-9**	**19GOR-10**	**19GOR-11**	**19GOR-27**	**19GOR-28**	**19GOR-29**	**19GOR-30**	**19GOR-31**
SiO_2	43.24	41.92	44.17	42.52	41.88	43.03	44.04	43.57	46.87	45.62	46.08	46.65	49.00	45.20	45.67	47.52	44.25	45.75	46.16	45.17	45.27
TiO_2	0.31	0.38	0.67	0.43	0.22	0.29	0.28	0.64	0.49	0.47	0.44	0.48	1.05	0.34	0.28	0.39	0.27	0.36	0.33	0.29	0.29
Al_2O_3	6.76	5.40	9.31	6.36	5.03	6.90	8.15	8.56	17.17	15.59	18.84	16.86	14.50	9.90	10.58	13.22	7.78	10.47	11.78	10.04	10.18
Fe_2O_{3T}	12.75	14.04	14.10	13.62	12.46	12.73	12.48	14.53	9.52	10.85	9.53	9.88	10.90	11.18	10.96	12.12	10.67	11.89	11.30	10.93	11.14
MnO	0.19	0.19	0.21	0.19	0.18	0.19	0.22	0.21	0.14	0.15	0.14	0.14	0.17	0.17	0.17	0.16	0.16	0.16	0.17	0.16	0.17
MgO	29.52	31.98	22.01	30.03	35.41	29.63	27.20	24.13	9.97	13.68	10.85	11.20	7.72	23.04	22.40	15.83	29.68	23.53	19.04	23.77	23.32
CaO	6.17	5.23	8.42	5.90	4.67	7.21	7.40	8.03	13.40	11.62	12.49	13.45	13.32	8.63	8.15	7.93	6.41	6.08	9.93	8.42	8.57
Na_2O	0.31	0.13	0.49	0.23	0.13	n.d.	0.19	0.28	1.42	1.28	1.45	1.28	2.74	0.79	0.82	2.23	0.36	0.96	0.80	0.79	0.77
K_2O	0.021	0.029	0.044	0.034	0.01	n.d.	0.03	0.03	0.061	0.063	0.105	0.065	0.354	0.044	0.278	0.215	0.023	0.093	0.180	0.047	0.024
P_2O_5	0.029	0.041	0.061	0.038	0.01	0.01	0.02	0.04	0.035	0.035	0.034	0.031	0.067	0.025	0.021	0.031	0.022	0.035	0.028	0.026	0.024
Total	**99.30**	**99.34**	**99.49**	**99.35**	**100.00**	**99.99**	**100.01**	**100.02**	**99.08**	**99.35**	**99.96**	**100.04**	**99.82**	**99.31**	**99.32**	**99.65**	**99.62**	**99.33**	**99.71**	**99.64**	**99.76**
LOI	4.86	6.63	5.83	5.28	5.34	7.16	6.36	5.10	2.61	2.81	3.09	3.08	2.72	3.15	4.07	5.35	7.98	8.50	4.25	2.81	3.45
Sc	1.22	6.74	12.3	5.78	n.d.	18.6	14.2	n.d.	15.4	21.1	18.9	33.5	41.7	11.3	14.8	22.8	7.47	1.69	29.5	4.83	1.73
V	94.8	57.6	100	139	84.0	113	87.2	171	99.1	231	177	261	347	89.0	165	218	69.6	171	192	116	127
Cr	1874	1028	981	3033	4773	1249	1520	2259	280	388	323	772	154	970	1689	960	704	1881	1510	1457	1191
Co	74.3	60.0	48.0	113	21.0	87.3	52.8	105	24.9	82.6	54.2	70.6	43.0	41.4	78.0	73.0	48.3	85.8	75.3	60.0	62.2
Ni	848	592	377	1394	1889	844	719	981	124	484	266	312	88.4	493	924	512	719	1030	681	719	749
Cu	35.1	26.6	43.1	60.3	37.0	43.4	30.8	76.0	47.9	104	104	112	125	41.8	68.4	85.9	24.8	82.6	99.8	57.2	49.5
Zn	40.6	28.9	35.8	61.9	64.0	56.0	49.2	82.0	22.7	53.2	44.5	47.9	58.3	26.7	49.0	54.7	25.4	57.6	52.5	38.5	40.5
Ga	4.74	3.03	5.37	7.10	5.00	6.08	5.84	10.0	7.30	14.7	13.5	17.1	16.0	4.34	7.83	10.23	3.43	7.69	9.55	5.84	6.18
Sr	22.8	17.7	20.2	41.9	42.8	4.88	7.15	50.5	37.6	62.8	81.8	83.0	119	10.4	38.1	93.7	9.36	21.8	27.6	13.1	12.2
Y	6.33	3.77	6.57	7.53	4.00	7.04	6.25	9.00	6.16	12.3	10.0	13.3	17.9	6.00	11.5	16.6	4.44	12.1	14.2	7.94	8.86
Zr	9.85	9.74	16.6	20.6	6.80	8.50	7.00	25.0	11.4	26.9	21.8	26.2	46.1	6.81	10.9	16.7	6.85	13.7	13.5	9.14	10.2
Nb	0.335	0.531	0.967	1.08	0.120	0.121	0.153	1.71	0.191	0.488	0.342	0.428	2.99	0.0588	0.0833	0.0979	0.0452	0.126	0.0743	0.0759	0.0887
Ba	10.5	3.63	2.80	9.54	6.00	0.525	0.976	7.48	3.38	6.58	8.77	8.15	53.3	0.788	19.4	32.7	0.263	4.35	1.31	0.460	0.620
La	0.301	0.463	0.834	0.981	0.150	0.138	0.159	1.32	0.245	0.539	0.433	0.512	2.49	0.0705	0.103	0.156	0.0755	0.144	0.117	0.0976	0.104
Ce	0.909	1.24	2.24	2.62	0.430	0.449	0.478	3.52	0.843	1.87	1.45	1.78	6.48	0.284	0.398	0.661	0.316	0.626	0.517	0.372	0.391
Pr	0.157	0.186	0.336	0.387	0.0900	0.0959	0.0894	0.540	0.161	0.358	0.280	0.344	0.983	0.0646	0.0855	0.145	0.0676	0.144	0.116	0.0804	0.0838
Nd	0.947	1.00	1.78	2.10	0.590	0.716	0.603	2.97	1.05	2.42	1.84	2.26	5.09	0.505	0.689	1.10	0.472	1.068	0.885	0.613	0.627
Sm	0.441	0.379	0.683	0.808	0.340	0.446	0.322	1.10	0.512	1.14	0.884	1.14	1.90	0.312	0.497	0.706	0.254	0.632	0.563	0.389	0.408
Eu	0.196	0.152	0.271	0.335	0.160	0.210	0.152	0.460	0.245	0.515	0.407	0.522	0.799	0.160	0.266	0.322	0.118	0.232	0.296	0.194	0.205
Gd	0.711	0.521	0.916	1.11	0.670	0.880	0.640	1.64	0.793	1.65	1.26	1.69	2.49	0.598	1.02	1.42	0.438	1.17	1.17	0.732	0.815
Tb	0.147	0.0969	0.176	0.207	0.130	0.180	0.136	0.290	0.153	0.331	0.250	0.336	0.462	0.132	0.237	0.324	0.0908	0.264	0.282	0.170	0.191
Dy	1.14	0.690	1.19	1.47	0.960	1.28	1.01	1.98	1.09	2.33	1.82	2.42	3.26	1.02	1.93	2.63	0.699	2.07	2.27	1.35	1.51
Ho	0.258	0.139	0.250	0.302	0.210	0.282	0.244	0.410	0.233	0.486	0.383	0.508	0.662	0.223	0.443	0.618	0.166	0.480	0.543	0.318	0.350
Er	0.763	0.387	0.680	0.811	0.590	0.807	0.745	1.09	0.655	1.31	1.07	1.40	1.80	0.664	1.29	1.86	0.457	1.45	1.63	0.929	1.03
Tm	0.110	0.0548	0.0916	0.114	0.0900	0.119	0.118	0.160	0.0946	0.181	0.152	0.203	0.249	0.0970	0.191	0.269	0.0692	0.213	0.245	0.140	0.153
Yb	0.702	0.352	0.574	0.752	0.530	0.732	0.776	0.980	0.593	1.18	0.981	1.28	1.59	0.623	1.25	1.78	0.453	1.39	1.62	0.920	0.998
Lu	0.107	0.0519	0.0852	0.109	0.0900	0.112	0.124	0.160	0.0882	0.171	0.140	0.181	0.227	0.0936	0.179	0.257	0.0672	0.209	0.239	0.134	0.144
Hf	0.323	0.289	0.495	0.659	0.250	0.331	0.255	0.820	0.370	0.814	0.680	0.846	1.33	0.236	0.397	0.586	0.228	0.474	0.488	0.327	0.355
W	0.0157	0.0334	0.0275	0.0170	0.00364	0.00412	0.00538	0.0172	0.00887	0.0152	0.0174	0.0167	0.0324	0.0115	0.0230	0.0168	0.00493	0.0191	0.0146	0.00884	0.0103
Pb	0.0427	0.0384	0.369	0.125	0.0800	0.0371	0.0486	0.170	0.0415	0.0568	0.0766	0.0517	0.137	0.00714	0.0151	0.00378	0.00329	0.00408	0.0103	0.0137	0.0148
Th	0.0194	0.0479	0.0804	0.0869	0.0200	0.0117	0.0195	0.120	0.0195	0.0340	0.0362	0.0389	0.211	0.00522	0.0128	0.0155	0.00829	0.0123	0.0114	0.00877	0.0166
U	0.0102	0.0141	0.0223	0.0266	0.0100	0.00681	0.00675	0.0400	0.00690	0.0134	0.0101	0.0132	0.0587	0.00135	0.00377	0.00979	0.00103	0.0456	0.00220	0.00263	0.00278
W/Th	0.807	0.698	0.342	0.196	0.182	0.351	0.276	0.143	0.456	0.447	0.481	0.428	0.153	2.20	1.80	1.08	0.595	1.55	1.28	1.01	0.619
U/Th	0.527	0.295	0.278	0.306	0.500	0.581	0.347	0.333	0.355	0.393	0.279	0.339	0.278	0.259	0.295	0.631	0.125	3.70	0.193	0.300	0.167

Table S1 cont.

	Gorgona									Curaçao					
Latitude (N)	2°57.415'		2°58.246'	2°58.182'	2°58.195'		3°00.166'		2°59.835'	12°05.150'	12°04.188'	12°06.396'		12°06.194'	12°08.15.8'
Longitude (W)	78°11.906'		78°10.274'	78°10.300'	78°10.303'		78°09.993'		78°10.043'	068°50.506'	68°50.251'	68°55.070'		68°51.079'	68°49.482'
	Tuff breccias		*D-basalts*			*E-basalts*				*Picrites*				*Basalts*	
Number	**19GOR-32**	**19GOR-33**	**19GOR-16**	**19GOR-25**	**19-GOR26**	**GOR23A***	**19GOR-22**	**19GOR-23**	**19GOR-24**	**CUR-04**	**CUR-05**	**CUR-11**		**CUR-09**	**CUR13-6**
SiO_2	46.15	45.27	48.82	48.88	47.94	50.00	51.07	51.58	48.91	47.26	46.60	46.33		50.36	51.20
TiO_2	0.22	0.28	1.22	0.84	1.36	1.41	1.28	1.29	0.65	0.65	0.54	0.55		0.97	0.98
Al_2O_3	9.06	9.94	13.75	13.87	13.71	13.80	13.75	13.73	15.62	10.30	8.64	8.13		14.93	14.55
Fe_2O_{3T}	10.58	11.58	14.54	12.83	15.98	10.50	13.52	13.37	9.79	11.22	10.58	11.35		10.35	10.42
MnO	0.16	0.16	0.22	0.19	0.24	0.20	0.17	0.18	0.16	0.16	0.17	0.17		0.17	0.18
MgO	23.08	25.48	7.24	8.14	6.90	9.16	7.07	6.98	10.09	20.11	24.94	26.02		8.52	8.28
CaO	9.67	6.54	10.53	12.46	10.52	10.90	10.97	10.57	13.31	8.93	7.67	7.57		12.21	11.50
Na_2O	0.66	0.44	3.05	2.52	2.88	2.88	2.07	2.15	1.56	1.42	0.75	0.44		2.29	2.74
K_2O	0.024	0.025	0.242	0.049	0.157	0.450	0.066	0.075	0.078	0.070	0.060	0.030		0.130	0.096
P_2O_5	0.020	0.021	0.094	0.059	0.109	n.d.	0.112	0.112	0.048	0.192	0.182	0.187		0.211	0.051
Total	**99.63**	**99.73**	**99.70**	**99.84**	**99.80**	**99.30**	**100.08**	**100.04**	**100.22**	**99.95**	**100.77**	**100.77**		**100.14**	**100.00**
LOI	6.33	7.81	1.87	1.88	1.45	n.d.	0.82	1.23	2.05	4.67	5.20	4.75		2.64	1.79
Sc	12.3	0.667	35.4	46.3	39.2	45.5	50.8	46.3	32.9	37.5	30.5	27.4		49.8	56.0
V	76.0	128	423	468	480	351	405	416	242	231	183	165		320	380
Cr	980	2037	229	324	209	497	79.2	76.3	463	2182	2340	2601		496	449
Co	39.4	83.7	49.0	65.8	51.9	58.9	46.6	49.2	46.4	79.1	85.8	85.4		46.24	53.54
Ni	473	1035	108	140	98.8	128	66.7	65.6	162.0	830	1036	1012		112.4	113.1
Cu	30.3	103	144	185	148	140	184	194	87.7	95.7	75.3	69.2		127.6	152.8
Zn	24.4	56.5	78.4	79.7	95.4	79.4	82.8	80.3	47.2	72.2	67.2	65.5		73.5	84.4
Ga	3.95	7.68	18.4	20.3	19.7	16.4	17.5	17.9	12.5	10.6	8.49	7.85		15.64	16.17
Sr	6.95	20.6	111	143	121	182	94.2	94.4	123	96.3	65.8	26.0		106.9	121.4
Y	5.62	9.22	28.0	27.3	33.0	21.6	26.8	25.8	12.2	12.5	9.97	9.44		18.11	19.5
Zr	5.09	9.19	63.7	52.6	76.2	90.1	70.9	73.3	31.3	34.6	27.4	26.5		49.28	48.05
Nb	0.0139	0.0617	1.23	0.959	1.49	9.70	5.04	5.07	2.10	2.59	2.01	1.96		3.60	3.31
Ba	0.257	0.317	40.2	22.0	33.2	108	14.1	17.7	7.79	22.0	17.5	6.21		12.15	9.16
La	0.0307	0.0578	1.63	1.26	1.99	7.87	3.89	4.15	1.66	2.03	1.65	1.62		3.01	2.71
Ce	0.138	0.299	5.41	4.07	6.80	19.4	10.8	11.5	4.67	4.82	3.95	4.01		7.597	6.8352
Pr	0.0322	0.0767	0.979	0.772	1.24	2.67	1.62	1.67	0.688	0.748	0.611	0.618		1.1627	1.0889
Nd	0.269	0.610	6.10	4.82	7.50	12.7	8.21	8.45	3.53	3.78	3.13	3.17		5.911	5.7790
Sm	0.192	0.441	2.6219	2.2677	3.1635	3.46	2.70	2.86	1.25	1.20	0.989	1.02		1.911	1.9527
Eu	0.110	0.210	1.06	0.992	1.26	1.24	0.982	1.02	0.500	0.432	0.359	0.371		0.712	0.777
Gd	0.443	0.900	3.74	3.43	4.43	3.98	3.46	3.62	1.63	1.58	1.32	1.36		2.48	2.66
Tb	0.108	0.212	0.752	0.680	0.834	0.658	0.654	0.659	0.297	0.284	0.237	0.242		0.446	0.488
Dy	0.877	1.67	5.11	4.88	5.90	3.93	4.54	4.69	2.12	1.83	1.52	1.57		2.88	3.23
Ho	0.204	0.383	1.10	1.03	1.25	0.817	0.987	1.02	0.457	0.395	0.332	0.340		0.617	0.716
Er	0.618	1.13	2.96	2.92	3.48	2.22	2.85	2.85	1.30	1.13	0.949	0.981		1.77	2.06
Tm	0.0904	0.167	0.424	0.420	0.501	0.328	0.429	0.413	0.193	0.170	0.143	0.146		0.267	0.321
Yb	0.617	1.06	2.72	2.63	3.25	2.03	2.78	2.74	1.23	1.05	0.891	0.916		1.69	2.03
Lu	0.0912	0.159	0.387	0.380	0.467	0.300	0.412	0.416	0.184	0.163	0.138	0.142		0.252	0.315
Hf	0.188	0.328	1.83	1.64	2.28	2.34	2.00	2.07	0.879	0.801	0.667	0.730		1.19	1.33
W	0.00334	0.0105	0.0720	0.0283	0.0291	n.d.	0.0418	0.0480	0.0234	0.0172	0.0355	0.153		0.0211	0.0239
Pb	0.00238	0.0111	0.143	0.155	0.124	0.772	0.156	0.237	0.107	0.118	0.103	0.110		0.204	0.133
Th	0.00848	0.00246	0.106	0.109	0.140	0.819	0.361	0.344	0.128	0.181	0.157	0.162		0.270	0.216
U	0.000587	0.00109	0.0360	0.0297	0.0443	0.187	0.0999	0.0969	0.0400	0.0358	0.0304	0.0322		0.0573	0.0503
W/Th	0.393	4.25	0.680	0.261	0.207	n.d.	0.116	0.140	0.182	0.0950	0.226	0.942		0.0782	0.111
U/Th	0.0691	0.443	0.340	0.274	0.315	0.228	0.277	0.282	0.311	0.197	0.194	0.199		0.212	0.233

Table S2. Highly siderophile element abundances corrected for loss on ignition (LOI), in ppb.

Number	Sample Type	LOI	Os	Ir	Ru	Pt	Pd	Re
Gorgona Island								
GOR4P	komatiitic basalt	4.32	0.9071	0.8467	2.020	17.00	17.28	0.9230
GOR23B	komatiite	4.61	0.8201	0.7805	4.142	11.96	14.20	1.233
GOR47	komatiite	3.68	0.8415	0.5678	2.819	13.10	15.04	0.8349
PC-5	komatiite	2.68	2.578	1.832	3.319	16.53	17.01	1.209
GOR152	komatiite	2.80	2.483	1.769	3.377	14.59	16.55	1.181
GOR153	komatiite	3.29	1.415	1.089	3.422	12.30	13.42	0.9289
GOR155	komatiite	5.97	2.633	1.985	3.061	16.21	16.76	0.5958
GOR156	komatiite	3.09	2.754	1.949	3.464	15.59	16.92	1.194
GOR157	komatiite	3.15	3.159	2.139	2.788	18.02	19.05	1.348
GOR159	komatiite	2.69	3.688	2.375	4.869	14.66	16.08	1.224
GOR159 (dup.)	komatiite	2.69	3.392	2.265	5.023	14.86	16.17	1.069
GOR160	komatiite	5.07	3.499	2.381	3.973	15.38	15.91	0.9859
GOR537	komatiite	1.83	2.430	1.803	3.776	16.08	17.36	1.102
GOR538	komatiite	2.88	2.273	1.658	5.067	12.34	12.62	0.825
GOR539	komatiite	4.21	2.781	2.109	3.812	17.83	21.90	1.029
GOR540	komatiite	4.64	2.219	1.653	3.703	16.36	16.40	0.8155
19GOR-1A	komatiite	3.51	2.550	1.832	3.226	16.32	19.06	1.164
19GOR-1B	komatiite	3.17	3.276	2.160	4.288	15.90	16.53	1.058
19GOR-1C	komatiite	3.12	2.297	1.642	3.872	14.87	16.86	0.9987
19GOR-1D	komatiite	2.73	2.795	1.985	4.120	16.32	17.48	1.197
19GOR-1E	komatiite	3.90	2.597	1.868	3.218	16.04	17.30	1.067
19GOR-2	komatiite	4.13	2.673	1.888	3.315	16.07	16.43	1.071
19GOR-3	komatiite	3.31	2.470	2.028	4.297	15.21	15.31	1.0342
19GOR-4	komatiite	3.58	2.258	1.678	3.450	12.09	15.00	1.0318
19GOR-5	komatiite	3.06	5.436	3.726	8.586	15.33	15.47	1.064
GOR1901	komatiite	2.74	2.684	1.942	3.205	17.14	17.22	1.114
19GOR-6	peridotite	4.86	1.503	1.480	5.420	5.312	6.440	0.3351
19GOR-7	peridotite	6.63	0.7294	1.0233	4.277	6.686	7.543	0.4166
19GOR-13	peridotite	5.28	7.328	4.205	10.42	9.501	9.762	0.5345
19GOR-13 (dup.)	peridotite	5.28	6.167	3.834	10.35	7.994	10.16	0.5018
19GOR-8	plagioclase peridotite	5.83	0.2562	8.792	2.299	11.42	14.03	0.7686
GOR503	dunite	5.34	4.370	4.263	7.684	11.662	5.012	0.1571
GOR507	wehrlite	7.16	0.125	0.059	3.459	7.975	7.214	0.2819
GOR509	olivine gabbro	6.36	2.410	1.972	5.810	13.343	9.728	0.4983
GOR535	olivine gabbro	5.10	0.285	0.346	2.298	9.775	11.265	0.5945
19GOR-9	picrite	3.15	2.292	1.768	3.739	8.868	10.84	0.3619
19GOR-10	picrite	4.07	0.6247	1.0081	3.596	7.748	10.35	0.1504
19GOR-10 (rep.)	picrite	4.07	0.5805	0.6433	3.743	7.505	10.67	0.1525
19GOR-10 (rep.)	picrite	4.07	0.5645	0.6216	3.683	7.547	11.18	0.1514
19GOR-11	picrite	5.35	0.3180	5.365	1.919	9.600	16.13	0.3506
19GOR-11 (dup.)	picrite	5.35	0.3248	5.637	1.891	9.872	15.61	0.3537
19GOR-27	picrite	7.98	17.89	12.061	5.297	7.798	7.568	0.3070
19GOR-28	picrite	8.50	2.550	1.796	4.085	9.615	11.88	0.3016
19GOR-29	picrite	4.25	0.5668	0.4334	2.646	9.565	12.67	0.4196
19GOR-30	picrite	2.81	2.467	1.887	4.312	8.311	10.14	0.2998
19GOR-31	picrite	3.45	0.6020	0.5293	3.179	8.653	9.827	0.3119
19GOR-32	tuff breccia	6.33	0.8313	0.6048	3.243	7.385	9.462	0.0868
19GOR-33	tuff breccia	7.81	0.8067	0.6452	3.919	7.711	14.00	0.1278

Table S2 cont.								
19GOR-14	poikilitic gabbro	2.61	1.270	0.9832	3.042	13.64		1.062
19GOR-14 (dup.)	poikilitic gabbro	2.61	1.206	0.9482	3.008	13.28	13.22	0.9402
19GOR-15	poikilitic gabbro	2.81	1.034	0.7158	2.185	12.37		0.7053
19GOR-15 (dup.)	poikilitic gabbro	2.81	0.9023	0.6964	2.136	12.50	12.67	0.6940
19GOR-17	gabbro	3.09	1.211	0.8882	1.991	12.77		1.121
19GOR-17 (dup.)	gabbro	3.09	1.064	0.8018	1.920	13.17	12.31	1.051
19GOR-18	gabbro	3.08	1.308	0.9211	2.580	12.13		0.9224
19GOR-18 (dup.)	gabbro	3.08	1.313	0.9345	2.701	11.98	11.51	0.9226
19GOR-19	poikilitic gabbro	2.72	0.0947	0.3140	0.5455	15.47	15.98	1.207
GOR23A	E-basalt	n.d.						
19GOR-22	E-basalt	0.82	0.0276	0.0445	0.0467	15.77	21.24	1.706
19GOR-22 (dup.)	E-basalt	0.82	0.0295	0.1029	0.0409	15.81	21.35	1.727
19GOR-23	E-basalt	1.23	0.0257	0.1125	0.0406	16.69		2.127
19GOR-23 (dup.)	E-basalt	1.23	0.0285	0.1065	0.0279	16.22	22.11	2.096
19GOR-24	E-basalt	2.05	0.0628	0.1039	0.2096	10.31		0.9169
19GOR-24 (dup.)	E-basalt	2.05	0.0602	0.0947	0.1538	10.46	13.03	0.8906
19GOR-16	D-basalt	1.87	0.2771	0.2769	0.7543	8.841	9.504	2.438
19GOR-25	D-basalt	1.88	0.4562	0.4702	0.9810	20.07		1.748
19GOR-25 (dup.)	D-basalt	1.88	0.4800	0.4810	1.0348	21.68	20.46	1.742
19GOR-26	D-basalt	1.45	0.1797	0.1487	0.4518	5.720		3.085
19GOR-26 (repl.)	D-basalt	1.45	0.2065	0.1509	0.4108	5.476	5.730	3.050
19GOR-26 (repl.)	D-basalt	1.45	0.1703	0.1264	0.4037	5.594	4.838	3.060
Curaçao								
CUR-04	picrite	4.67	1.811	1.367	3.386	9.804	11.56	0.3201
CUR-05	picrite	5.20	3.144	2.150	4.743	11.51	10.34	0.2839
CUR-11	picrite	4.75	4.002	2.842	5.115	13.77	10.42	0.3663
CUR-09	basalt	2.64	0.0182	0.0265	0.3932	6.942	21.97	0.8680
CUR13-6	basalt	1.79	0.0280	0.0270	0.4540	8.486	7.570	0.7788

Table S4. Tungsten isotopic compositions of Gorgona Island rocks determined using MC-ICPMS.

Lab-ID	Sample	Rock type	Mass (g)	[W] (ng/g)	Yield (%)	N	$\mu^{182}W_{meas.}$ (±2σ)[a]	$\mu^{183}W_{meas.}$ (±2σ)[a]	$\mu^{182}W_{meas.}$ (±2σ)[a]	$\mu^{184}W_{meas.}$ (±2σ)[a]
							normalized to $^{186}W/^{184}W = 0.92767$ ('6/4')		normalized to $^{186}W/^{183}W = 1.98590$ ('6/3')	
EE07-08	GOR-503	Dunite	19.3996	3.6	22	1	-22.0 ± 14.2	-19.8 ± 13.5	4.1 ± 15.6	13.1 ± 9.0
EG04-04	GOR-505	Dunite	20.5730	n.d.	n.d.	1	-21.6 ± 14.2	-4.7 ± 13.5	-13.8 ± 15.6	3.1 ± 9.0
DP01-04	GOR-507	Wehrlite	36.0233	2.0	61	1	-18.8 ± 14.2	-21.6 ± 13.5	10.8 ± 15.6	14.4 ± 9.0
DM01-04	GOR-509	Ol Gabbro	27.5654	5.0	41	1	-61.6 ± 14.2	-2.8 ± 13.5	-56.5 ± 15.6	1.9 ± 9.0
EC01-04	GOR-509	Ol Gabbro	44.7426	5.0	37	3	-50.3 ± 6.8	-8.9 ± 7.7	-37.6 ± 5.9	5.9 ± 5.2
Combined	*GOR-509*	*Ol Gabbro*	*72.3080*			*4*	*-53.1 ± 12.6*	*-7.3 ± 8.7*	*-42.3 ± 19.5*	*4.9 ± 5.8*
EE01-03	19GOR-7	Peridotite	30.6381	13.9	30	4	-3.0 ± 13.0	-13.1 ± 10.5	14.1 ± 7.6	8.7 ± 7.0
EG07-08	19GOR-10	Picrite	20.0850	23	20	1	-19.5 ± 14.2	-16.47 ± 13.5	1.2 ± 15.6	11.0 ± 9.0
EG01-03	19GOR-17	Gabbro	30.0778	10.3	55	5	-1.0 ± 11.9	-1.8 ± 11.4	1.2 ± 10.2	1.2 ± 7.6
EE04-06	GOR-535	Ol Gabbro	31.4300	17.2	19	3	1.0 ± 12.6	-8.9 ± 5.9	13.7 ± 7.7	5.9 ± 3.9

[a]The uncertainties (2σ) for measured $\mu^{i}W$ (n = 1) represent the long term reproducibility (2SD) as determined for replicate measurements of the terrestrial rock standard BHVO-2 (Hellmann et al., 2019). Uncertainties are 2SD if N ≥ 3. n.d. - not determined.

Supplementary Figures

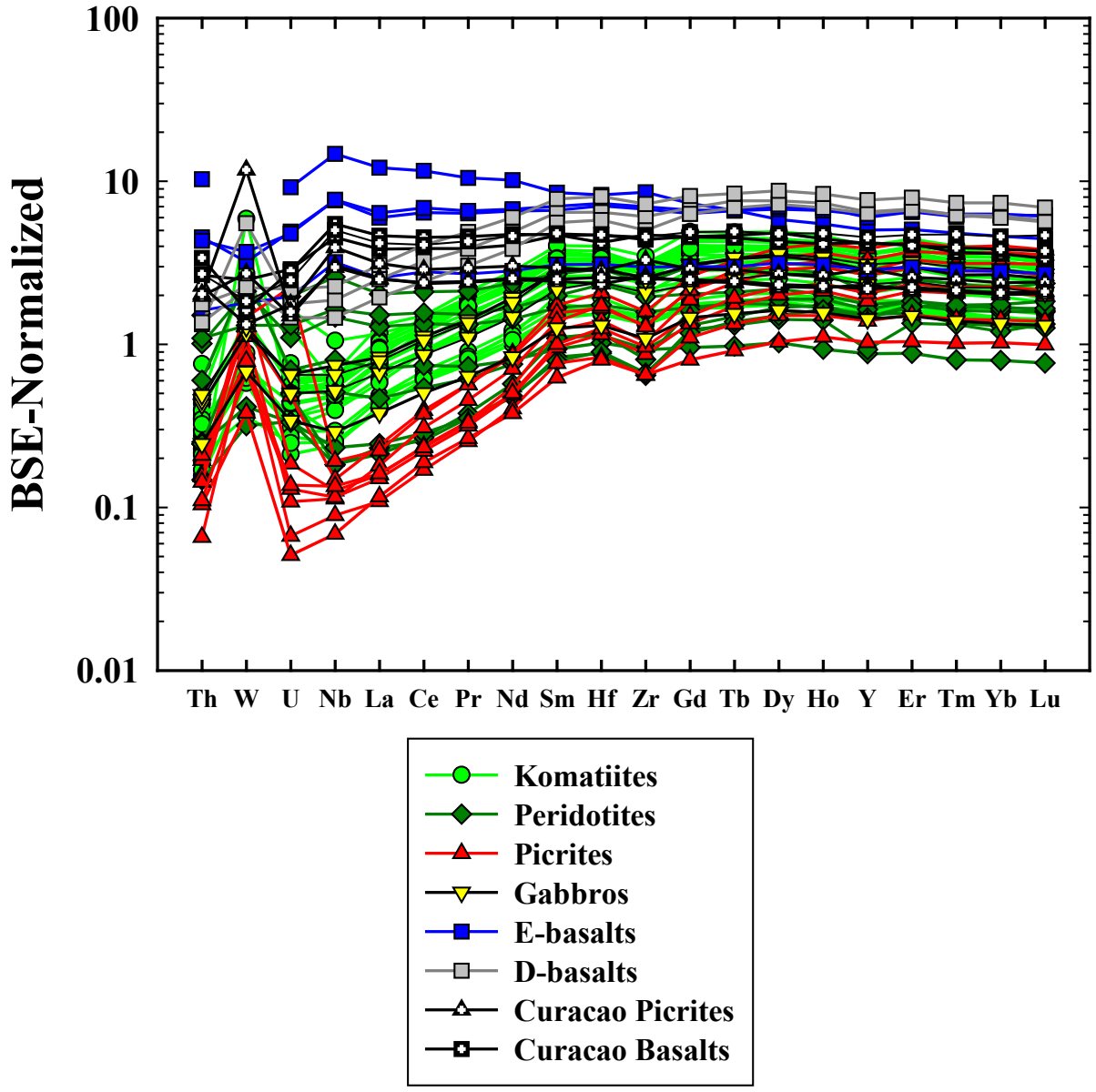

Figure S1. Plot of bulk silicate Earth (BSE) normalized concentrations of trace element concentrations of Gorgona Island and Curaçao rocks ordered from the most highly incompatible on the left to the least highly incompatible on the right. Bulk silicate Earth concentrations from McDonough and Sun (1995) and Arevalo and McDonough (2008).

10

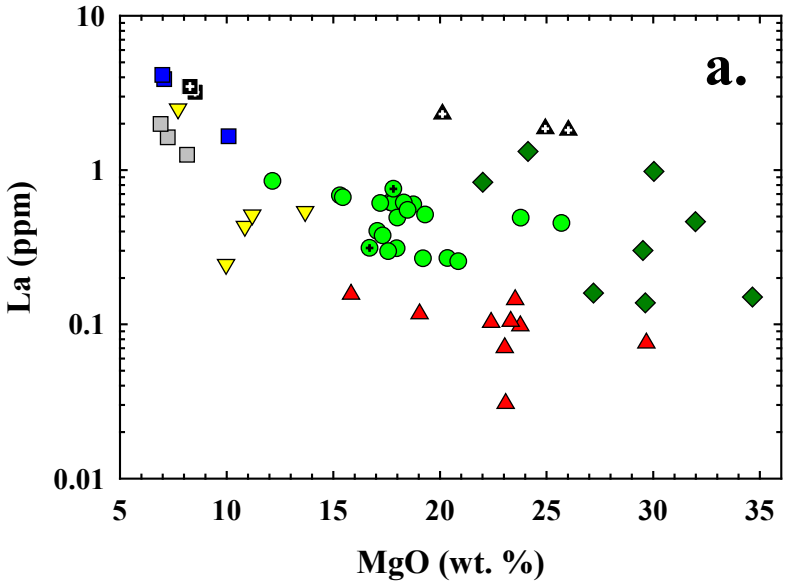
a.
La (ppm)
10
1
0.1
0.01
5
10
15
20
25
30
35
MgO (wt. %)

11

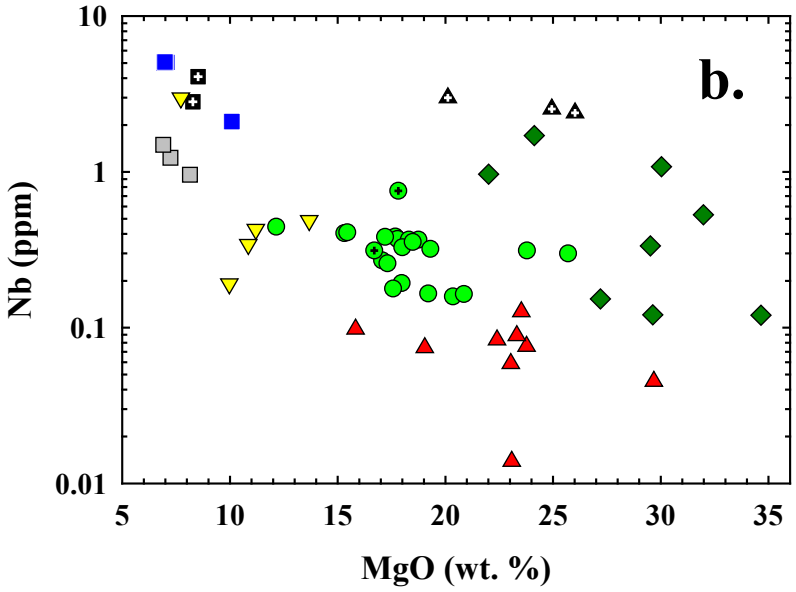
b.
Nb (ppm)
10
1
0.1
0.01
5
10
15
20
25
30
35
MgO (wt. %)

12

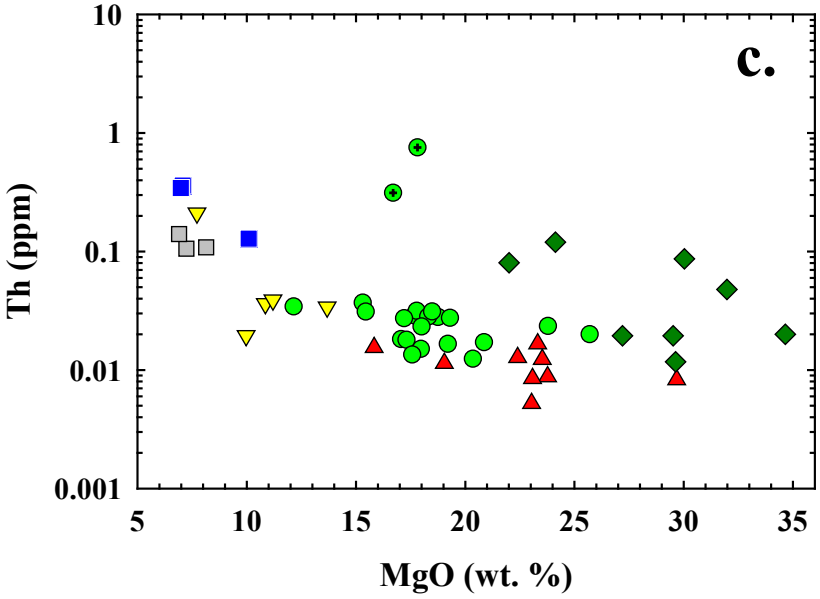

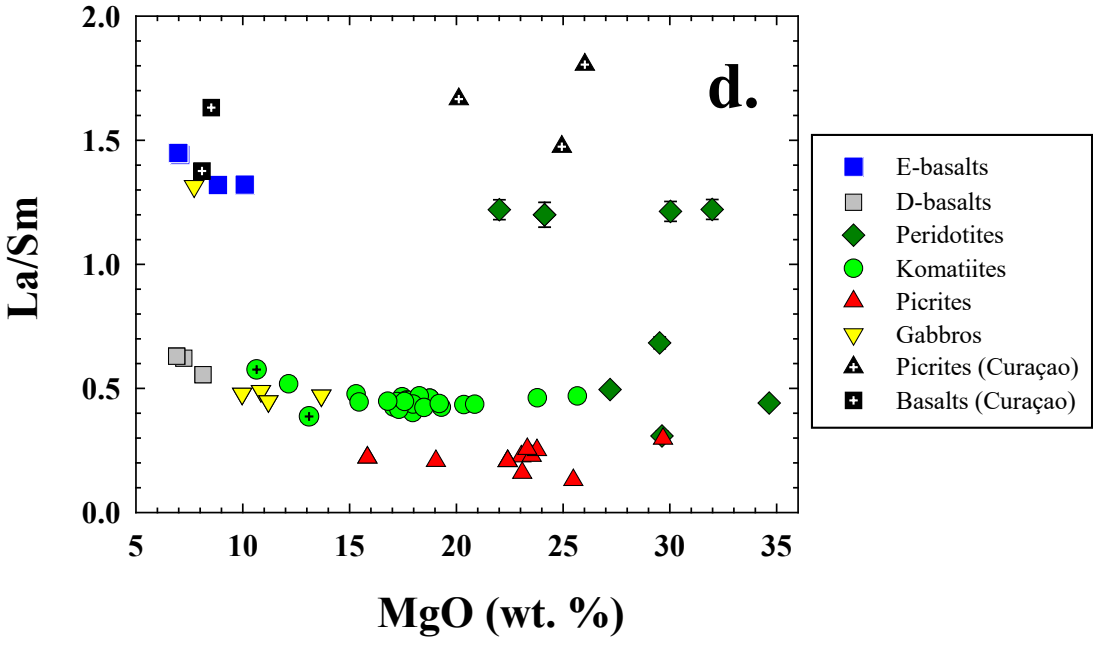

Figure S2a-d. Plots of MgO (in wt. %) versus: a) La, b) Nb, c) Th (all in ppm) and d) La/Sm for Gorgona and Curaçao rocks. Komatiites GOR23B and GOR47 with elevated $\gamma^{187}Os$ are shown as green circles with crosses. Note the general, but poorly defined negative correlation across the suite and the clear division between enriched (La/Sm > 1) and depleted samples.

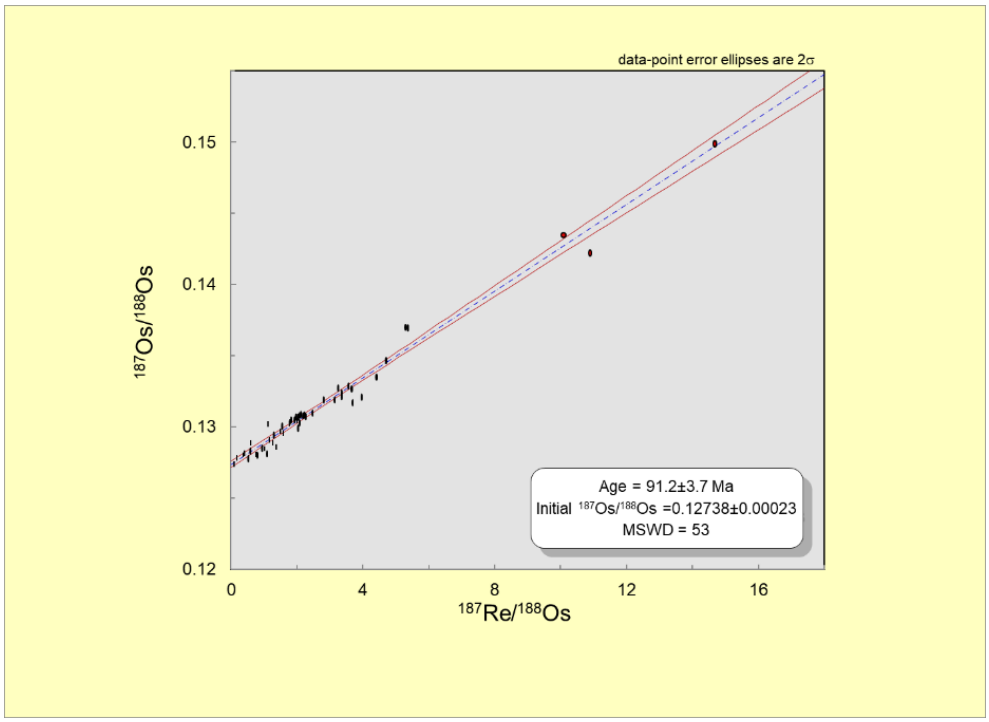
data-point error ellipses are 2σ
0.15
0.14
0.13
0.12
$^{187}Os/^{188}Os$
0
4
8
12
16
$^{187}Re/^{188}Os$
Age = 91.2±3.7 Ma
Initial $^{187}Os/^{188}Os$ =0.12738±0.00023
MSWD = 53

a.

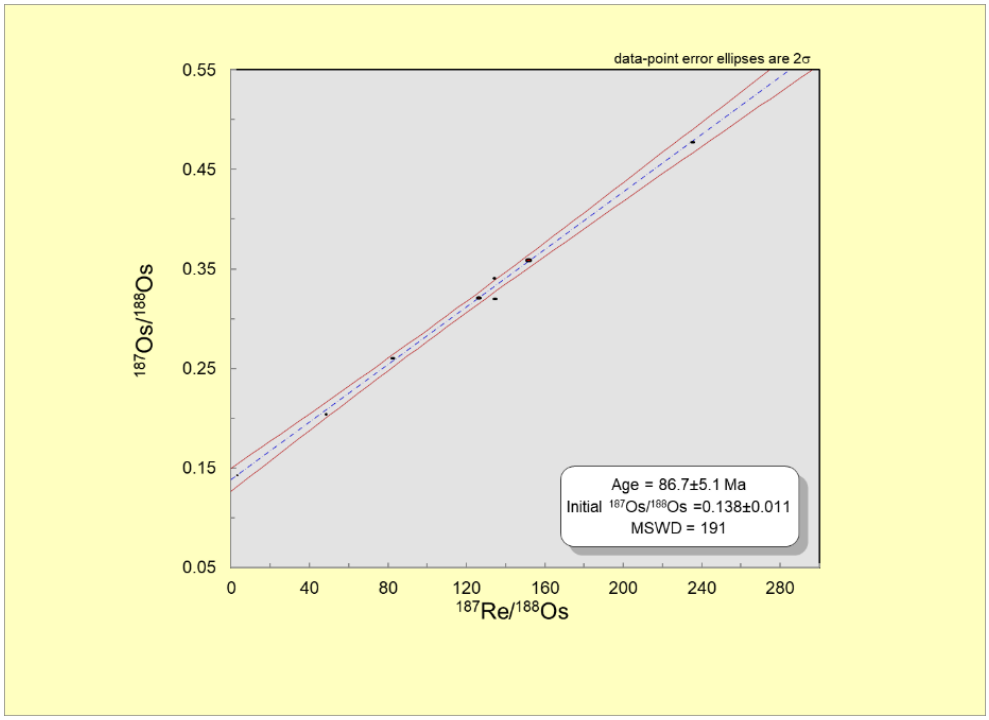
data-point error ellipses are 2σ
0.55
0.45
0.35
0.25
0.15
0.05
$^{187}Os/^{188}Os$
0
40
80
120
160
200
240
280
$^{187}Re/^{188}Os$
Age = 86.7±5.1 Ma
Initial $^{187}Os/^{188}Os$ =0.138±0.011
MSWD = 191

b.

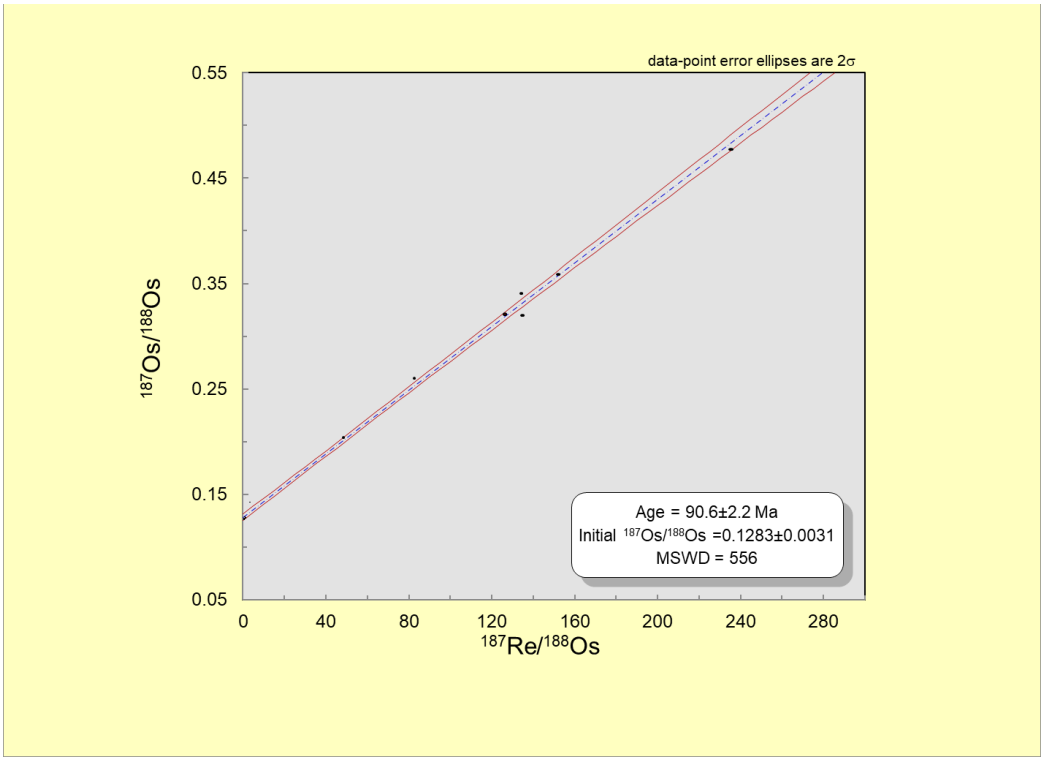

c.

Figure S3a-c. $^{187}Re/^{188}Os$ versus $^{187}Os/^{188}Os$ isochron figures for: a) Gorgona komatiites, picrites and peridotites, b) Curaçao basalts (including data from Walker et al., 1999), and c) Curaçao combined basalts and picrites (including data from Walker et al., 1999). Data were regressed and isochrons generated using the *Isoplot 3.00* program (Ludwig, 2003). Analytical uncertainties are the size of the symbols or smaller.

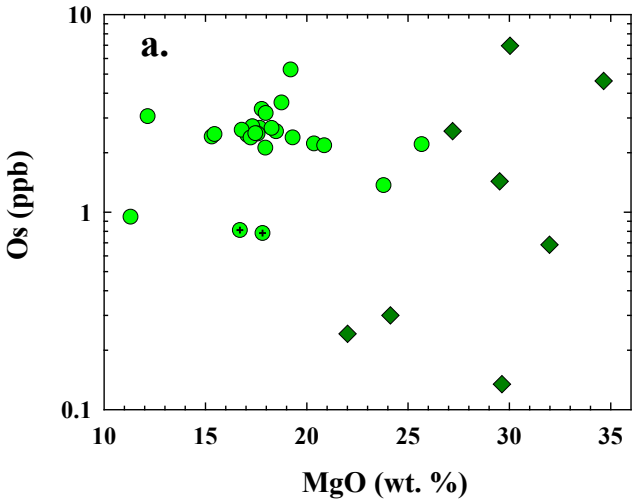
a.
Os (ppb)
10
1
0.1
10
15
20
25
30
35
MgO (wt. %)

33

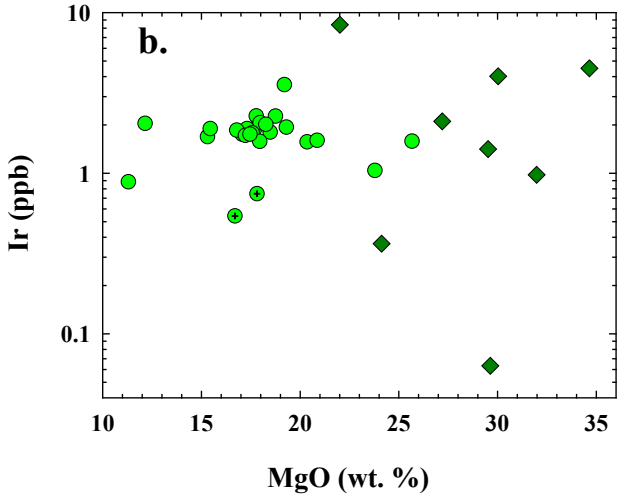
b.
Ir (ppb)
10
1
0.1
10
15
20
25
30
35
MgO (wt. %)

34

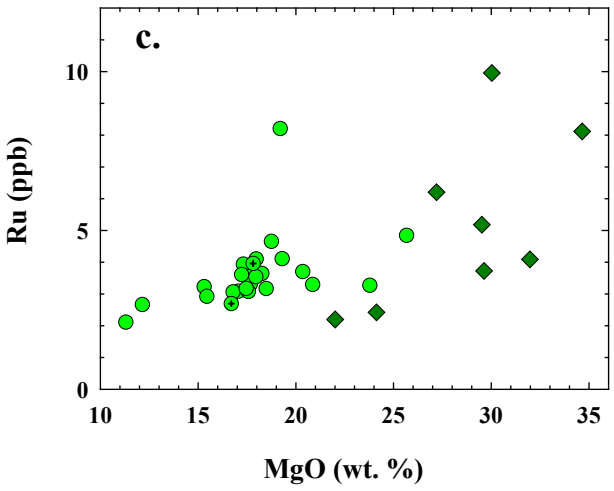
c.
Ru (ppb)
10
5
0
10
15
20
25
30
35
MgO (wt. %)

35

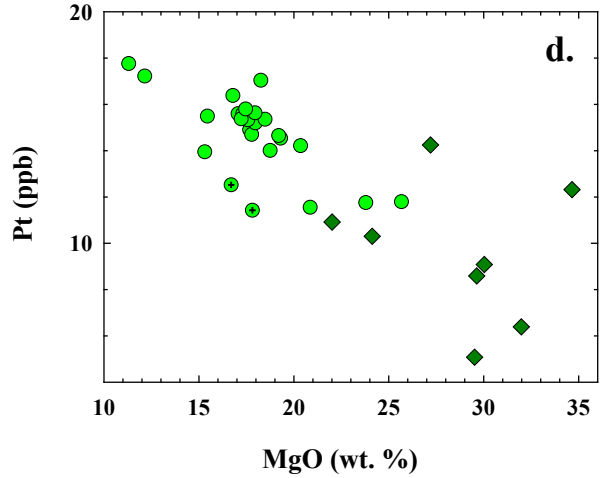

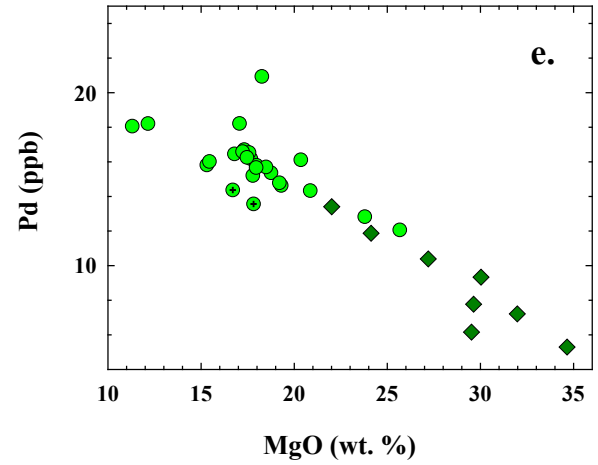

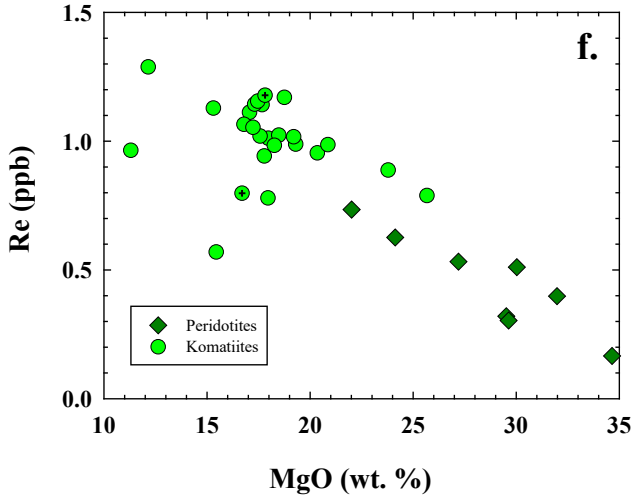

Figure S4a-f. Plots of MgO (in wt. %) versus HSE abundances (in ppb) for Gorgona komatiites and peridotites. Komatiites with strongly elevated $\gamma^{187}Os$ (GOR23B and GOR47) are shown as green circles with crosses.

42

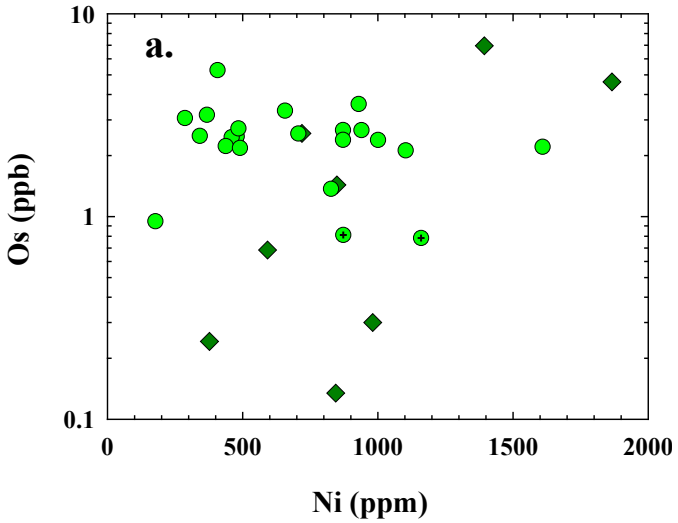
a.
Os (ppb)
10
1
0.1
0
500
1000
1500
2000
Ni (ppm)

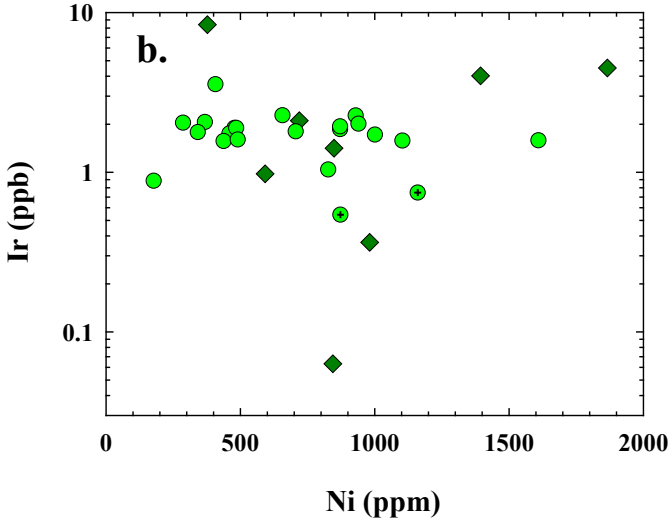
b.
Ir (ppb)
10
1
0.1
0
500
1000
1500
2000
Ni (ppm)

43

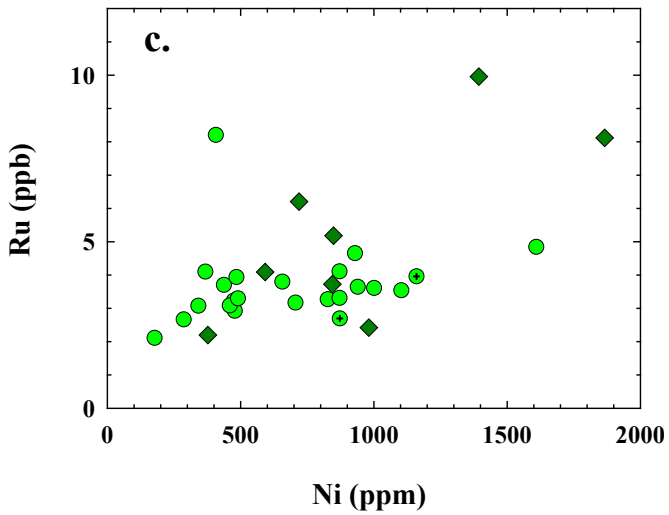
c.
Ru (ppb)
10
5
0
0
500
1000
1500
2000
Ni (ppm)

44

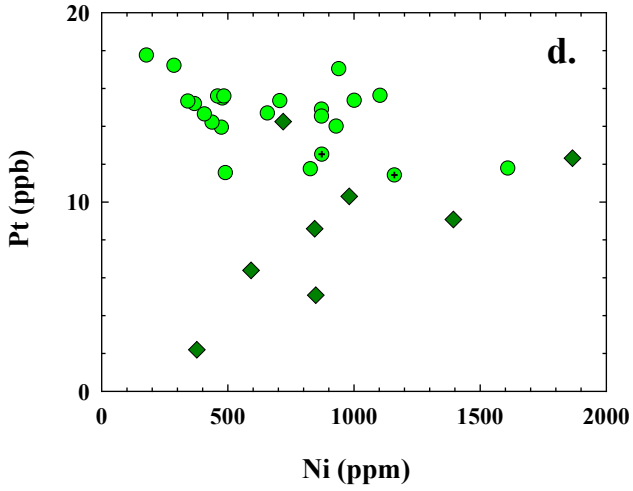

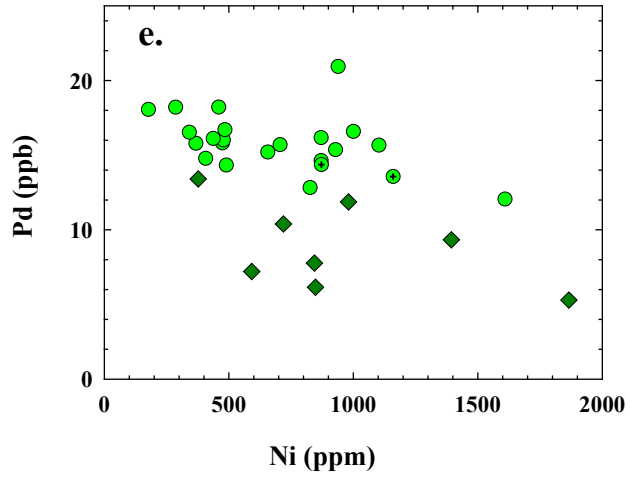

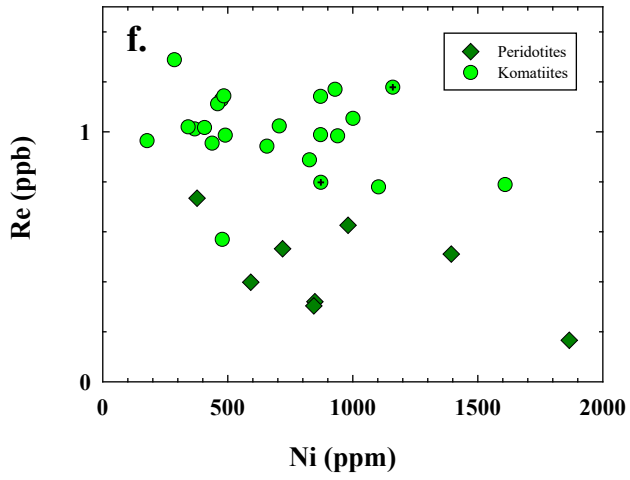

Figure S5a-f. Plots of Ni (in ppm) versus HSE abundances (in ppb) for Gorgona komatiites and peridotites. Komatiites with strongly elevated γ^{187}Os (GOR23B and GOR47) are shown as green circles with crosses.

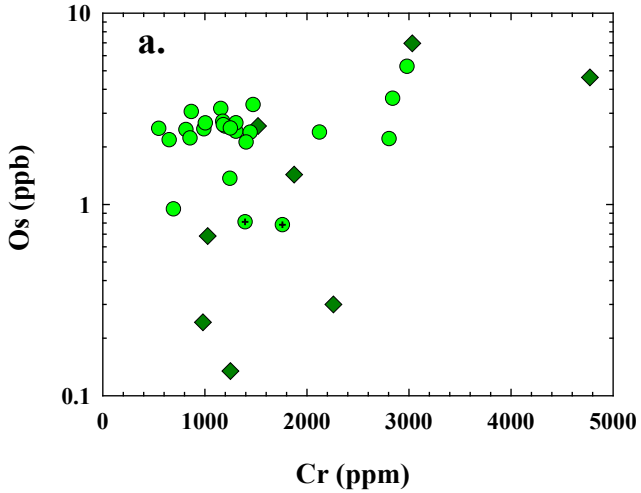
a.
Os (ppb)
10
1
0.1
0
1000
2000
3000
4000
5000
Cr (ppm)

51

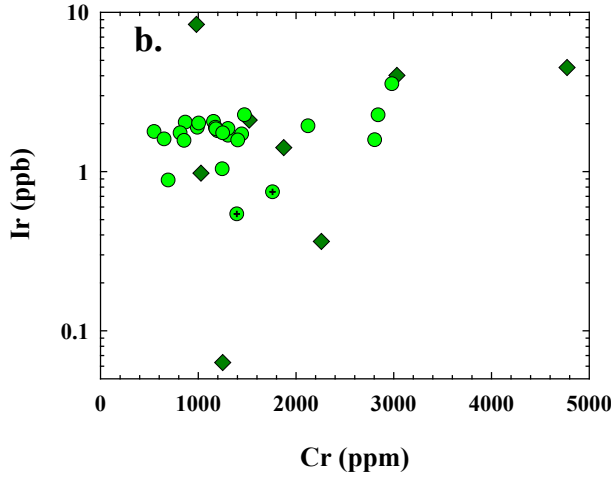
b.
Ir (ppb)
10
1
0.1
0
1000
2000
3000
4000
5000
Cr (ppm)

52

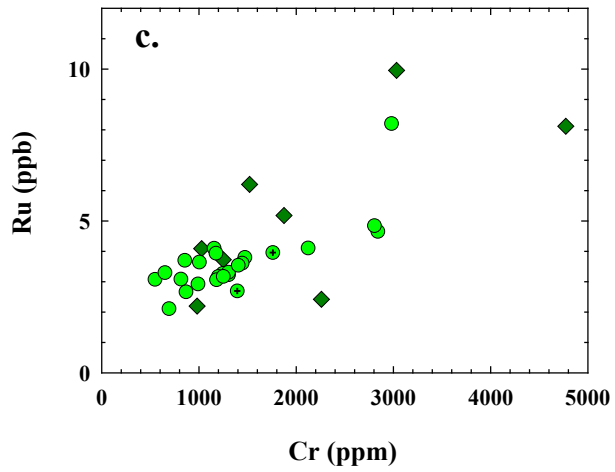
c.
Ru (ppb)
10
5
0
0
1000
2000
3000
4000
5000
Cr (ppm)

53

54

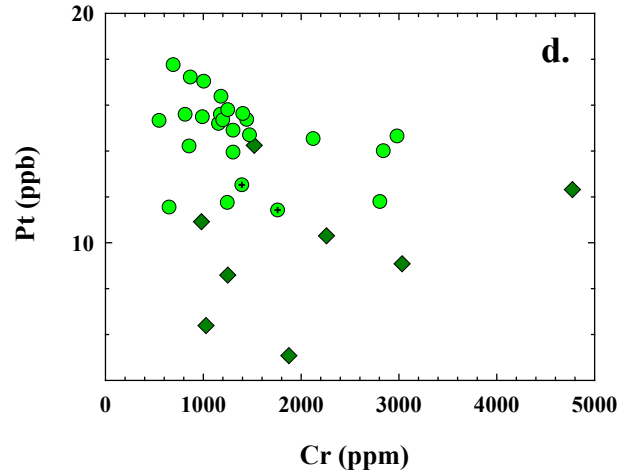

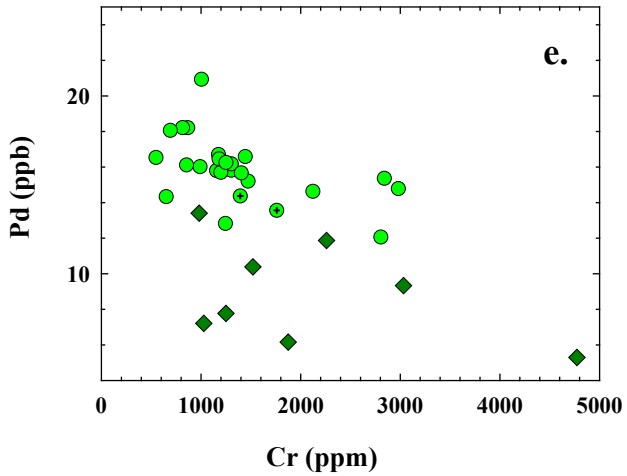

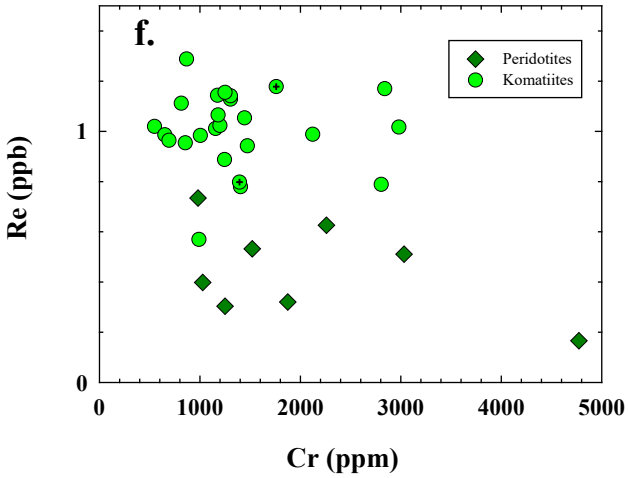

Figure S6a-f. Plots of Cr (in ppm) versus HSE abundances (in ppb) for Gorgona komatiites and peridotites. Komatiites with strongly elevated γ^{187}Os (GOR23B and GOR47) are shown as green circles with crosses.

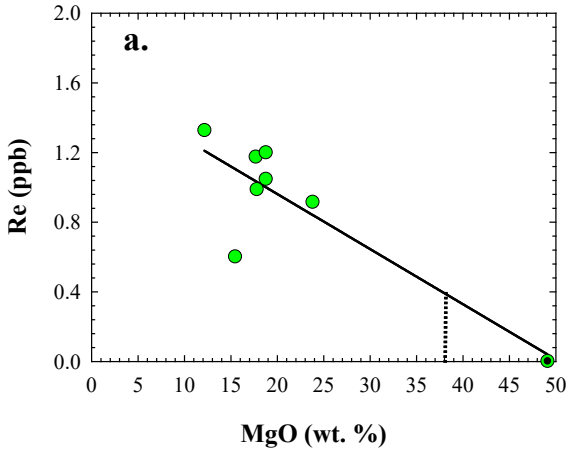

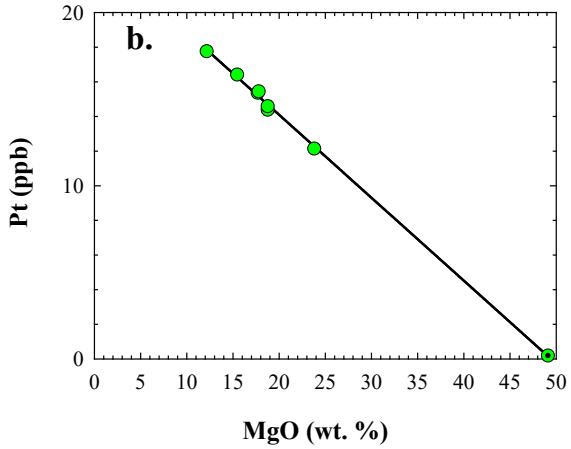

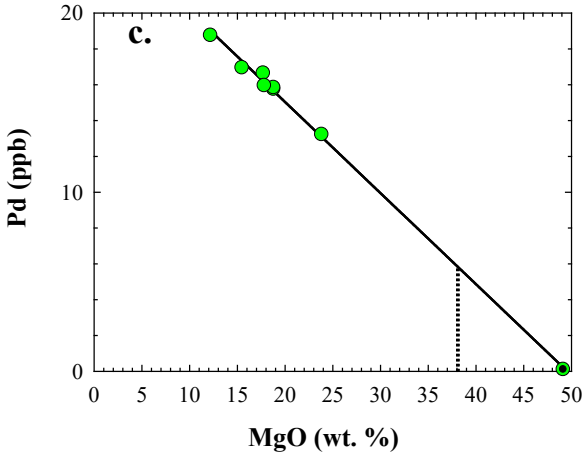

Figure S7a-c. Plots of MgO (in wt.%) versus Re, Pt and Pd, from komatiites samples GOR-153 to 160, which are presumed to be samples of the same, or closely-related flows. Regression results are projected to an estimated olivine composition (circle with dot). Analytical uncertainties are the size of the symbols or smaller.

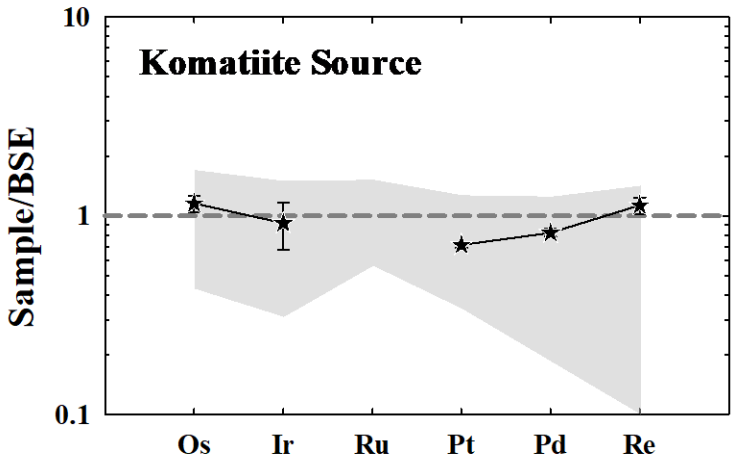

Figure S8. The projected, Primitive Mantle normalized abundances of Os, Ir, Pt, Pd and Re in the mantle source of the dominant komatiites. Uncertainties in the projected concentrations are shown with the error bars. The gray field shows the range of compositions defined 95% of modern abyssal peridotites, with data compiled by Walker (2016).

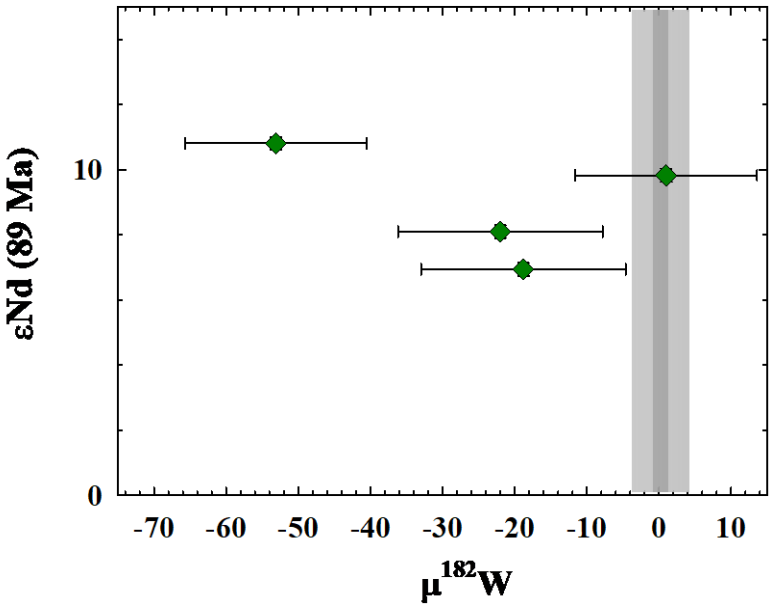

Figure S9. $\mu^{182}W$ versus initial εNd for four Gorgona peridotites with variable $\mu^{182}W$. Neodymium isotopic data are from Révillon et al. (2000).

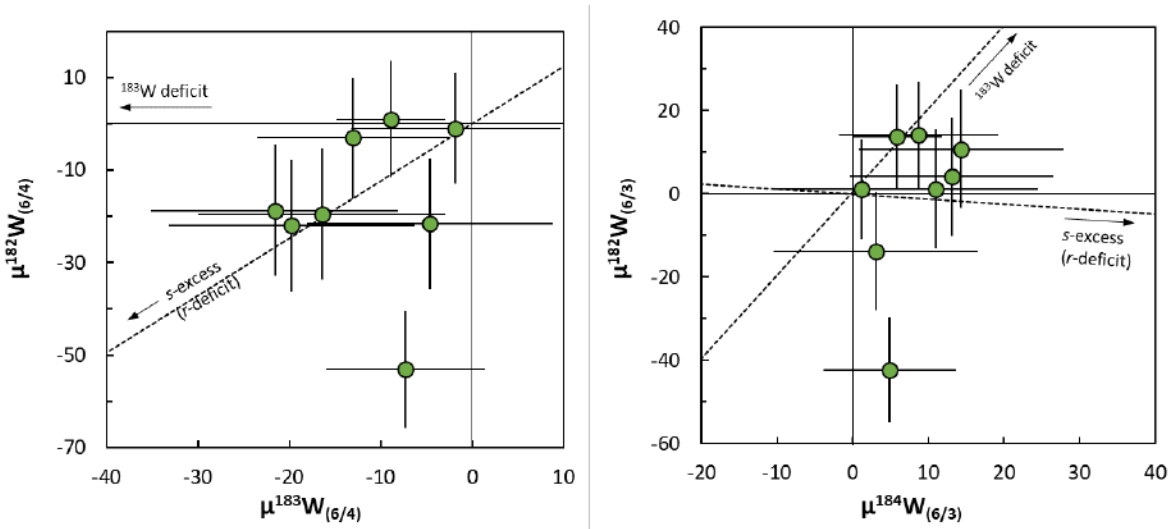

Figure. S10. Plots of $\mu^{182}W$ versus $\mu^{183}W$ and $\mu^{184}W$ for Gorgona samples. Samples do not all plot along a theoretical *s*-process line (Bisterzo et al., 2011), suggesting that the variation in ^{182}W is purely radiogenic in origin.

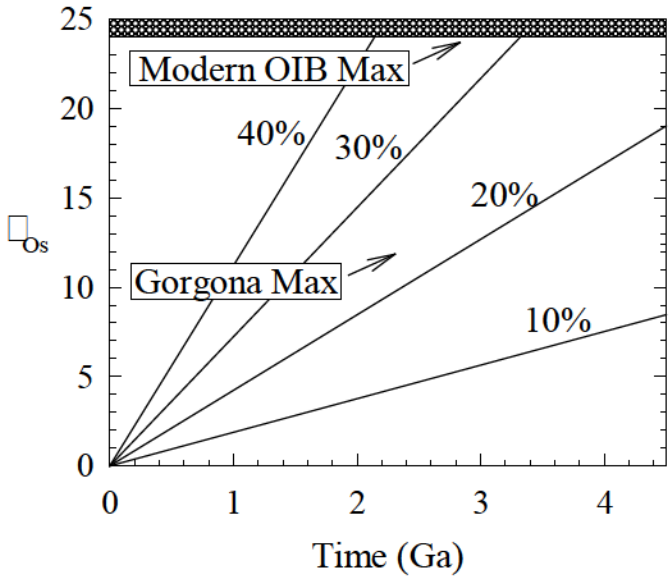

Figure S11. $\gamma^{187}Os$ versus Time (in Ga) for hybrid mantle reservoirs generated via the mixing model reported in Walker et al. (1999). Diagonal lines indicate growth trajectories for different mantle/basalt mixtures with the percentage of basaltic crust additions labeled. The evolution growth trajectories show that considerable time and/or considerable contamination is necessary to generate $\gamma^{187}Os$ values $\geq +12$ via mixing oceanic basalt with fertile mantle.